Project funded by the European Commission under the 6th (EC) RTD Framework Programme (2002- 2006) within the framework of the specific research and technological development programme “Integrating and strengthening the European Research Area”

Project UpWind

Contract No.:
019945 (SES6)

“Integrated Wind Turbine Design”

AUTHOR:	Ervin Bossanyi
AFFILIATION:	Garrad Hassan and Partners Limited
ADDRESS:	St Vincent’s Works, Silverthorne Lane, BRISTOL BS2 0QD, England
TEL.:	+44 (0) 117 972 9900
EMAIL:	Ervin.bossanyi@garradhassan.com
FURTHER AUTHORS:	Work Package partners
REVIEWER:	
APPROVER:	

Document Information

DOCUMENT TYPE	Deliverable 5.10
DOCUMENT NAME:	Work Package 5 – Control systems: Final report
DOCUMENT NUMBER:	11593/BR/10
REVISION:	B
REV. DATE:	10th February 2010
CLASSIFICATION:	R0: General public
STATUS:	

Abstract: This document summarises the main results arising from UPWIND Work Package 5: Control systems.

Contents

Principal contributors

Garrad Hassan	Ervin Bossanyi (Work package leader), Barbara Savini
Alstom	Michele Rossetti, Carlo-Enrico Carcangiu
CENER	Mikel Iribas Latour
ECN	Dennis Wouters, Tim van Engelen
GE Global Research	Parag Vyas
IWES	Martin Geyler, Melanie Hau, Boris Jasniewicz
REpower	Svenja Wortmann
Risø	Helen Markou
Stuttgart University	David Schlipf

STATUS, CONFIDENTIALITY AND ACCESSIBILITY								
Status			**Confidentiality**			**Accessibility**		
S0	Approved/Released	●	**R0**	General public	●	Private web site		
S1	Reviewed		**R1**	Restricted to project members		Public web site	●	
S2	Pending for review		**R2**	Restricted to European. Commission		Paper copy		
S3	Draft for comments		**R3**	Restricted to WP members + PL				
S4	Under preparation		**R4**	Restricted to Task members +WPL+PL				

PL: *Project leader* **WPL:** *Work package leader* **TL:** *Task leader*

1. Introduction

Further improvement in the cost-effectiveness of wind turbines drives designers towards larger, lighter, more flexible structures, in which more 'intelligent' control systems play an important part in actively reducing the applied structural loads. This strategy of "brain over brawn" will therefore avoid the need for wind turbines to simply withstand the full force of the applied loads through the use of stronger, heavier and therefore more expensive structures.

As well as contributing to the further development of control algorithms for achieving such load reductions, WP5 has recognised the need to demonstrate that these load reductions can be achieved in practice, by carrying out full-scale tests on well-instrumented turbines in the field. This will provide the confidence required to incorporate these control techniques into the design of new, larger and innovative turbines.

As the penetration of wind energy increases, real issues are already arising relating to the control of the electrical network and its interaction with wind farms. These issues must be resolved before the penetration of wind power can increase further, and some of the tasks within WP5 have also addressed this need.

The specific objectives of this work package are:

- Further development of control algorithms for wind turbine load reduction, of the sensors and actuators which are required for the algorithms to be effective, of efficient methods of adjusting and testing controllers, and the application of these techniques to new larger and innovative turbines.
- Investigation and evaluation of different load estimation algorithms, using various sets of available sensor signals. Incorporation of promising structures to load reducing controller algorithms. Identification of potential problems to overcome when taking into account fault prediction information in controller dynamics.
- Field tests to demonstrate that the load reductions and estimated loads can be achieved reliably, so that future designs can take advantage of the implied reduction in capital costs.
- Development of wind turbine and wind farm control techniques aimed at increasing the acceptable penetration of wind energy, by allowing wind turbines to ride through network disturbances, and to contribute to voltage and frequency stability and overall reliability of the network.

The work package is divided into three broad areas:

Task 5.1 Controller design and implementation
Task 5.2 Field testing and evaluation
Task 5.3 Wind farm electrical control

A number of sub-tasks have been carried out within each of these areas. This report summarises the main results from each aspect of the work. In many cases, the detailed results are presented in other deliverables of the work package, and references to these are given where appropriate.

2. Controller design

2.1 State-of-the-art controller for the 5MW reference turbine

An early task in this work package was to design a state-of-the-art power production controller for the UPWIND 5MW reference turbine, bringing it up to date with the latest commercial techniques so that it can be used as a basis for further work.

The turbine is a generic 126 m diameter 3-bladed offshore turbine of fairly conventional design. Although not representative of any one particular turbine, it is fairly representative of typical commercial turbines in this class. The hub height is 90m above the nominal surface, with a sea depth of 20m. Figure 2.1 provides an illustration of the basic proportions of the turbine, and the key operational parameters are summarised in Table 2.1.

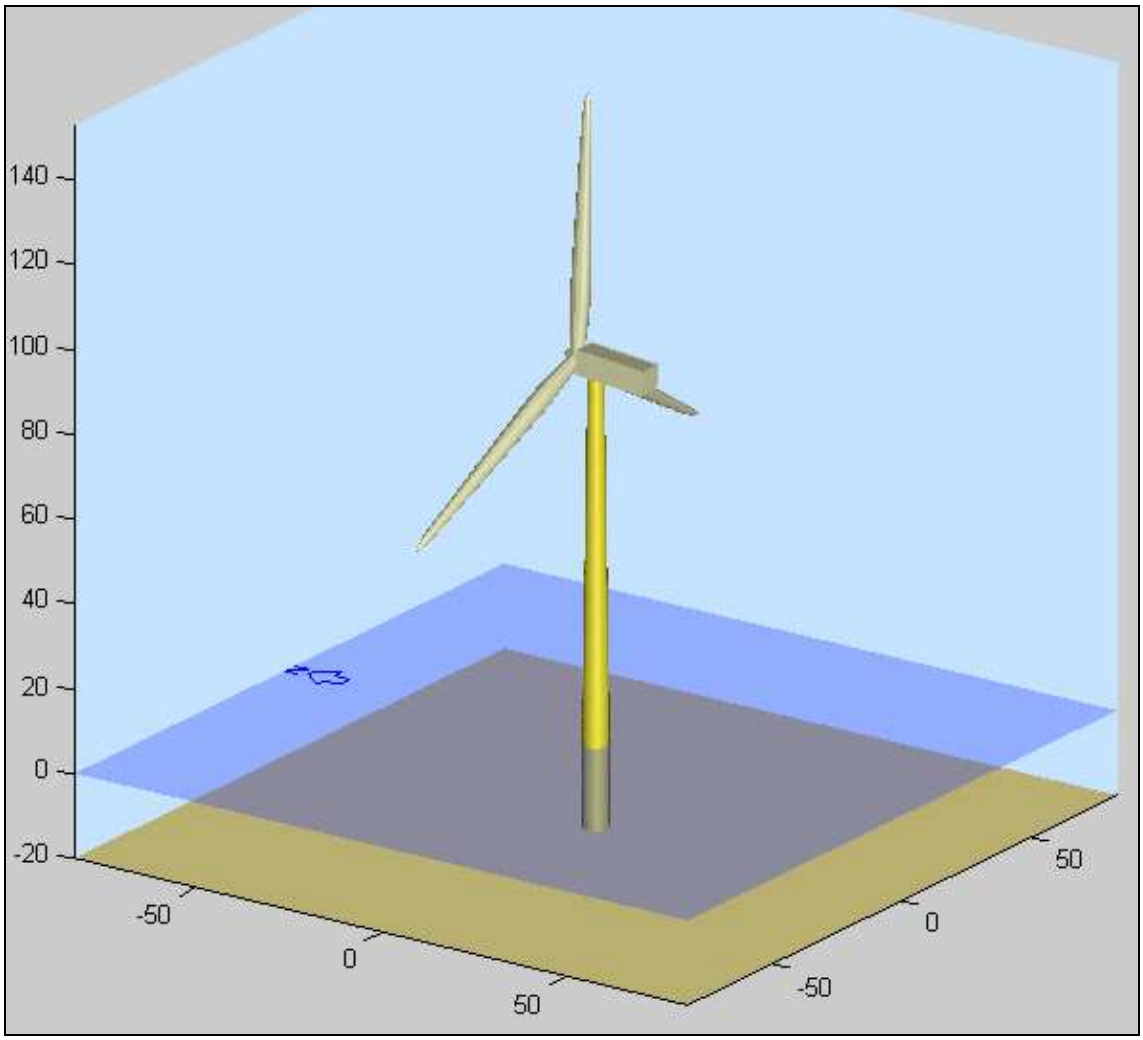

Figure 2.1: The 5 MW reference turbine

In accordance with widespread current practice, the power production control is based on the principles of variable rotor speed with full-span pitchable blades which pitch in the feathering

direction. The turbine reaches its rated power of 5 MW at the rated wind speed of 11.3 m/s. The main principles of the controller are based on previous work [1], [7].

Rotor diameter	126	m
Number of blades	3	
Hub height	90	m
Tilt angle of rotor to horizontal	5	deg
Cone angle of rotor	-2.5	deg
Rotor overhang	5	m
Gearbox ratio	97	
Rotational sense of rotor, viewed from upwind	Clockwise	
Position of rotor relative to tower	Upwind	
Aerodynamic control	Full span pitch	
Generator	Variable speed	
Cut in wind speed	4	m/s
Rated wind speed	11.3	m/s
Cutout wind speed	25	m/s
Rated rotational speed	12.1	rpm

Table 2.1: Key operational parameters

The controller is based on the following principles:

- Optimisation of power production below rated wind speed, by allowing the rotor speed to vary in proportion to wind speed until the maximum operational rotor speed of 12.1 rpm is reached, subject to a speed exclusion zone to prevent excitation of the first vibrational tower mode by the blade passing frequency (3P).
- Nominally constant speed operation at 12.1 rpm, using speed regulation by torque control below rated and by collective pitch control above rated.
- Modification of generator torque control to help with damping of torsional resonance in the drive train.
- Combined torque and pitch control to ensure smooth transitions at rated and maximise energy capture.
- Additional contribution to collective pitch control to improve the response to extreme gusts.
- Modification of collective pitch control in response to nacelle acceleration, to help with damping of fore-aft tower vibration.
- 1P individual pitch control to reduce asymmetric rotor loads, especially 1P loads on rotating components and low frequency loads on non-rotating components.
- 2P individual pitch control to reduce 3P fatigue loads on non-rotating components.

The controller design has been carried out using classical linear control design methods applied to a high-order linearised model of the turbine dynamics at a number of operating points. The controller has then been tested in detailed non-linear turbulent simulations and further adjusted, using some non-linear controller features where appropriate, to achieve a satisfactory controller performance across a range of operating conditions.

The controller design is reported in detail in Deliverable 5.1.1 [9]. Some illustrations demonstrating the performance of key features of the controller in the test simulations are presented in the next section.

2.1.1 5MW controller: sample simulation results

Figure 2.2 shows how the controller achieves smooth transitions between below-rated and above-rated operation. Speed regulation at 12 rpm is maintained, whether by torque or

collective pitch control. The phasing-out of individual pitch control and fore-aft tower damping at lower power levels is clearly seen; when they are active however, they have a negligible effect on the power output.

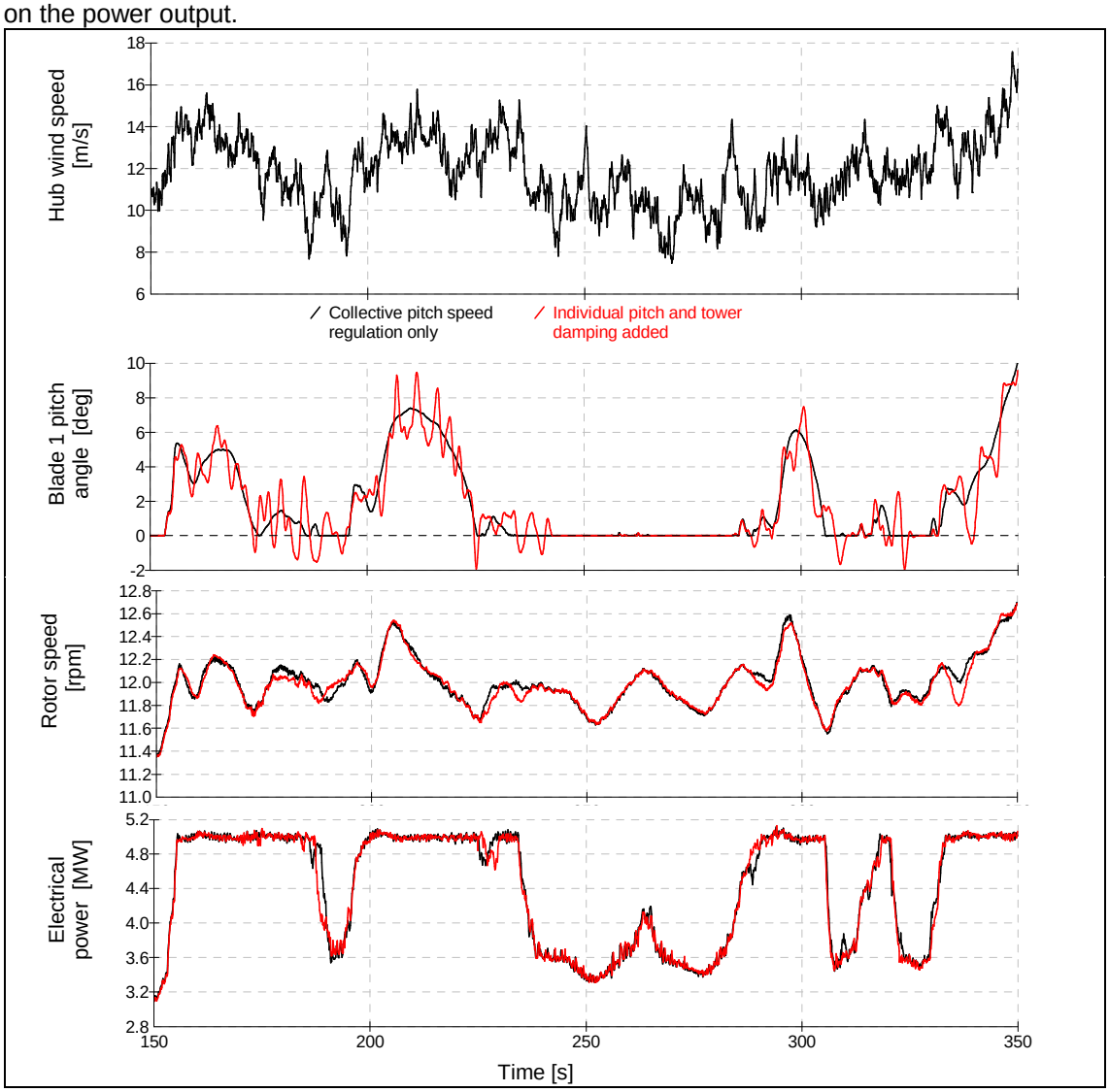

Figure 2.2: 5MW controller performance around rated wind speed

Figure 2.3 demonstrates the effect of the additional contribution to collective pitch control to improve the response to extreme gusts. Both the overspeed and the tower vibration resulting from the IEC edition 2 extreme operational gust at cut-out wind speed are significantly reduced. This feature is also beneficial for the extreme gust at rated wind speed, but is designed to have negligible effect on normal operation in turbulent wind at any wind speed.

The effect of the individual pitch control is best illustrated by examining the effect on the blade root out of plane (My) loading, the rotating hub moment My or Mz (the effect is very similar on these two loads) and the non-rotating My (nodding) or Mz (yawing) moment at the yaw bearing (again the effect on these two loads is very similar). A turbulent wind simulation at 19m/s mean wind speed has been selected to demonstrate the effect. The turbulence intensities are 16.7% (longitudinal), 13.1% (lateral) and 9.3% (vertical). The results are very similar at other wind speeds across the above-rated range. Obviously the effect decreases below rated as the individual pitch control is phased out.

Spectra of the principally-affected loads are shown in Figure 2.4. The upper two plots are for loads on rotating components, where the large fatigue-dominating peak at 1P (0.2 Hz) is completely removed by the 1P (first harmonic) individual pitch control. That leaves a smaller peak at 2P, which is removed by the 2P (second harmonic) individual pitch control.

The lower graph represents the non-rotating loads, where the 1P individual pitch loop removes the 0P (low-frequency) variations (it would also remove any 2P component if it were present), while the 2P loop attenuates the fatigue-dominating 3P peak (it would also remove any 1P component if it were present).

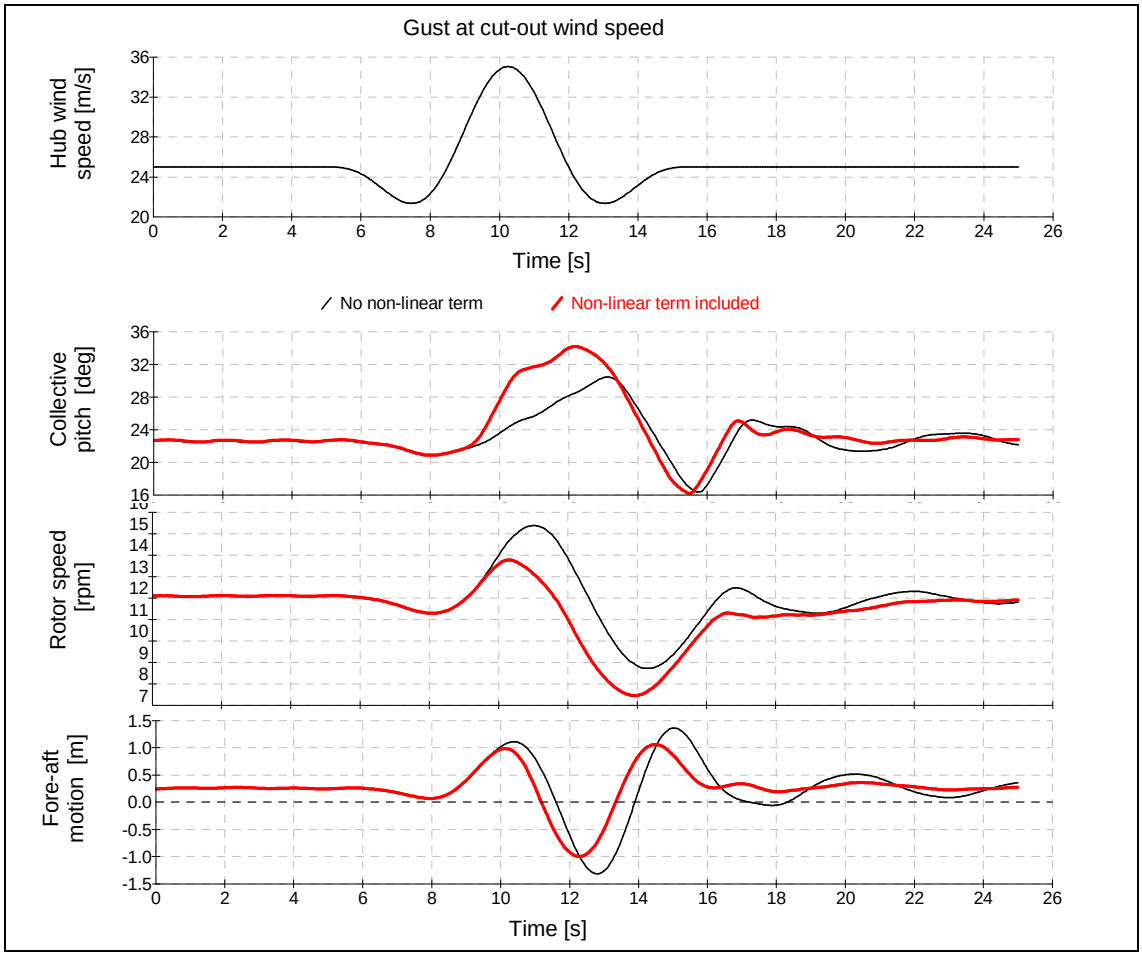

Figure 2.3: Effect of non-linear term on extreme gust at cut-out wind speed

The 5MW reference turbine with this new controller design was subsequently used as the basis for further work, both in this work package (for example the LIDAR work in Section 2.4), and in other UPWIND work packages (for example Work Package 4 on Offshore Support Structures).

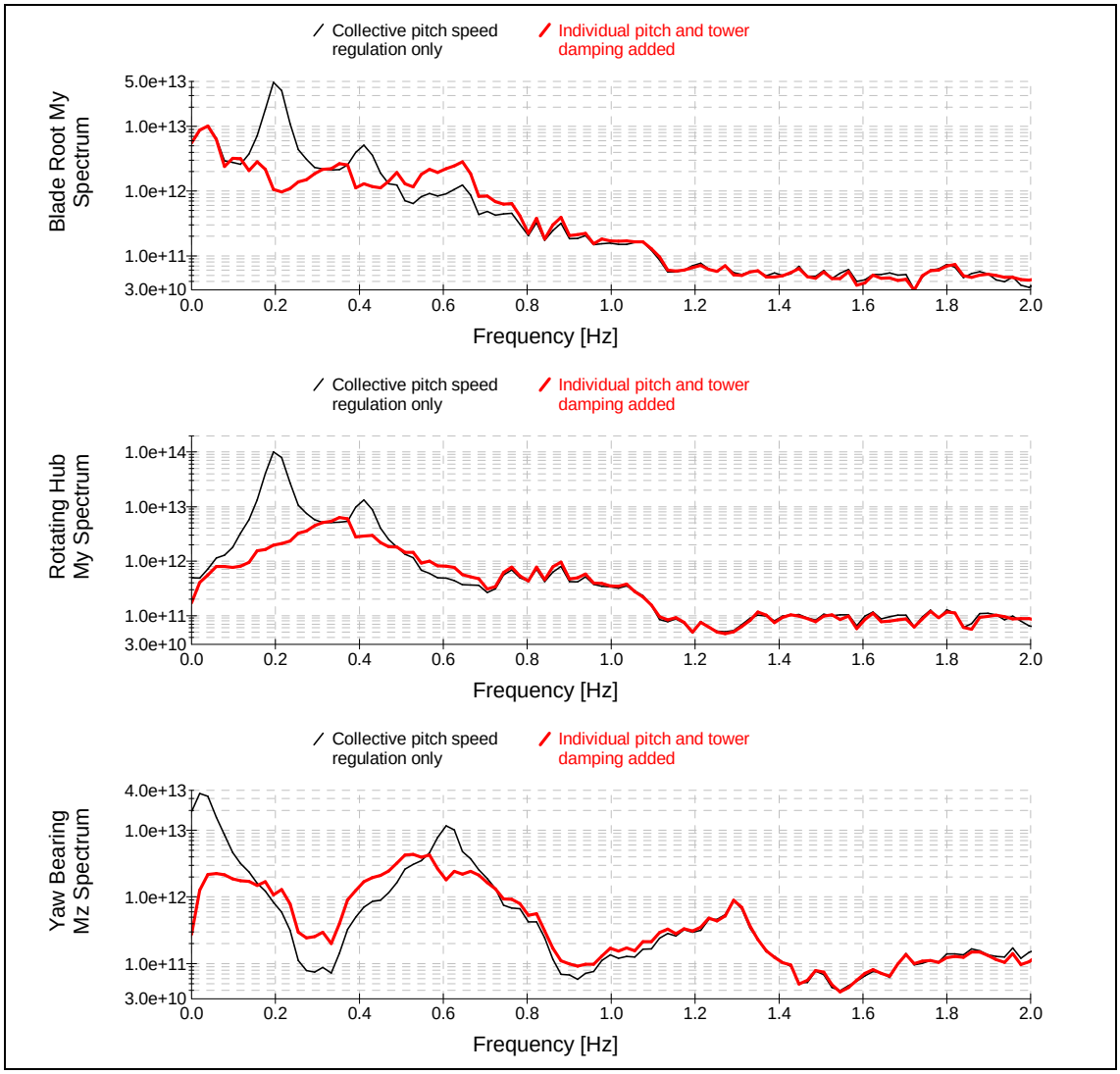

Figure 2.4: Load spectra: effect of individual pitch control

2.2 Supervisory control implications of IPC

A big effort in control design has been made in the last years to reduce wind turbine fatigue loads. Individual pitch control (IPC) is a promising technique [1], [7], [11] and it focuses on reducing fatigue asymmetric loads moving each blade individually accordingly to load measurements as presented earlier on in the paper. Although when compared to a collective pitch controller this strategy is capable of reducing asymmetric fatigue loads, attention must be paid to the corresponding extreme loads as the blades might be pitched at different angles during shutdowns. We investigate here the impact of using this technique on the supervisory logic design in order to limit extreme loads [12].

The supervisory control algorithm includes the procedure for normal turbine start up and shutdown as well as over speed and over power trips and the logic for determining failures of the subsystems such as pitch and yaw. A full set of load calculations according to IEC Edition 3 has been run to compare the effect of collective and individual pitch controller strategies on fatigue and extreme loads on the 5MW reference wind turbine.

2.2.1 Shutdown cases

Shutdown cases are analyzed to compute wind turbine extreme loads. A standard procedure when a shutdown is triggered is to pitch the blades quickly to feather. If an individual pitch controller is employed in a normal operative condition the instantaneous difference between blade pitch angles could be quite large. As a consequence if a shutdown occurs and the whole manoeuvre is carried out with the blades pitched at different angles, asymmetric loads could be higher than in the case of collective pitch control. This is also the case when the safety system is suddenly triggered, for example in an emergency stop. As an example we report here the case of a grid loss shutdown, with the fault occurring 5.25 seconds after the beginning of a gust. As represented in Figure 2.5 the blades are not aligned during the shutdown and in this case the rotating hub My will be 45% higher and the tower base Mz will be 34% higher than the ones obtained with a collective pitch controller.

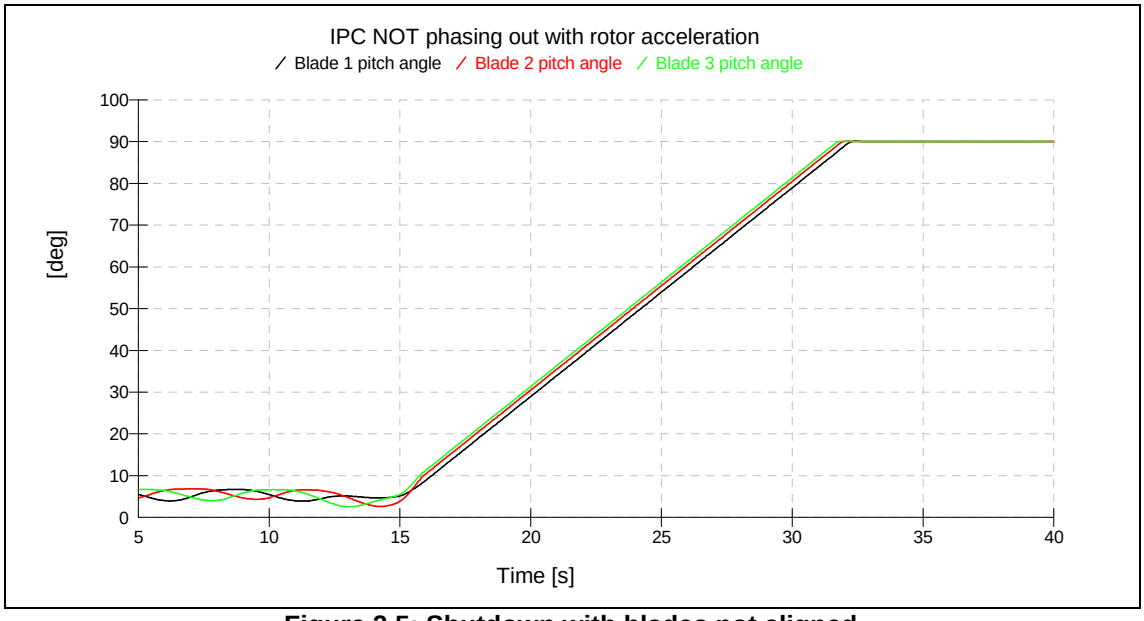

Figure 2.5: Shutdown with blades not aligned

In order to reduce extreme loads the individual pitch contribution is phased out with rotor acceleration, so that when the rotor accelerates for example during a gust and a shutdown is likely to occur the blades will be almost aligned before the shutdown begins, as reported in Figure 2.6 for the same grid loss case presented above. This feature is also beneficial in

reducing overspeed in normal power production when speed regulation and IPC may be 'competing' to use the available pitch rates. The differential pitch contribution can be continuously phased out during the shutdown if necessary.

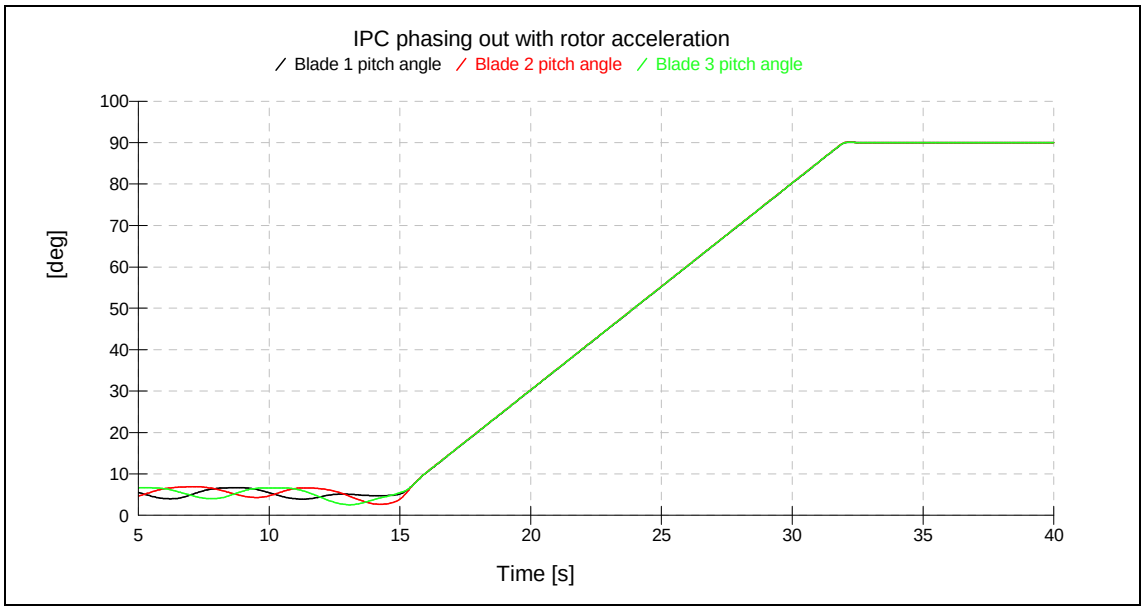

Figure 2.6: Shutdown with blades aligned

The example reported here is the case of a grid loss shutdown, with the fault occurring 5 seconds after the beginning of a gust. Figure 2.7 shows that by phasing out the individual pitch contribution it is possible to limit extreme loads while preserving the benefits of the individual pitch controller in normal conditions. The ultimate loads obtained are comparable to those obtained with the collective pitch controller.

2.2.2 Load sensor failure cases

IPC computes differential pitch actions based on load measurements (blade root or hub loads for example). This requires sensors, and any sensor is capable of failure. The potential impact of these failures on the controller performance and loads also has to be assessed and failure detection strategies should be implemented in the supervisory logic to detect fault events.

Load sensor failures could consist for example of sensor freezing or saturation to full scale or zero. In order to detect these failures the following approaches could be used:

- Check signal consistency over 1 period,
- If blade root loads are used, compare the one-revolution loads mean (Dm) and peak-to-peak (Dr) maximum difference between blades to detect anomalies on one blade.

The quantity Dr is the maximum normalized absolute difference on the three blades of the average load value (where k is the generic controller timestep):

$$Dm_{ij}(k) = (\overline{m}_i(k) - \overline{m}_j(k)) / M(k) \qquad i, j = 1,3$$

$$M(k) = \sum_i \overline{m}_i(k)$$

$$Dm(k) = \max(|Dm_{ij}(k)|)$$

where $\overline{m}_i$ is the flapwise (or edgewise) bending moment of blade i averaged on 1 revolution.

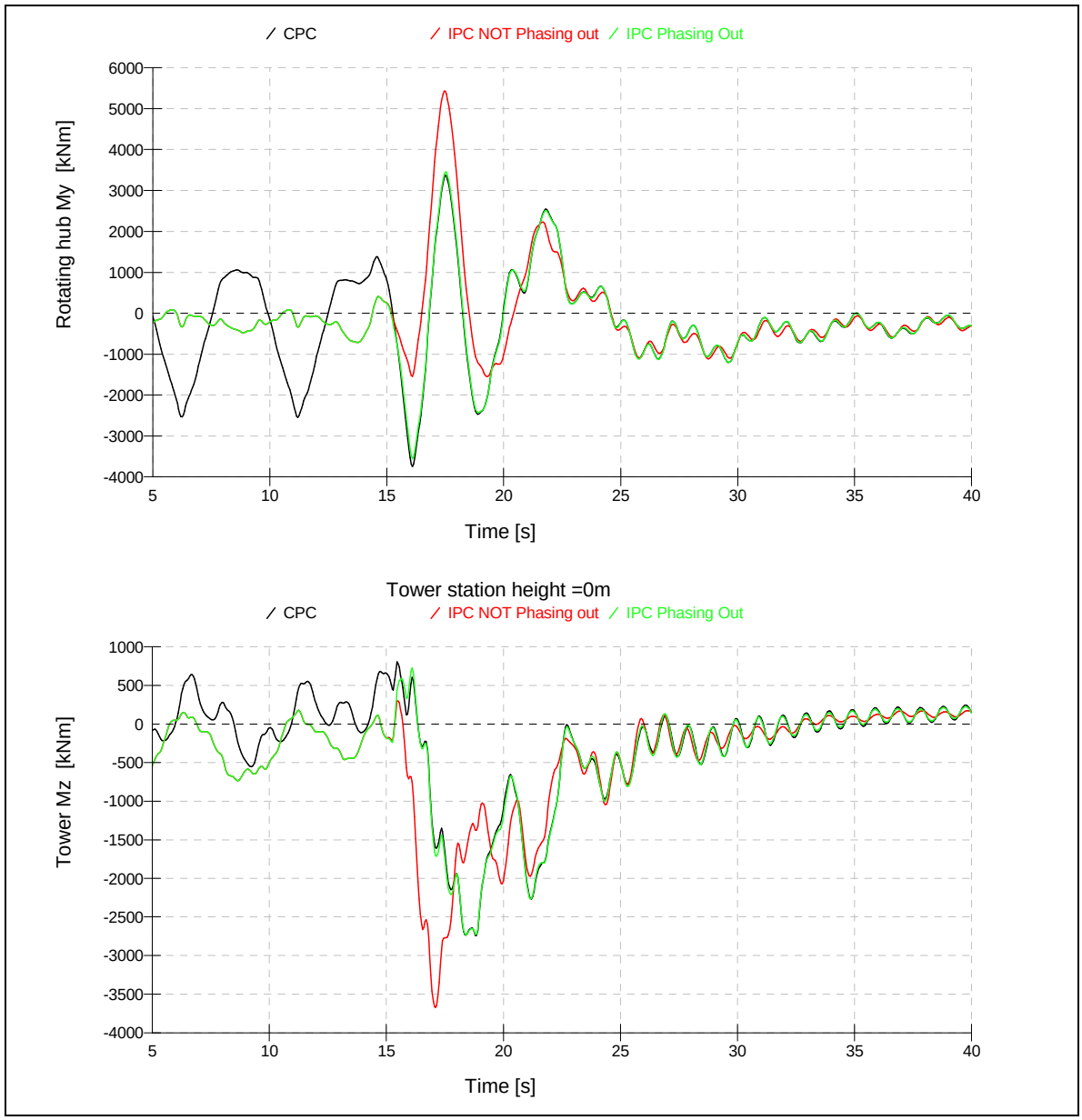

Figure 2.7: Effect of IPC phasing out with rotor acceleration on loads

The quantity Dr is the maximum normalized absolute difference on the three blades of the peak-to-peak load value:

$$Dr_{ij}(k) = (\bar{r}_i(k) - \bar{r}_j(k)) / R(k) \qquad i, j = 1,3$$

$$R(k) = \sum_i \bar{r}_i(k)$$

$$Dr(k) = \max(|Dr_{ij}(k)|)$$

where $\bar{r}_i$ is the peak-to-peak flapwise (or edgewise) bending moment of blade i averaged on 1 revolution.

Figure 2.8 shows the values of indexes Dm and Dr in case of no failure, one blade sensor seizure and one blade sensor saturation to zero. The two quantities described above are capable of detecting these types of failure by changing their value from a no fault condition

reported in black line. However the analysis on fatigue loads shows that the impact of a not-detected load sensor failure has a small impact on IPC performance.

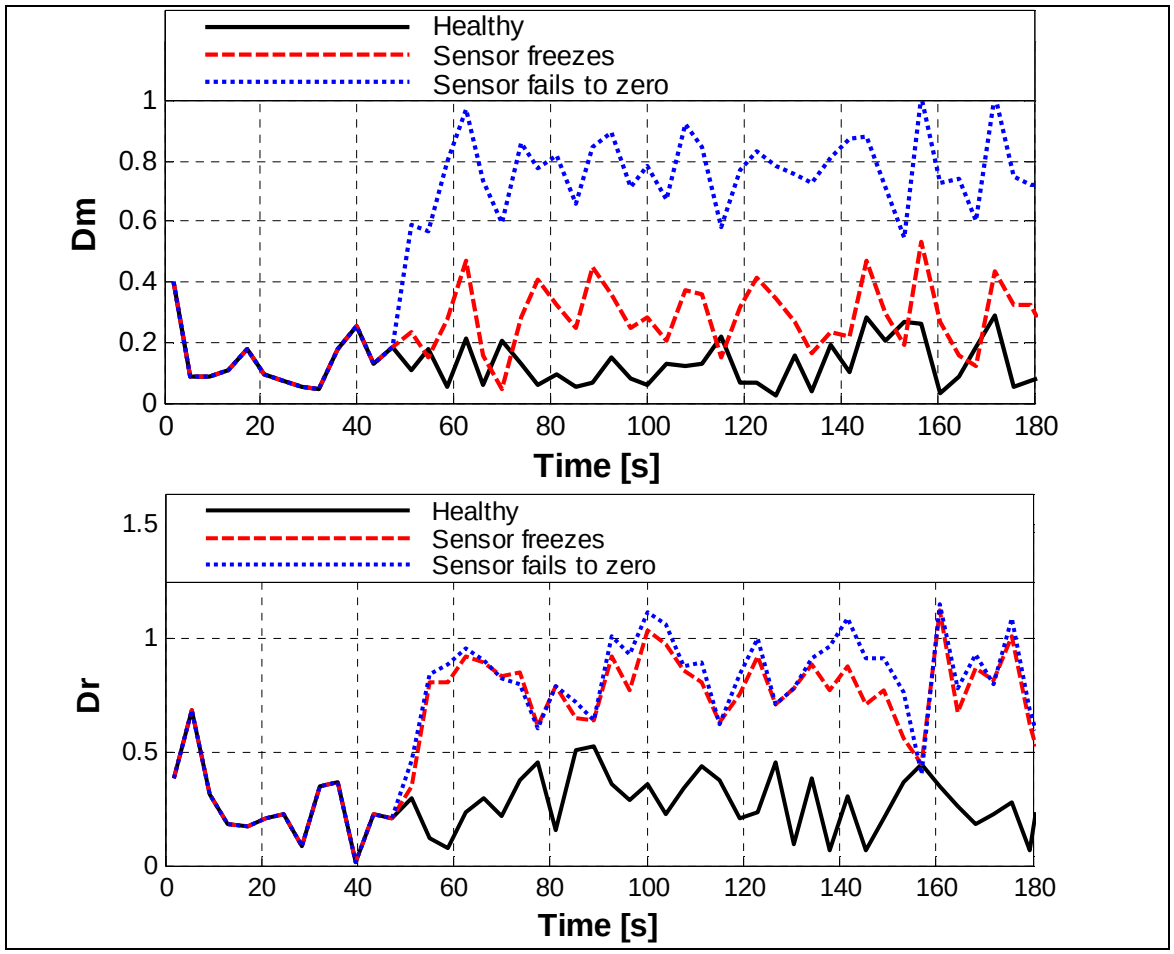

Figure 2.8: Indexes for blade load sensor failure

2.2.3 Load calculation analysis

A load calculations analysis based on IEC 61400-1 edition 3 has been run to compare both fatigue and extreme loads against the ones achieved with a CPC. While the full results are reported in [13] in terms of ultimate loads the conclusion from the load calculations is that the largest difference is a 10% reduction when using IPC, with most components within 2%. Moreover, ultimate loads occur mostly in the same load cases for the two control strategies.
In terms of fatigue load comparison IPC is capable of improving most of load components, especially the asymmetric ones as expected from the control design. In particular blade root My, rotating hub My and Mz are reduced up to 30%. Reduction of 11% is achieved for the stationary hub and tower Mz.

2.2.4 Conclusion

Although IPC is capable of reducing asymmetric loads in normal power production, extreme loads caused by shutdown carried out with blades not aligned can be much higher than if a collective pitch controller is used. For this reason strategies to align the blades before the shutdown occurs should be implemented in the supervisory logic.

Critical conditions can be gust cases or pitch failure cases with the generator speed increasing, but if the differential pitch action is scheduled with the rotor acceleration these extreme asymmetric loads may be no greater than they were without IPC.

The load calculation analysis showed that when this expedient is used and suitable logics especially for pitch failure detection are employed the ultimate loads are comparable with the ones achieved by using a collective pitch controller. It is important to note that while not increasing ultimate loads IPC is then capable of improving fatigue loads. The maximum improvement is a reduction up to 30% on asymmetric loads.

The potential impact of load sensor failures on controller performance and loads has been analyzed and the effect of failure modes modeled up to now is to reduce IPC performance without leading to severe load conditions. However, strategies to detect load sensor failures should be implemented in supervisory logic.

Possible developments of this work can be to investigate other possible methods for a safe blade alignment during shutdowns and a more detailed investigation of possible failure modes and analysis of the implications on loads.

The full results of this work including load calculation results are presented in Deliverable 5.1.2 [13].

2.3 Online estimation of mechanical load for wind turbines

The continuous estimation of mechanical loads occurring during wind turbine operation is useful in many ways. One field of application is condition monitoring of extreme and fatigue loads, in terms of both maintenance and operating control. Although off-line data processing is sufficient for long term influences, the continuous estimation is useful if a rapid influence from the operating control to changing wind conditions is intended.

Another very important field of application is to provide a basis for feedback control measures to reduce mechanical loads [14]. Estimated loads can be used as input signals for load reducing controllers instead of directly measured strain. This is beneficial in two respects. Sensor installation is not only costly due to installation and maintenance, but sensor faults themselves might lead to turbine malfunction – which implies yet another field of application. Hence, our work focuses on load estimators that are based on measurements available on today's large scale wind turbines.

Three different time scales can be established according to the application area:

- A slow time scale referring to the offline calculation of extreme and fatigue loads in terms of maintenance,
- a medium time scale if rapid response of the operating control to changing conditions is intended, and
- a fast time scale for load reducing feedback control measures.

The continuous estimation method based on state space observers investigated in our work is suitable for all three time scales. This section summarises the results obtained at Fraunhofer IWES regarding the choice of a suitable structure for the estimator, its design, and a field test on a commercial 5MW turbine [15], [16].

2.3.1 Overall system

In our work, we focus attention on the estimation of the tower bending moments. An observer is used to estimate the states of a wind turbine model and a wind speed model. To this end, the observer employs the readings of the accelerometers measuring the tower top fore-aft and side-side movement, the pitch angle commanded by the collective pitch controller, and the rotor speed, each of which is an available signal on today's large scale wind turbines. It compares these signals with those of a model running in parallel with the real system. The internal states of the model are continuously corrected according to the deviation between the measured, real signals and the estimated signals of the model.

Estimating wind speed and turbine states by state space observers or Kalman filters has been proposed earlier [14] and is used in several studies, see for example [17],[18],[19], even though many of them use those in the context of state space controllers and do not explicitly account for the estimation performance. There are a lot of publications dealing with simulations of load reducing control systems. A few concern field tests with wind turbines in the class below 1MW, see for example [10],[20],[21]. But, to the authors' knowledge, no field tests have been reported so far on large-scale systems.

2.3.2 Linear time-invariant model and state-space observer

A simple linear time-invariant model for steady-state operation of the controlled wind turbine is used; see [16] for further details. Keeping the model simple, that is linear and of low order, is advantageous for both online-implementation and application in model-based control.

The mechanical part is a linearised multibody system consisting of rigid beams, where the tower is modelled by two beam elements and the rotor blades are modelled by a single beam element each. Another single beam element is used for the drive train, which is connected to the rotor

blades and an inertia element modelling the generator. The joints connecting the elements are springs and dampers, whose parameters are determined by modal analysis. To eliminate the periodicity of the rotor related quantities, a coordinate transformation, sometimes called the Coleman or multiblade transformation, is used [22]. Different degrees of freedom are locked so the resulting system includes the following modes: first and second tower fore-aft and side-side modes, first tower torsional mode, first drive train mode, first rotor blade flapwise and edgewise modes.

The aero-dynamic forces are assumed to attack at a single point on each rotor blade. They are calculated using a steady-state approximation neglecting dynamic effects such as dynamic inflow and dynamic stall. The linearised aerodynamic coefficients are derived from the power and thrust coefficient data.

Putting together the mechanical and the aero-dynamical model yields a linear time-invariant state-space system with about 25 states whose inputs are the three wind speed components in multiblade coordinates. This model is valid in the neighbourhood of a decent operating point characterised by mean wind speed.

Again, for the wind speed model, we employ a very simple approximation: a constant deviation from the steady-state mean wind speed uniformly distributed over the rotor area. In terms of linear systems theory, this is a single integrator. Different, more complex models have been suggested in literature; see for example [18],[19] and the references therein. But, firstly, the wind power is concentrated at low frequencies and an integrator is sufficient to capture the slowly varying mean wind speed. And secondly, since we restrict ourselves to collective signals, it is unlikely that spatially distributed effects are reproduced correctly on basis of the measurement signals.[1]

A state space observer is used to estimate wind speed and turbine states. The latter include deflections of the tower, which determine the tower bending moments. To correct the model's internal states the deviation between the real and the estimated measurement signals is fed back. Because four signals are measured, the observer feedback design is a multivariable control problem. This problem is solved using linear quadratic theory [23]. For the online-implementation of the observer it is beneficial to reduce the model order and remove less relevant modes. This is done by a model reduction method, called residualisation, that preserves the steady state gain of the system and is therefore suitable if the low-frequency behaviour of the model has to be retained [24].

2.3.3 Field test

The field test has been carried out on a Multibrid M5000, a commercially available 5MW wind turbine designed for large offshore wind farms [25]. From the operating control system we get measurements of the tower top accelerations and the collective pitch angle. For the field test, strain gauges mounted on the tower centre at 60 m height with adhesive measure the tower bending moments. The measurement sequences are time series of 10 minutes length.

In Figure 2.9 the estimated and the measured tower bending moments are compared in an example for a measurement sequence with mean wind speed 18 m/s and turbulence intensity 10%. The upper plots show a section of the sequence and the lower plots show the power spectral densities of the sequence. On the left hand side the fore-aft bending moment is shown and on the right hand side the side-side bending moment.

The spectral density of the fore-aft bending moment is estimated very well with deviations at 5P to 7.5P. Measured and estimated moments match exactly at the first tower eigenfrequency

[1] For instance, the static part of the cyclic wind speed components due to wind shear is unobservable without measuring individual blade related values [16].

around 1.5P. The first side-side tower eigenfrequency is located around 1.5P, too, and here the estimation of the side-side tower bending moment works as well as the fore-aft estimation. At frequencies higher than the first eigenfrequency the estimated signal is noisy. However, the level of noise is admissible, as can be seen in the time domain plot. So we conclude that a sound foundation for the application of model-based control for tower load reduction is readily available – without assembly of additional sensors.

Furthermore, preliminary results indicate that the same sensor configuration allows for the estimation of the collective blade loads. This can be seen from Figure 10, where the estimation results of the flapwise and edgewise collective blade bending moments[2] are shown using the same observer and the same data sequence as for the results in Figure 9. Again, the upper plots show a section of the sequence and the lower plots show the power spectral densities of the sequence.

There is fair correlation in the time domain and a good correlation in the frequency domain – except for a dominant frequency peak at 1p in the spectral density of the edgewise bending moments. This peak is due to rotor asymmetries, which are not included in the model.

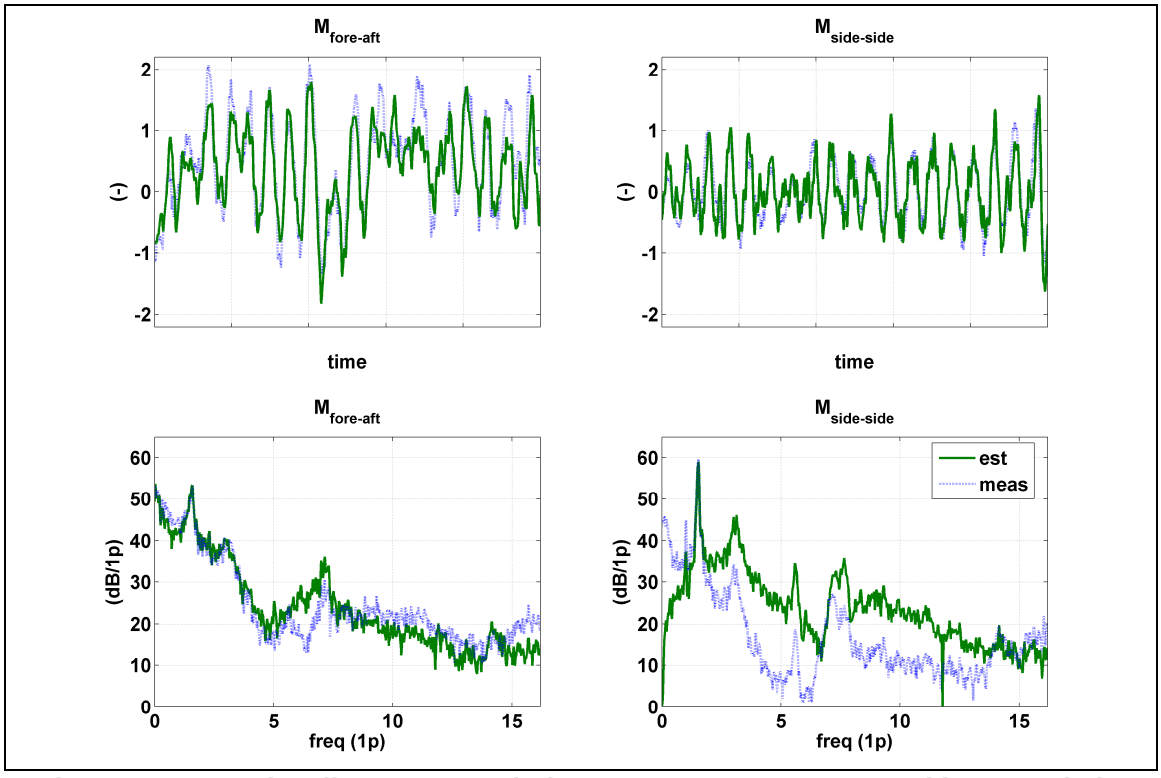

Figure 2.9: Tower bending moments during measurement sequence with mean wind speed 18 m/s and turbulence intensity 10%: time and frequency domain. Left: fore-aft. Right: side-side

[2] The collective blade bending moments are defined by the mean value of the three individual blade bending moments, e. g. $M_{flap,0} = (M_{flap,1}+M_{flap,2}+M_{flap,3})/3$.

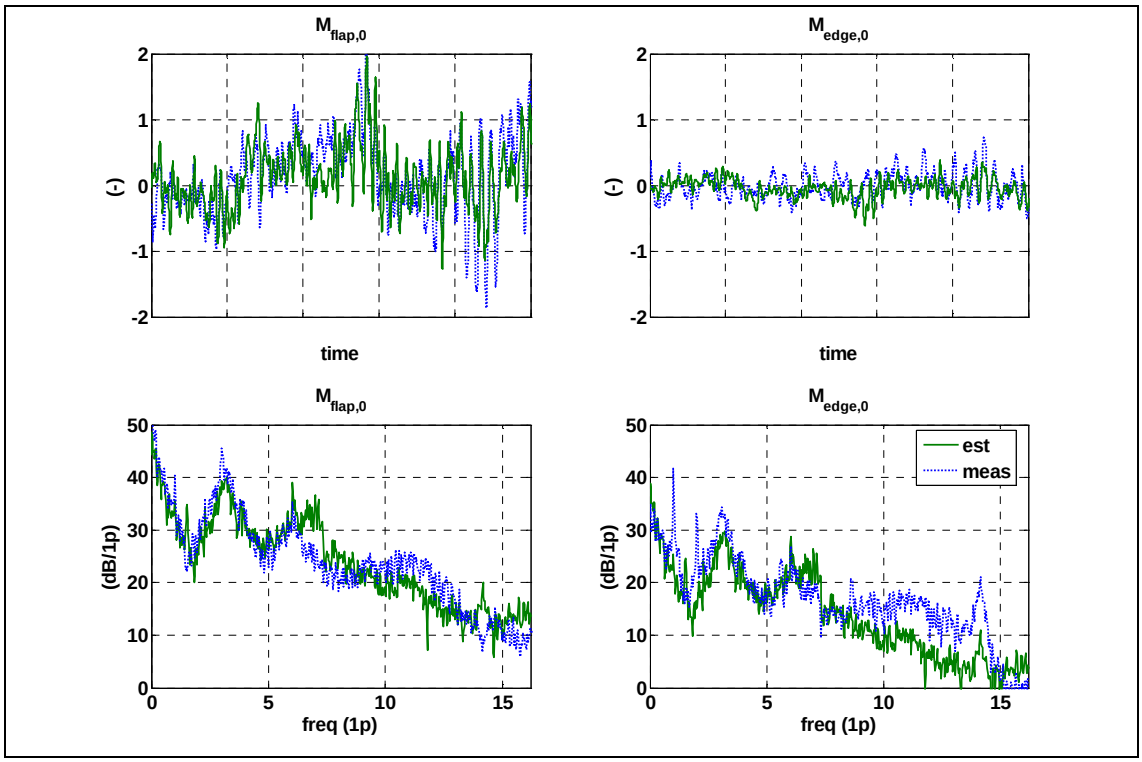

Figure 2.10: Collective blade bending moments during measurement sequence with mean wind speed 18 m/s and turbulence intensity 10%: time and frequency domain. Left: flapwise. Right: edgewise

2.3.4 Conclusion

The experiments using field test data show that tower load estimation is possible on the basis of readily available sensor signals. With the observer-based estimation approach it suffices to use measurements of the tower top acceleration, the collective pitch angle, and the rotor speed. That is, no additional strain sensors are necessary.

In addition, preliminary results suggest that the estimation of blade related loads might also be possible. To this end, the effects originating from rotor asymmetries and their integration into the model should be investigated.

This work is reported in detail in Deliverables 5.2 [15] and 5.3 [16].

2.4 LIDAR assisted collective pitch control

LIDAR (Light detection and ranging) systems are able to provide preview information of wind disturbances at various distances in front of wind turbines. This information can be used to improve control of wind turbines trough a predictive feedforward control structure. To estimate the load reduction of extreme and fatigue loads by LIDAR assisted pitch control, LIDAR measurements were simulated with GH Bladed and the UpWind controller [9] was extended by a update to the pitch rate increment from the processed simulated measurements, as shown in Figure 2.11.

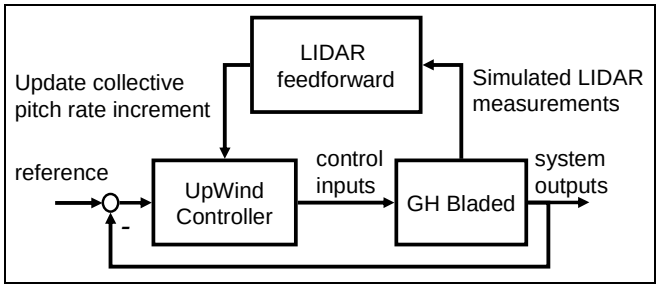

Figure 2.11: Extended control loop

2.4.1 Update collective pitch increment

According to [26], the feedforward law was designed to compensate the effects of the effective wind speed $\dot{v}_{eff}$ to the rotor speed Ω. The update to the collective pitch increment $\dot{\beta}_{FF}$ was obtained with $\dot{\beta}_{FF} = \frac{\delta\beta}{\delta v}\dot{v}_{eff}$, where $\frac{\delta\beta}{\delta v}$ is the derivative from the static pitch over static wind speed (see Figure 2.12).

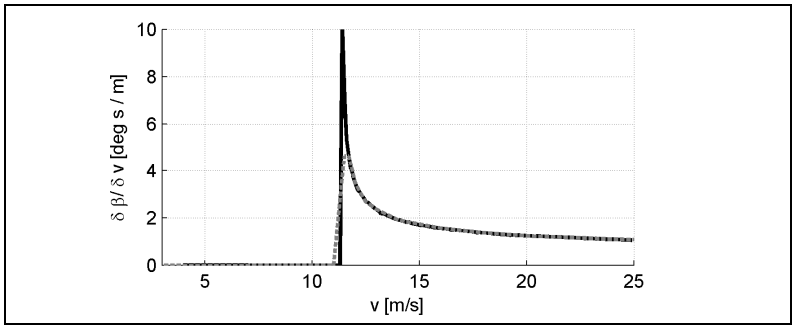

Figure 2.12: Theoretical (black) and used (grey) feedforward law

The prediction time was chosen to τ =0.5s to overcome the pitch actuators. The parameter of the feedback controller were reduced in a first try to have in turbulent wind field simulations approximately the same standard deviation of the rotor speed as the original UpWind controller, but reduced loads. But more sophisticated tuning of all feedback loops should be done in future work.

2.4.2 Simulated LIDAR measurements

Within GH Bladed different LIDAR systems can be simulated, but for first evaluation a pulsed LIDAR system was chosen and a circle is swept in 2.4s with 12 points in each of five different distances, which could be carried out with a real system [27], see Figure 2.13.

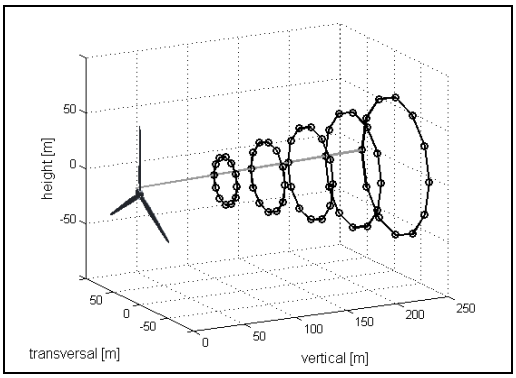

Figure 2.13: Sketch of scanning LIDAR system

The probe volume of 30m [28] was considered in the calculation of the line-of-sight wind speed. The effective wind speed was obtained by assuming perfect alignment with the turbine and a moving average over the last full circles, considering the time shift between the different distances. To account for uncertainties of Taylor's Frozen Turbulence Theorem [29], the signal was filtered with a low pass filter with mean wind speed dependent cut-off frequency.

2.4.3 Results for extreme loads

Error! Reference source not found. compares the pitch angle, rotor speed, and tower base bending moment for an "Extreme operating gust" for the UpWind controller and the LIDAR assisted controller. Additional the detection of the gust by the LIDAR system is plotted, showing the effect of spatial and temporal filtering.

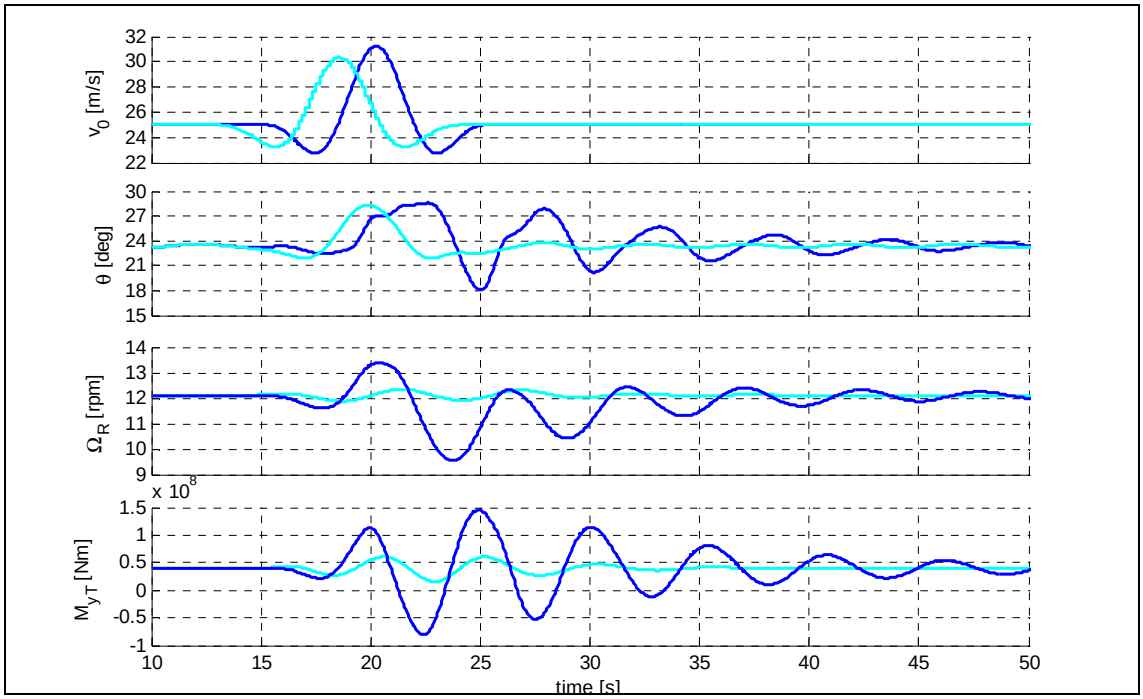

Figure 2.14: top: Wind gust (dark) and LIDAR measurement (light); rest: collective pitch angle, rotor speed and tower base fore-aft bending moment for UpWind controller only (dark) and with feedforward (light)

2.4.4 Results for fatigue loads

To estimate the load reduction potential of the proposed controller, various simulations were analysed. The controller with the feedforward can significantly reduce the influence of the wind disturbance to rotor speed and to the tower base fore-aft bending moment below the 1P-frequency (see Figure 2.15).

The standard deviation of rotor speed and pitch angle and the damage equivalent loads (DEL) over the different wind speeds can be seen in Figure 2.16.

Using a Weibull distribution with average 8.5 m/s and shape factor 2, the lifetime DEL for the tower base fore-aft moment can be reduced by 11.1% compared to the UpWind controller.

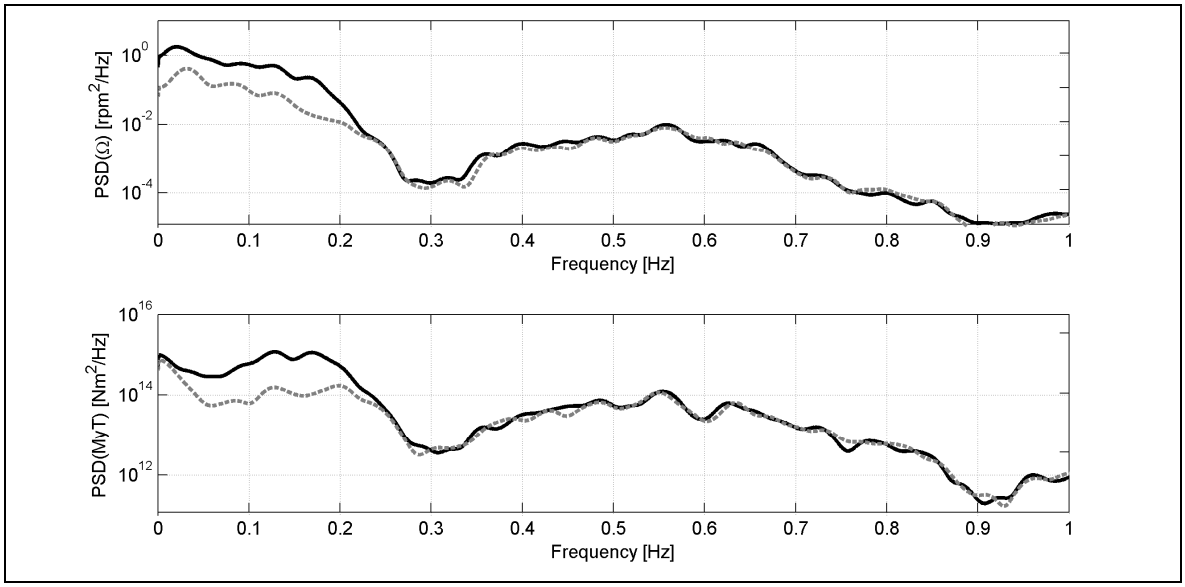

Figure 2.15: Power spectral density of rotor speed and tower base fore-aft bending moment for the simulation with 21 m/s, UpWind controller only (black) and with feedforward (grey)

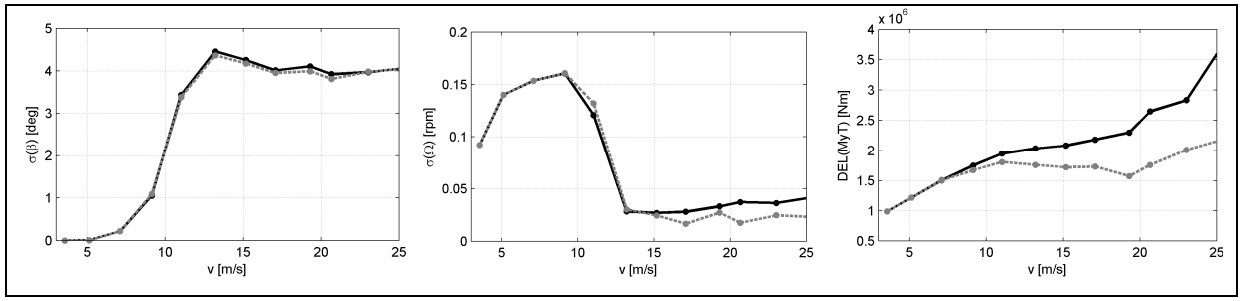

Figure 2.16: Standard deviation of rotor speed and pitch angle and DEL of tower base fore-aft moment (20 yrs lifetime N=2E06, m=4), UpWind controller only (black) and with feedforward (grey)

2.5 Dual pitch control for out of plane blade load reduction

A rotor blade layout with two pitch actuators, for example one at the blade root and another at about 2/3 radius, allows the aerodynamic efficiency to be reduced above rated wind speed in different ways (dual pitch control). In full load conditions relatively more energy can be extracted from the inner part of the rotor than from the outer part. This approach appears to allow for reducing the slowly varying level of the out-of-plane blade root moments by around 15%. This is explained through basic expressions of the radial dependence of aerodynamic loading and demonstrated through time domain simulations.

2.5.1 Radial dependence of aerodynamic loading

Assume equal aerodynamic efficiency in each circle of the rotor plane. The power of the inflowing wind per unit radius (pu) is proportional to the radius r of the circle. So, this must also hold for the extracted pu power p, which depends on the pu tangential aerodynamic force ftg_b(r) as follows:

$$p = \sum_{1}^{B} ftg\_b(r).r.\Omega$$

where B = no. of blades and Ω = rotational speed.

Equal efficiency is obtained if ftg_b takes the same value at each radius r. Since the leadwise relative wind speed r.Ω far exceeds the flapwise wind speed (~(1-a)*U_a) over most of the rotor plane, and drag is of negligible importance in attached flow conditions, the tangential pu force ftg_b(r) can be approximated by

$$ftg\_b(r) \cong 0.5\rho.Cl(r).c(r)..r.\Omega.(1-a).U_a$$

which does not vary over r if the product Cl(r)*c(r) is inversely proportional to r. Then, equal aerodynamic efficiency is achieved over the rotor. Approximate Cl*c by K/r (K constant). Under the assumptions made, the pu axial aerodynamic force fax_b(r) obeys

$$fax\_b(r) \cong 0.5\rho.K..r.\Omega^2$$

The pu aerodynamic torque mdr_b(r) and out-of-plane moment mfl_b(r) in the blade root relate to the pu tangential and axial force in a straightforward way:

$$mdr\_b(r) = ftg\_b(r).r \cong 0.5\rho.K.r.\Omega.(1-a).U_a$$
$$mfl\_b(r) = fax\_b(r).r \cong 0.5\rho.K.r^2.\Omega^2$$

It is clear that the pu driving torque mdr_b(r) and pu axial force fax_b(r) increase in proportion to radius r whereas the pu root flap moment mfl_b(r) increases in proportion to r^2. Therefore lower blade flap moments should be achievable if the extraction of wind energy is moved towards the inner part of the rotor plane in high wind speeds.

2.5.2 Blade load response to pitch changes in inner and outer part of rotor

For the 5MW UPWIND reference wind turbine we derived a linear servo-aeroelastic model with the computer program TURBU Offshore [30] in a wind speed of 15m/s. The average operating conditions comprise a pitch angle of 12.4 degrees, rotor speed of 12.1 rpm and electric power of 5MW. The model includes blades with 14 elements of which the twist angles can be varied independently. The twist variations of elements 1 up to 9 (r=41.7m) and of elements 10 up to 14 (r=63.0m) were clustered. Thus, one collective pitch control signal was retained for the inner 66% of the rotor and another for the outer 34%. Figure 2.17 shows the response of aerodynamic loads to changes in both pitch angles. Pitch adjustment in the outer part appears twice as

effective for the aerodynamic driving torque and the axial force. For the blade root flap moment this is even three times. This quantifies the analytic finding that the blade flap moment is more sensitive to spanwise distributed pitching than the driving moment.

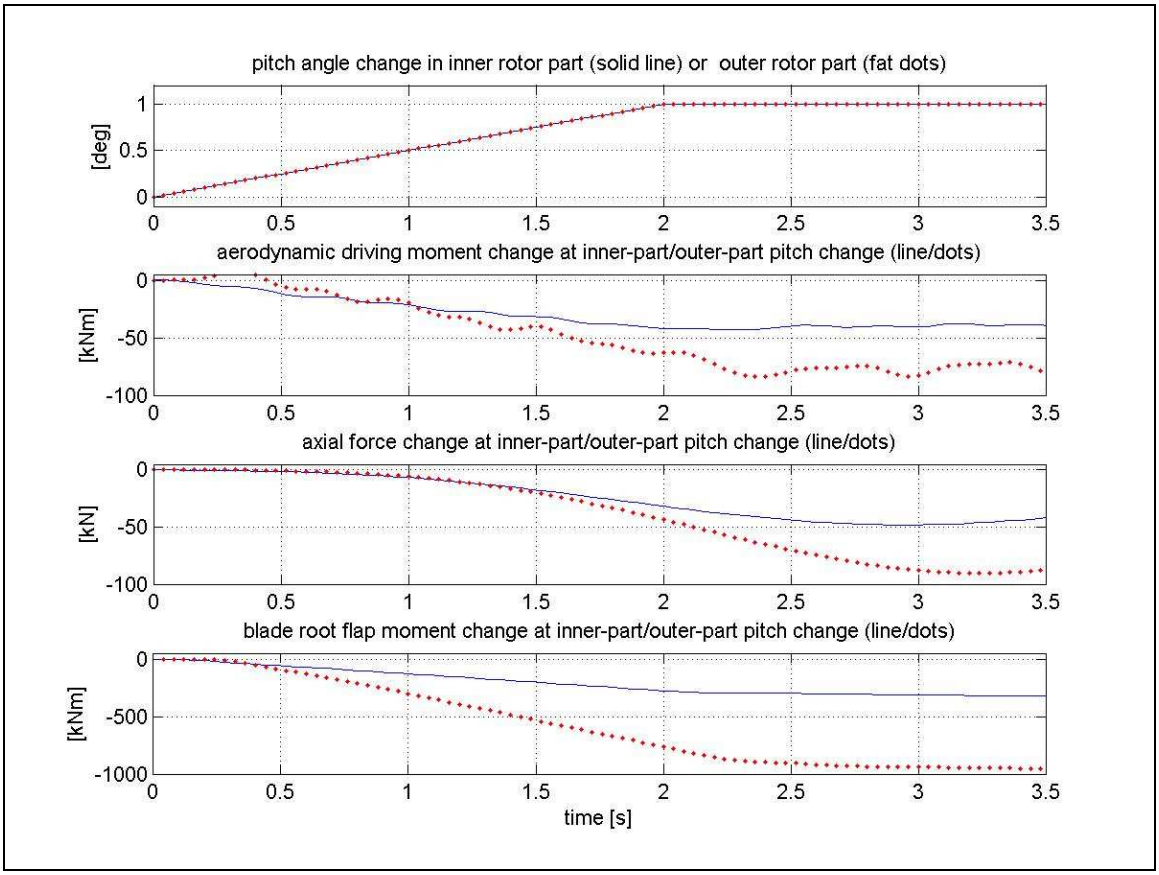

Figure 2.17: Aerodynamic load response to pitch changes

2.5.3 Basic control design and parallel time-domain simulation in turbulent wind

A basic `single pitch' controller has been designed for PD-feedback of the generator speed to equal pitch speed setpoints for the inner and outer blade parts. Filters are used against tower and blade vibration and rotational sampling. The PD-gains are scaled with a schedule factor that decreases from 5 to 1 at increasing pitch angle. A smooth torque/speed-curve applies with rated power delivery in above-rated wind speeds. The dual pitch controller is similar; now different PD-gains apply for the inner and outer pitch angles, respectively 50% and 125% of the single pitch gains. The overall control strength would remain unchanged because of the aforementioned two times stronger response of the driving moment to outer pitch changes. The schedule factor now depends on weighted outer and inner pitch angles.

Both controllers have been implemented in a Simulink scheme together with two instances of the servo-aeroelastic model of the wind turbine. Pitch servo actuation was simulated through an integrator and a low pass filter (0.1s). The wind field was provided as three helix-like realisations for axial wind speed variations which include tower shadow, wind shear and rotationally sampled turbulence [31],[32]. This set-up is easily configurable and allows for fast, parallel simulation (1 minute or less for 10 minutes 'real-time').

Figure 2.18 shows in the upper two boxes the wind speed as the instantaneous average over the rotor blades (box 1), the rotor speed (box 1), and the pitch angles (box 2) during a simulation in 15 m/s average wind speed with 16% turbulence. The rotor speed and power behaviour is equal for single and dual pitch control; this also holds for generator power (not shown). The inner pitch

adjustments are 2.5 times smaller than the outer ones (fat lines in lowest plot box) because of the different PD-gains.

The lower boxes show the blade root flap moment with dual pitch control and the absolute difference compared to single pitch control (box 3), and the percentage reduction in the flap moment relative to the 600s-mean value obtained using single pitch control (box 4). Rotational sampling effects are filtered from the shown signals. An appreciable 15% reduction is achieved in the flap moment level that varies with the rotor uniform wind speed variations. The thrust force and driving torque are equal for single and dual pitch control (not shown).

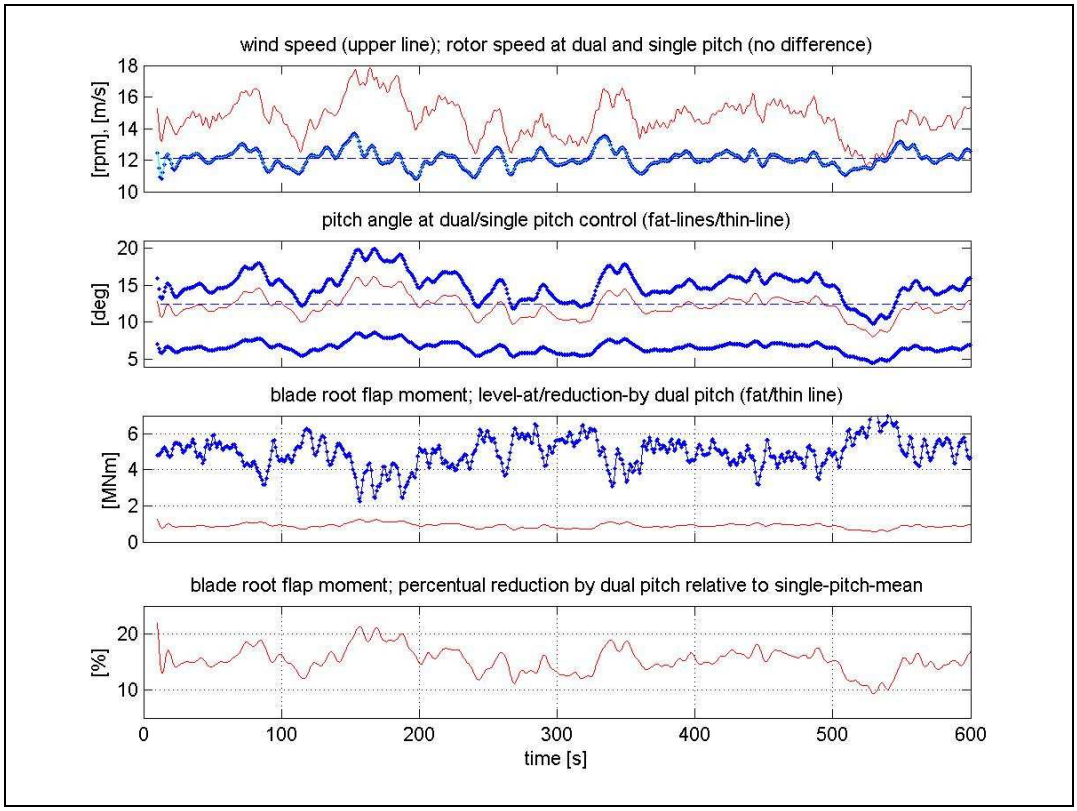

Figure 2.18: Simulation with single and dual pitch control

Figure 2.19 shows the lift and drag polars for two inner elements (5, 9) and two outer elements (10, 14). The asterisks mark the angle of attack (AOA) and lift coefficient (Cl) regions during single pitch control. The O-marks represent the AOA- and Cl-regions for dual pitch control. The higher average AOA in the O-marked regions for the inner elements agrees with a lower average inner pitch angle; the decreased AOA-width of these regions agrees with weaker dynamic pitch adjustment. For the outer elements the opposite holds: lower average AOA and increased AOA-width in the O-marked regions by stronger pitching. The `working-regions' show that linear parts of the lift polars apply on all four elements for both single and dual pitch control. Therefore the linearised aerodynamic behaviour assumed in the simulation model is valid for these conditions.

2.5.4 Conclusion

Low-frequency out-of-plane blade root bending moments in above-rated wind speeds can be reduced by typically 15% when the outer third of the rotor blades is pitched around 2.5 times more towards feather than the inner 2/3 part. Of course the potential saving in structural cost must be weighed against the additional cost and maintenance requirements of the dual pitch mechanism.

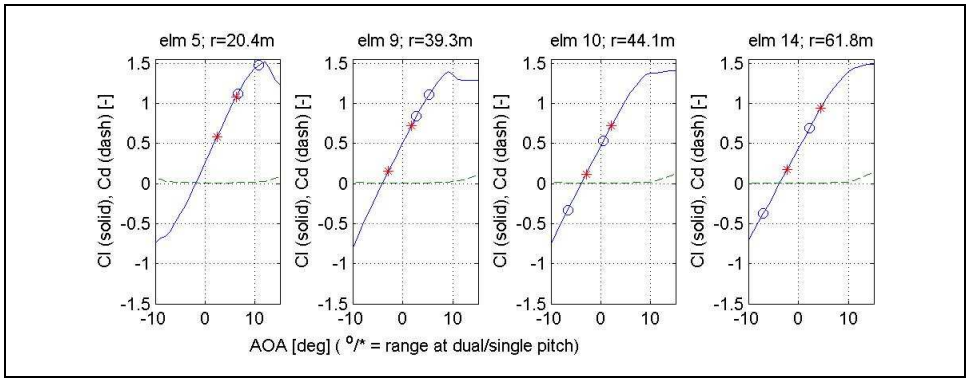

Figure 2.19: Angle of Attack and Lift Coefficient range

2.6 Gradual cut-out strategies for high winds

Most wind turbines are designed to cut out at a specific wind speed, usually 25 m/s. There is some variation in how the high wind cut-out is implemented: it is likely to be based on some combination of instantaneous trip conditions and conditions averaged over a longer period. For example, the cut-out could be triggered if any one of several conditions is detected, such as

- 10-minute average nacelle anemometer wind speed reaches 25 m/s,
- 5-second gust on nacelle anemometer reaches 35 m/s,
- 60-second average pitch demand exceeds a certain value,
- etc.

It may be advantageous to design the high wind cut-out strategy to be based entirely on pitch angle so that the nacelle anemometer signal is not required at all.

Once the cut-out is initiated, it is usual for the turbine to follow some relatively benign normal shutdown procedure, which will involve ramping the pitch up and the speed and power down until the turbine reaches an idling state. It will usually remain in this state until the measured wind speed averaged over a suitable period falls below a pre-set value, when a start-up will be initiated.

The actual cut-out wind speed is chosen to trade off the energy lost by not operating in higher winds against the additional loading which would be incurred by continuing operation in higher winds. This should include consideration of the additional loading cycles caused by each cut-out: the higher the cut-out wind speed, the smaller the number of cut-out events per year. Of course it should also include consideration of the loading cycles incurred when the turbine is idling in high winds. For each individual turbine, typical cut-out strategies of this sort are perfectly good.

At large penetrations of wind power however, the cut-out strategy may have a very significant effect for the wind farm and for the electricity network. During a storm, when the wind speed over a wide area may be rising to 25 m/s and higher, there may come a point when large numbers of turbines start to cut out within a short space of time. Other generation will have to be available and ready to pick up the load, to avoid severe system problems. It becomes extremely important to be able to predict this sudden shortfall as accurately as possible so that other generating plant and/or load management measures can be ready in time.

One way to alleviate problems is to implement a more gradual shut-down, so that as the wind speed increases above 25 m/s the output is gradually reduced, but only reaches zero at some much higher average wind speed, for example 35 m/s or even higher. By reducing the power, the additional loading incurred is much less than if full power were maintained over the whole range, which makes this approach feasible. This approach greatly reduces the probability of sudden large shortfalls in generation during a storm, and it also means that the wind power which will be available from a region can be predicted much more accurately. With a sharp cut-out, a small wind speed prediction error either side of 25 m/s could mean a difference of 100% in the wind power output, but with a smooth cut-out the same wind speed prediction error will result in a much smaller error in the predicted power. This approach was proposed many years ago in [33], but is now becoming of real interest in areas of high wind power penetration.

One task in this work package aimed to investigate the feasibility of this approach in more detail, by calculating the change in loading which would be incurred with such a strategy. The increase in loading during operation in the ramp region above 25 m/s was calculated, compared to the loading which would have been incurred with the turbine idling. However the ramping strategy also generates some additional energy from those high winds, so the possibility of starting the ramp at a lower wind speed was also investigated. This means that the total fatigue loading

might be no higher with the ramping strategy, and the energy output might still be the same as before. This would mean that the benefit of improved wind power predictability and reduced variability in high winds could be achieved with existing designs, without any change to the fatigue load envelope and without any loss of annual energy output.

An earlier investigation [34] for a 2MW turbine indicated that a ramping strategy between 25 and 50 m/s resulted in only a modest increase in fatigue loading, as long as suitable strategies were implemented for active damping of both fore-aft and side-side tower vibrations.

However as well as fatigue loads it is also important to investigate whether this strategy might imply any change to the extreme loads which might be experienced during operation above 25 m/s, compared to what would be experienced if the turbine were idling in these conditions.

This study investigates the design of suitable power ramping strategies for the UPWIND 5MW reference turbine by thorough consideration of the trade-offs between energy output, fatigue loads and extreme loads. Two parallel investigations were performed:

1. Starting from the full state-of-the-art controller designed during this project (section 2.1), a power ramp was designed which caused the power to ramp down to approximately zero at 35 m/s. Some modifications to the power production controller were introduced in order to achieve better control of loading in the high wind region. The ramp and controller parameters were adjusted crudely to achieve suitable balance of fatigue loading and power production, and the resulting system was used for a full set of load calculations in order to asses the extreme load implications.

2. Starting from the original controller for this turbine, a more gradual ramp was designed to bring the power down by 50% at 50 m/s, following previous work as reported in [34]. The more gradual ramp is clearly preferable from the point if view of the electrical system, but is likely to result in higher loading. However the number of hours spent at the highest wind speeds is so small that the increase in fatigue loading was expected to be small.

The study assumed a Class 1 wind regime described by a Rayleigh distribution with a mean wind speed of 10 m/s. For this wind regime, the hourly mean wind speed would be expected to exceed 25 m/s for about 64.7 hours per year, and to exceed 35 m/s for about 0.6 hours per year.

2.6.1 Ramp 1: zero power above 35 m/s

Ramp 1 was designed to start somewhere in the region of the normal 25 m/s cut-out wind speed, and aimed to reduce the power approximately linearly with wind speed until zero power is reached at around 35 m/s mean wind speed. Higher mean wind speeds than this would be very rare, and this ramp might be expected to significantly decrease the power variability and increase its predictability during storms. Clearly if the mean wind speed increased very rapidly from below 25 to above 35 m/s over a whole large area there could still be a significant problem, but the probability of this happening is very small.

The power ramp can be achieved by reducing either the rotational speed, the torque, or both. This ramp was initially designed to reduce the speed from the nominal 12.1 rpm at 25 m/s to 60% of this (7.26 rpm) at 28 m/s. The first tower mode is at 0.29 Hz and so would be excited by the blade passing frequency when the speed is 5.74 rpm or 47% of nominal. To avoid this, the speed remains at 60% as far as 32 m/s, with the torque being reduced instead. Above 32 m/s, the speed is reduced rapidly to 40% of nominal, with the torque rising to compensate, and thereafter the speed and torque are both reduced together to reach 10% at 35m/s, resulting in an air-gap power of 1% of nominal (the zero-load losses have not been defined for this turbine, but this is probably low enough to get zero output power). Subsequently it was found that the starting wind speed for the ramp could be reduced to 23 m/s, because the loss of energy output

between 23 and 25 m/s was more than compensated by the gain between 25 and 35 m/s, and of course the fatigue loads were lower. This power ramp is plotted in Figure 2.20.

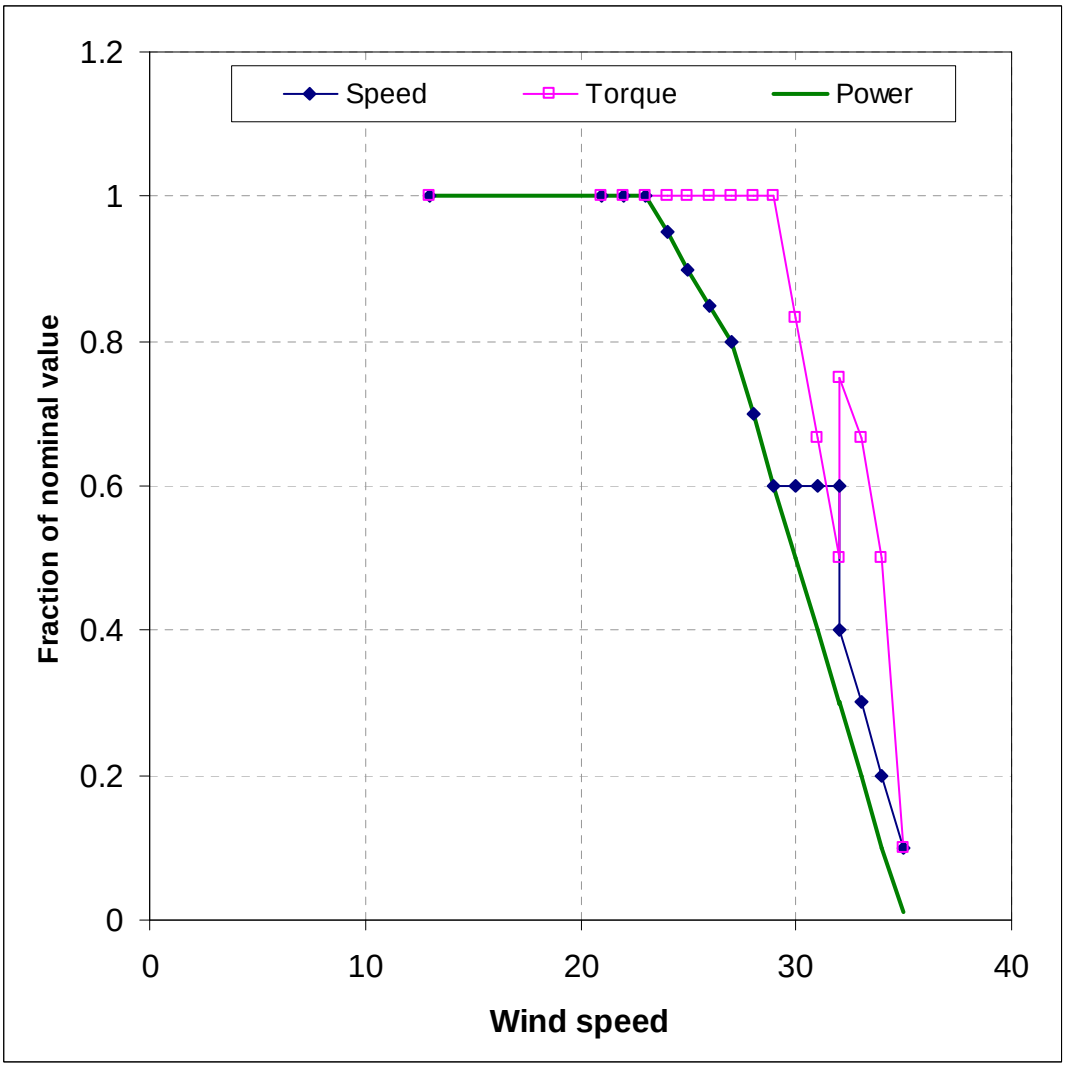

Figure 2.20: Ramp 1 as a function of wind speed

In order not to require a measurement of wind speed, the steady-state pitch angle corresponding to each point in the ramp was determined by running a short simulation with the appropriate steady wind speed and the desired generator speed and torque set-points, and allowing the pitch angle to settle to an equilibrium value (using the normal pitch controller dynamics).

The ramp can now be defined as a function of steady-state pitch angle, as shown in Figure 2.21. To use this, the controller uses a low-pass filtered version of the collective pitch angle (the mean of the three blade pitch angles, which are different because of individual pitch control), to determine the speed and torque set-points. A 10-second first-order lag was found to work well for the low-pass filter.

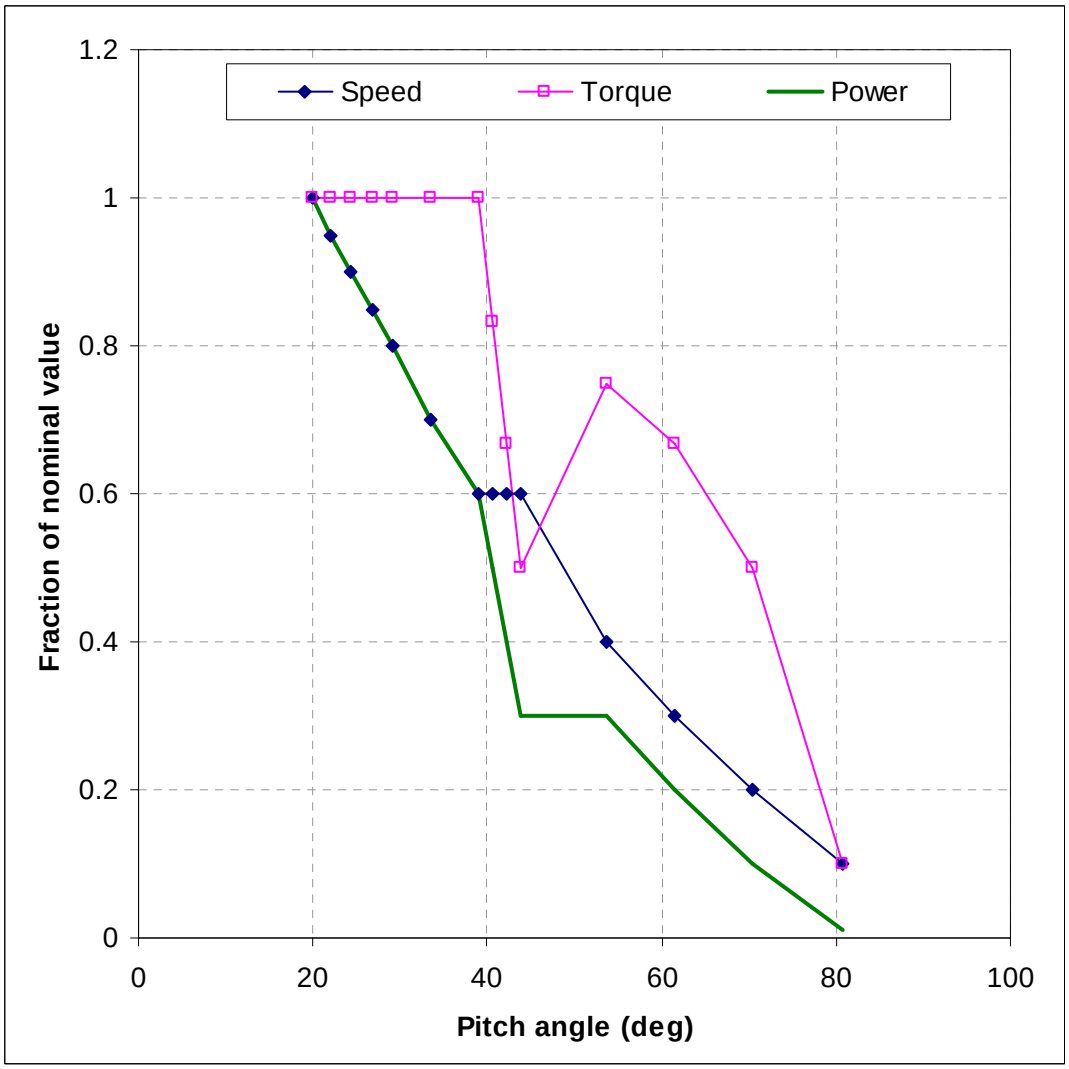

Figure 2.21: Ramp 1 as a function of pitch angle

Some initial turbulent wind simulations were carried out at wind speeds up to 35 m/s to assess the fatigue loading, and compare it against the case of a sharp cut-out at 25 m/s followed by idling up to 35 m/s. The results motivated two further modifications to the control algorithm:

- In the standard algorithm, when operating above rated the torque demand is varied in inverse proportion to the speed error, to keep the power output (excluding the drive train damping contribution) constant as the speed varies around the set-point. This 'constant power' strategy no longer makes sense once the torque and speed are very small, so the controller was made to revert to 'constant torque' operation at high pitch angles. This was done by calculating the torque demand as a weighted average of the 'constant power' torque demand and the 'constant torque' torque demand, the weighting changing linearly with pitch angle from fully 'constant power' below 28.65º to fully 'constant torque' above 37.24º. Note that the terms 'constant torque' and 'constant power' are in quotes because with the ramp applied, neither is actually constant but changes with low pass filtered pitch angle.

- Side-to-side tower vibrations became quite severe at high wind speeds (as was also reported in [34]), so as well as the standard drive train damping torque a further contribution to generator torque demand was added on, derived from measured side-to-side nacelle acceleration and calculated in such a way as to enhance the damping of the first tower side-to-side mode of vibration. To achieve very much damping this technique requires rather

large generator torque variations, leading to increased hub, shaft and tower top torque (Mx) fatigue loading as well as large power variations. However even a small amount of additional damping was sufficient to bring down the vibration level so that the tower base Mx fatigue loading was only slightly above the base case, without too much increase in the hub, shaft and tower top Mx loading. The side-to-side damping was only used in high wind speeds, being phased in linearly with pitch angle with no damping below 25.8º and full damping above 40.1º. The damping torque was calculated from the measured side-to-side nacelle acceleration by passing it through a specially tuned fourth-order filter with transfer function whose continuous time representation is

$$\frac{1+2\zeta_1 s/\omega_1+s^2/\omega_1^2}{\left(1+2\zeta_2 s/\omega_2+s^2/\omega_2^2\right)\left(1+2\zeta_3 s/\omega_3+s^2/\omega_3^2\right)}$$

where ω_1 = 2.485 rad/s, ζ_1 = 0.441,
ω_2 = 1.8695, rad/s, ζ_2 =0.1938,
ω_3 = 2.9165 rad/s, ζ_3 = 0.7071

The resulting controller was used for a full set of fatigue load calculations, and the results compared against the original controller. The changes in some of the key fatigue loads are reported in Table 2.2, along with the energy output.

	Base case	**Ramp 1**	**% Change**
Blade root Mx (kNm)	10079.4	10092.5	0.1
Blade root My (kNm)	8668.4	8728.4	0.7
Blade root Mz (kNm)	166.0	166.1	0.1
Stationary Hub Mx (kNm)	1949.2	2052.9	5.3
Stationary Hub My (kNm)	8569.7	8666.9	1.1
Stationary Hub Mz (kNm)	8606.1	8681.8	0.9
Yaw bearing Mx (kNm)	2143.0	2253.2	5.1
Yaw bearing My (kNm)	8945.5	9034.7	1.0
Yaw bearing Mz (kNm)	9415.3	9495.8	0.9
Tower base Mx (kNm)	27414.5	28480.3	3.9
Tower base My (kNm)	55219.0	55789.1	1.0
Tower base Mz (kNm)	9415.2	9495.7	0.9
Annual energy output (GWh)	22.9	23.1	0.9

Table 2.2: Effect of Ramp 1 on energy and key fatigue loads

These results indicate that in terms of energy output and fatigue loading there should be no problem to introduce such a ramp. Fatigue loads are well contained, with only one or two small increases. Energy output is even slightly increased, so it might be possible to change the ramp shape slightly, for example by starting it at slightly lower wind speed, if a further reduction in fatigue loading was required.

The next step was to run a set of extreme load calculations for both cases. With the turbine operating instead of idling in the higher winds, it is possible that significant changes could be seen in the extreme loads.

The load cases which were run are those defined by the IEC 61400-1 edition 3 standard. The external wind conditions were class IA. No idling or maintenance load cases were considered as these would have remained identical for both cases. A summary of the operating conditions associated with each load case is provided in Table 2.3.

Load case	Description of operating condition
dlc1.3*	Extreme turbulence model
dlc1.4*	Extreme coherent gust with direction change
dlc1.5*	Extreme wind shear (vertical and horizontal)
dlc2.1	Transducer failure, software overspeed trip (n4 speed trip)
	Collective pitch runaway towards fine
dlc2.2	Transducer failure, safety system overspeed trip (nA speed trip)
	Pitch seizure, 1 blade pitch runaway (towards fine and feather)
dlc2.3	Extreme operating gust with grid loss
dlc4.2	Normal stop with extreme operating gust
dlc5.1	Emergency shutdown
* For the base case, idling simulations were run for wind speeds above cut-out.	

Table 2.3: Summary of extreme load cases

The external conditions are designed to capture events with a statistical return period up to 50 years in order to generate a conservative 20 year design load envelope. It was assumed that the standard's equations defining external conditions for power production were valid beyond the current industry standard 25m/s cut-out wind speed. In fact; the IEC standards do not define a maximum limit for the cut-out wind speed.

An initial load comparison was carried out between ramp control operation, from 4m/s to 35m/s, and normal power control, from 4m/s and 25m/s. The comparison of ultimate loads across the main turbine components is reported graphically in Figure 2.22.

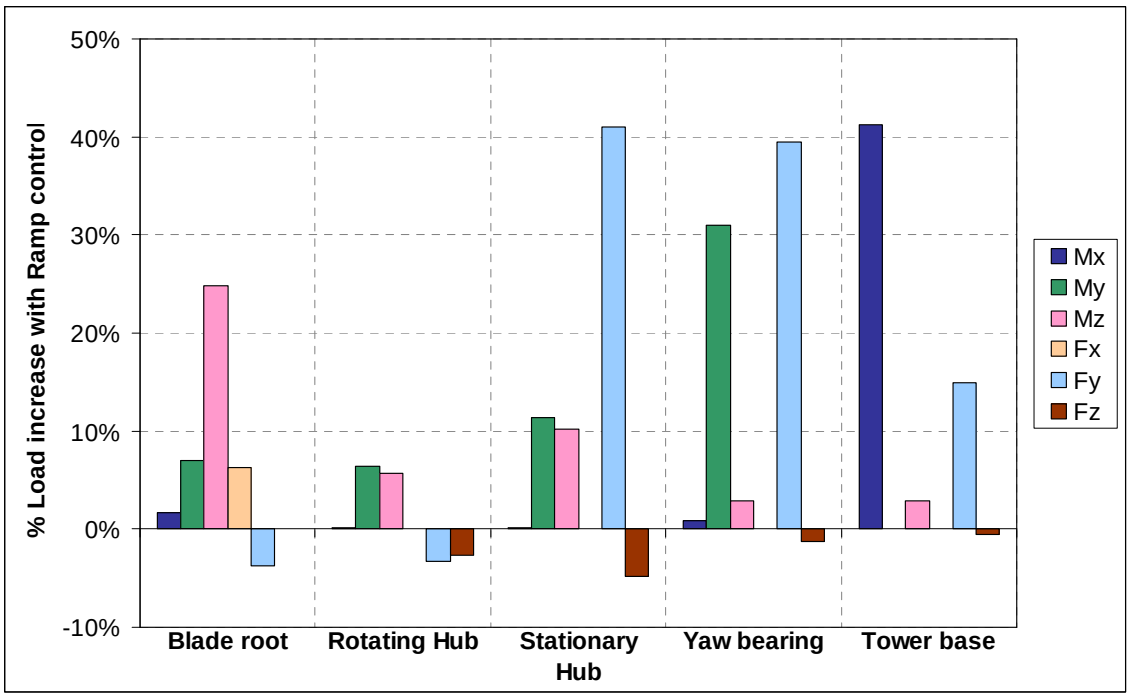

Figure 2.22: Load comparison between ramp control and normal control

Figure 2.22 shows a significant penalty in side-side loading with ramp control. Tower base Mx and Fy are nearly 45% higher with ramp operation to 35m/s than under normal operation. It was found that DLC5.1 was driving the side-side extreme loads in the ramp control case. DLC5.1 simulations include an emergency stop in turbulent wind. The driving case occurred at 35m/s mean wind speed.

The comparison reported above gives an indication of the extreme load implications of pushing past the current industry standard cut-out wind speed. However, this comparison was not fully comprehensive as it compared power production loading with ramp control from 4 and 35m/s and normal control operation between 4 and 25m/s, without considering the loading generated while the turbine under normal control was idling between 25 and 35m/s.

To investigate this, additional idling simulations were run under DLC1.3 and DLC1.5 environmental conditions. The updated load comparison is reported in Figure 2.23

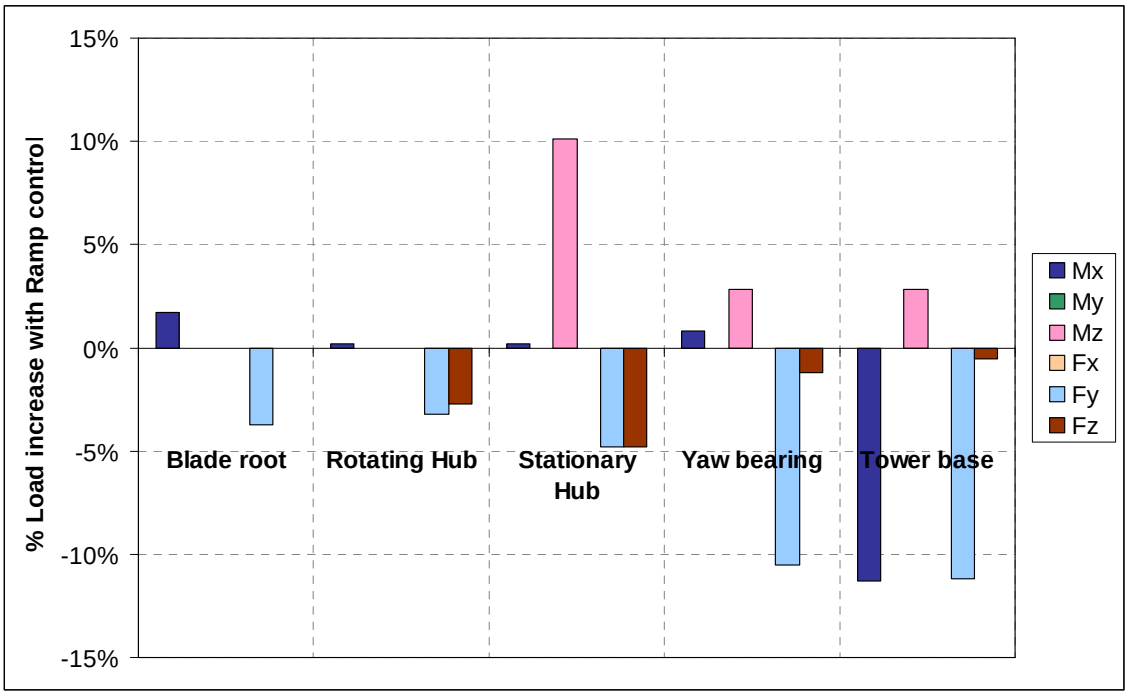

Figure 2.23: Load comparison with additional idling cases in the base set

The inclusion of the DLC1.3 idling cases has significantly increased the side-side loading, in particular the extreme tower base Mx of the base set and so the ramp control load is now approximately 10% lower. A large number of extreme load components are reduced with high wind operation under ramp control. One reason for this is that under normal operation, the extreme loads for a number of components occur at 25m/s wind speed while the turbine is still operating at fully rated power. With ramp control operation, the wind turbine is slightly derated at this wind speed which gives the turbine greater operational flexibility to respond to the extreme events which would usually cause a shutdown under normal control.

The results show that operation in high winds with ramp control can actually reduce the extreme load envelope across certain load components and are no higher than 11% across the main load components in this study. The results also highlight the significant extreme loading that can be incurred during idling operation and suggest that the wind turbine design standards do not necessarily choose the most conservative approach through the current definition of the ultimate load cases.

2.6.2 Ramp 2: half power above 50 m/s

In this study the base case controller for the 5MW Upwind reference turbine is the NREL controller described in [Jonkman]. This does not include any additional load reduction strategies for the tower or the blade root loads. In order to assess the possibility of operating the turbine in high winds speeds above 25m/s (storm conditions), in terms on additional loading 'experienced' by the turbine, weighed against additional power production, three cases are investigated:

Case 1: nominal operation up to 25m/s, i.e. operation with the base case controller, and idling above 25m/s

Case 2: nominal operation up to 50m/s i.e. rated power output with the torque and rotor speed set-points unchanged.

Case3: nominal operation up to 25m/s and implementation of a storm control strategy above 25m/s, in which the rotor speed set-point is reduced as a function of a filtered wind speed signal. This ramp is designed to reduce the speed from the nominal 12.1 rpm at 25 m/s to 50% of this (6.05 rpm) at 50 m/s

In Figure 2.24, Figure 2.25 and Figure 2.26, the mean, maximum, minimum and standard deviation of the rotational speed, power output and pitch angle for the implemented storm control strategy, over the whole operational range is shown. [Simulations in HAWC2 over the whole operational range. Discuss use of wind speed signal as an input].

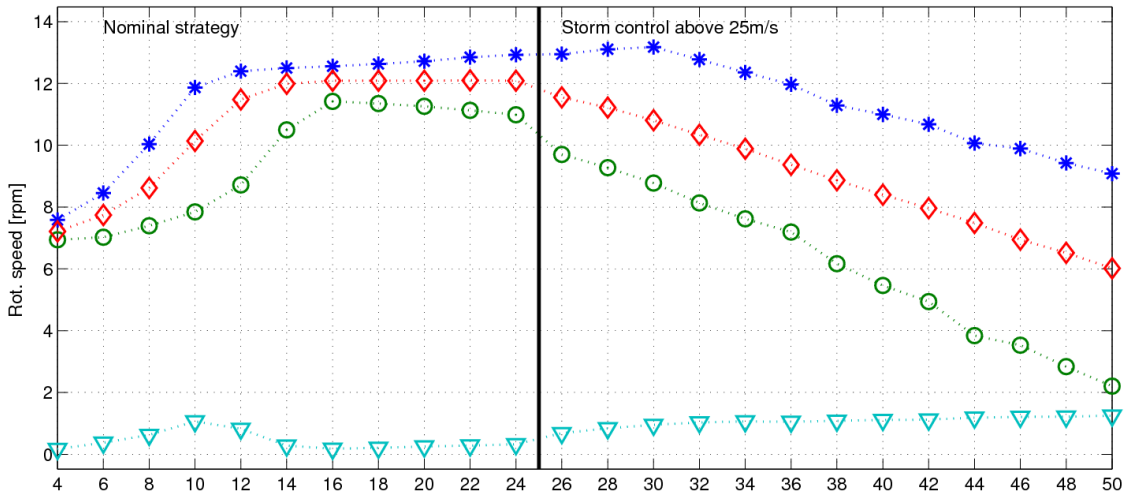

Figure 2.24: Rotational speed over the whole operational range for Case 3: reduced rotational speed set-point above 25m/s. ◊ mean value, ○ min value, ∗ max value, ▽ standard deviation

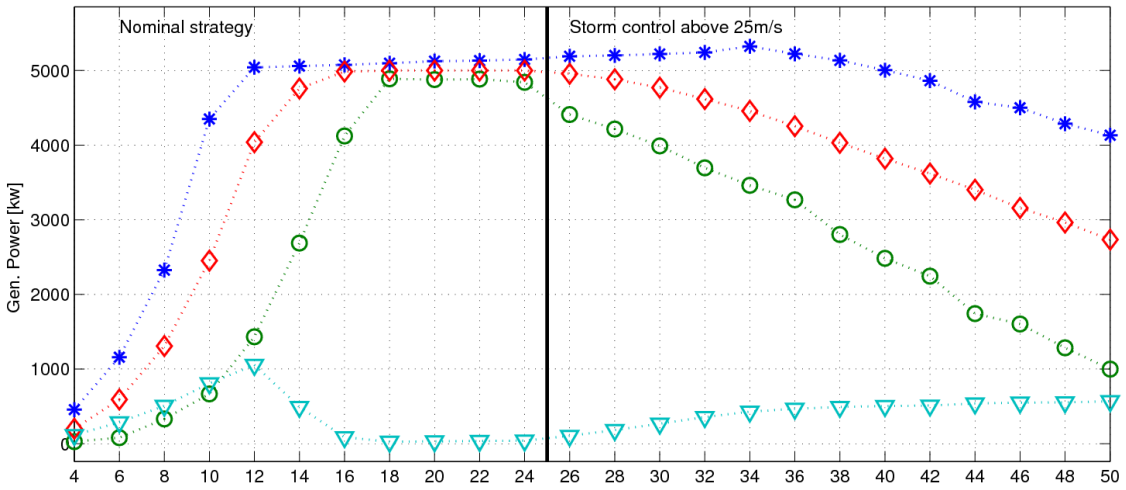

Figure 2.25: Power output over the whole operational range for Case 3: reduced rotational speed set-point above 25m/s. ◊ mean value, ○ min value, ∗ max value, ▽ standard deviation

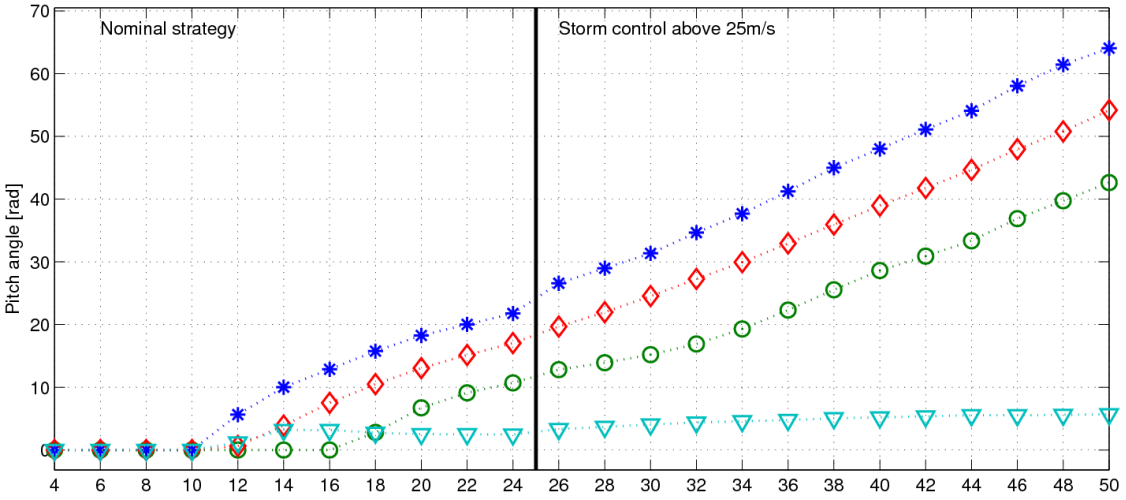

Figure 2.26: Pitch angles over the whole operational range for Case 3: reduced rotational speed set-point above 25m/s. ◊ mean value, ○ min value, ∗ max value, ▽ standard deviation

A rainflow analysis to determine the fatigue loads on the tower top, tower bottom, main shaft and the blade roots, during operation of the turbine, for all the above defined three cases, has been undertaken. From these results the following will be determined: firstly what the percentage increase of loading in Case 3 is compared to nominal operation (Case 1); and if it is realistic and needed to implement additional load reduction strategies in order that the loads on the turbine are comparable to the nominal loads with the turbine shut-down above 25m/s.

The study assumes a Class 1 wind regime described by a Rayleigh distribution with a mean wind speed of 10 m/s. For this Class, the hourly mean wind speed is expected to exceed 25 m/s for about 64.8 hours per year, and to exceed 35m/s for about 0.6 hours per year. For a Class II and Class III turbine, the hours at high wind speeds are even fewer. Although the ramp is more gradual than that described in the previous section, and is thus likely to result in higher loads, the number of hours spent at the highest wind speeds is so small that the increase in fatigue loading

is expected to be small, A similar study using the same ramp was undertaken for a 2MW turbine, as reported in [34], in which an increase in the tower loads, especially the side-to-side, was seen. The implementation of active tower dampers was sufficient for the loading on the turbine when operating at reduced power above 25m/s, to be comparable to that when idling above 25m/s.

The fatigue loading on the turbine when allowing the turbine to operate above 25m/s is investigated for the 5MW Upwind reference turbine and is summarised in Table 2.4.

- When running at **rated power** above 25m/s (Case 2) the tower loads, both fore-aft and side-to-side are decreased compared to idling, the blade flap and blade torsion fatigue loads increase by 30.63% and 113% respectively.
- With the **storm control** strategy (Case 3), the side-to-side tower loads are increased, by 44.39%, the blade loads are much reduced compared to Case 2, although they are still higher than the base case scenario.

Sensor	Case 2	Case 3
Tower fore-aft moment	-19.02%	-15.40%
Tower side-to-side moment	-35.26%	44.39%
Tower tilt moment	3.31%	3.09%
Tower yaw moment	-0.20%	2.06%
Shaft moment	0.01%	0.01%
Blade flap moment	30.63%	14.94%
Blade edge moment	-10.72%	-11.33%
Blade torsion moment	113.71%	18.03%

Table 2.4: Percentage change in loading for Case 2 (rated power and nominal controller above 25m/s) and Case 3 (reduced power above 25m/s with ramp2), relative to the base case, Case1 (idling above 25m/s).

In order to operate at higher wind speeds with the suggested power reduction strategy without resulting in substantially increased loads on the turbine, the tower side-to-side fatigue loading and the blade root loads need to be decreased. Before implementing additional load reduction controllers, it is currently being investigated whether reducing the cut out wind-speed (the turbine is operating in above results up to 50m/s), will reduce the loads. The relative contribution to fatigue damage per time series (%) for the tower side-to-side moment is seen, for example, in Figure 2.27. When running above 25m/s with a reduced power output, the highest contributions to the tower side to side fatigue damage is in the winds-speeds from 38m/s to 44m/s, and thus operating up to only 35m/s or 40m/s, would contribute to reduced side-to-side fatigue loads.

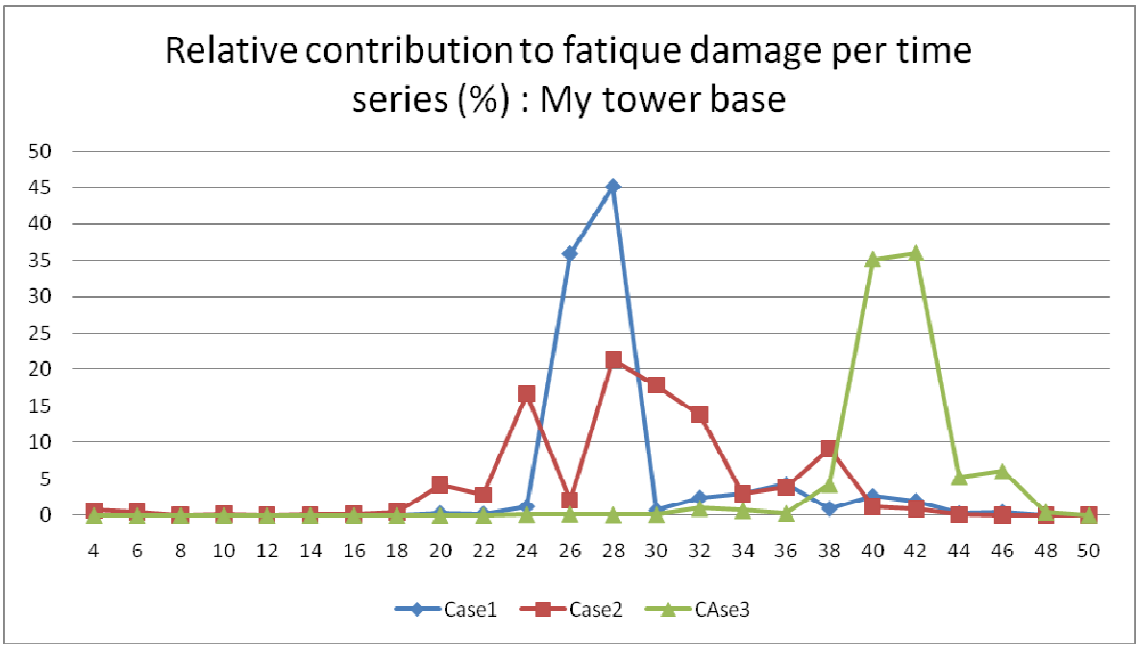

Figure 2.27: Relative contribution to fatigue damage per time series (%) for the tower side-to-side moment for Case 1 (nominal operation), Case 2 (rated power above 25m/s), Case 3 (ramp down of power above 25m/s)

3. Controller implementation

3.1 System identification of wind turbines operating in closed loop

With the increasing size and power of wind turbines onshore and offshore, the importance of good control for stabilisation and load reduction becomes ever more important. The basic tool for the design of a controller is the linear model of the plant to be controlled in different points of operation. At the design stage, linear models based on linearization of nonlinear aeroelastic codes are generally used. However, differences in the as-built turbine may mean that these models are not accurate enough if controller re-tuning is required when commissioning the real turbine.

Identification in open loop operation of dynamic systems is a common solution for this kind of problem. Since it is difficult and dangerous to operate WT in open loop, identification in closed loop operation has been considered. Different procedures and new algorithms for identifying the main plant dynamics operating in closed loop have been created. This new set of algorithms deals with main problems which can appear in the WT plant models, like controllers operating in cascade, filters in the loop and time-varying and non linear controllers, and of course, without the measurement of the wind speed.

The algorithms and procedures were originally developed based on simulations run with Bladed, FAST and HMS, for standard IEC61400 turbulent winds. Recently, some experimental data have been obtained at NREL's CART2 Wind Turbine.

3.1.1 Closed loop identification algorithms

Assuming that the real system is linear around an operating point, the objective of system identification in closed loop operation is to search for a plant model that in feedback with the controller operating on the true plant, will lead to a closed loop transfer function, (sensitivity function), that is as close as possible to that of the real closed loop system.

Consider Figure 3.1 where the controller is implemented (R/S). The effective plant input u, is obtained from the external excitation ru through filtering by the output sensitivity function Syp. The output sensitivity has a maximum in the frequency region close to the critical point in the Nyquist plane. Therefore the frequency spectrum of the effective input applied to the plant will be enhanced in this region, so the quality of the identified model in these critical frequency regions for stability and performance will be improved.

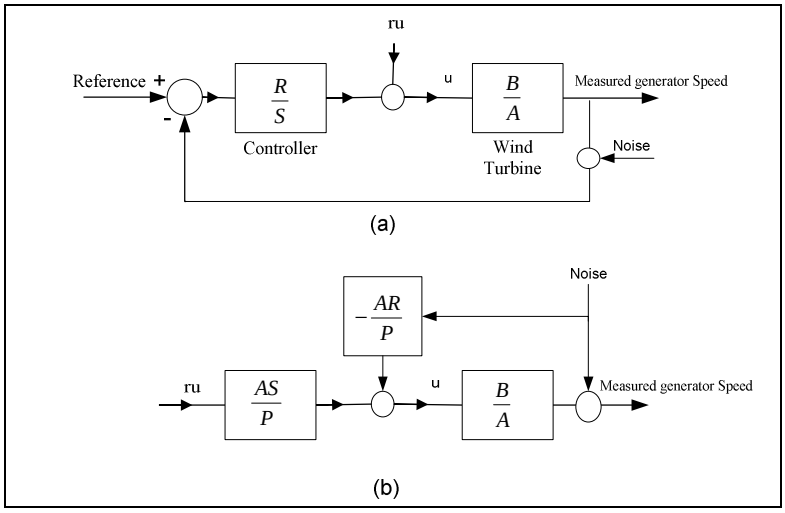

Figure 3.1: a) Identification scheme in closed loop. b) Equivalent scheme

One may expect that the open loop techniques based on the whitening of the prediction error will still provide good results in closed loop operation. However the feedback introduces a correlation between the measurement noise and the plant input. This leads to an important bias on the estimated parameters [35].

The set of algorithms used and created for the identification of the WT belong to the family of the close loop output error (CLOE) algorithms. The objective of CLOE algorithms is to identify a plant model that in feedback with the actual controller, gives a closed loop transfer function as close as possible to the real operating one. This set of algorithms is summarized in Figure 3.2.

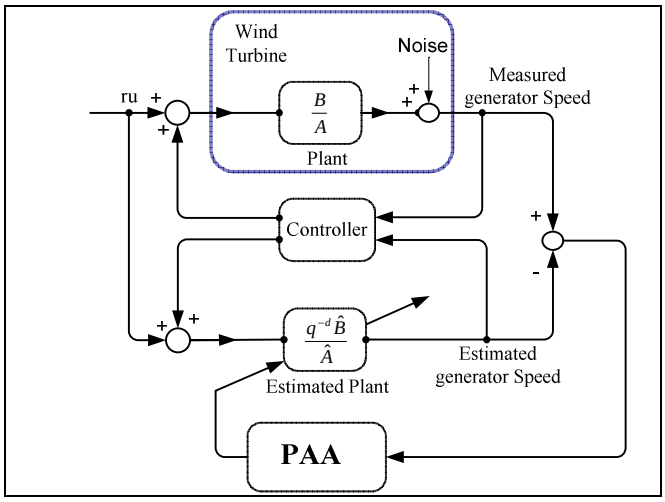

Figure 3.2: CLOE algorithms

The estimated parameters are arranged in a vector θ. The measurements can also be arranged in a vector Φ, and used in the parameter adaptation algorithm (PAA), defined by the following equations:

$$\hat{\theta}(t+1) = \hat{\theta}(t) + F(t)\,\phi(t)\,\varepsilon(t+1)$$

$$\varepsilon(t+1) = \frac{\varepsilon^0(t+1)}{1+\phi^T(t)\,F(t)\,\phi(t)}$$

$$\varepsilon^0(t+1) = w_1(t+1) - \hat{\theta}(t)\,\phi(t)$$

$$F(t+1) = \frac{1}{\lambda_1(t)}\left[F(t) - \frac{F(t)\,\phi(t)\,\phi^T(t)\,F(t)}{\frac{\lambda_1(t)}{\lambda_2(t)} + \phi^T(t)\,F(t)\,\phi(t)}\right]$$

3.1.2 Identification of Torque Loop

It is well known that in a variable-speed wind turbine operating at constant generator torque there is a very little damping for the drive train mode, since torque does not vary with generator speed [36]. The very low damping can lead to large load oscillations at the gearbox. Coupling with the in-plane collective modes and the tower side to side modes are also sometimes present in these plant models. The torque loop usually plays a vital role in damping these modes, and it is probably one of the most difficult loops to be tuned in the commissioning of the turbine.

The procedure and algorithm developed for the identification of the plant of this loop depends on the operational conditions. However it is important to realize that no measurement of the wind is used in the process of identification.

The algorithm to be used in the identification of the transfer function between the Torque demand and the generator (or rotor) speed can be arranged for different complexities of the loop. According to this, simple control schemes like PID controllers in feedback with the plant, to several cascade controllers and filters in the loop schemes can be used for the identification.

The method begins with the application of an input excitation signal, the design of which is critical for the success of the identification. An example of input / output signals used in the process of identification of the torque loop is shown in Figure 3.3. The influence of the input on the output of the plant is small. The input excitation signal is normally between 3% and 7% of the nominal torque demand. This means that the amount of energy needed for obtaining the identified models is small, which is important for the stability and safety of the method.

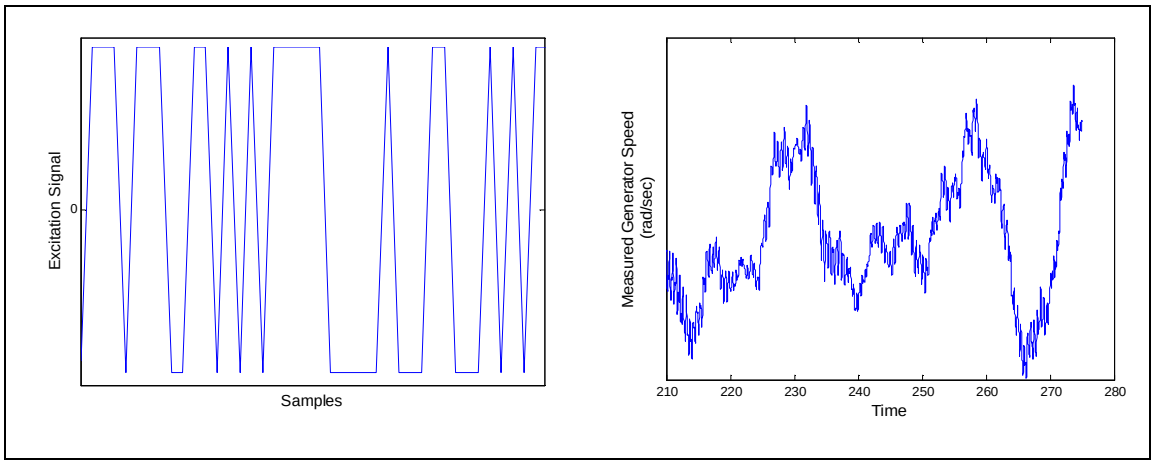

Figure 3.3: Input – Output pair for identification of torque loop

Several models have been obtained using this technique. Figure 3.4 shows a comparison between three models: the one coming from the linearization tool of Bladed, the one coming for the case of constant wind speed, and finally the model indentified in the presence of the 3-dimensional turbulent wind speed. The first two models look similar because they are obtained exactly under the same wind speed. The third looks a little bit different but correlates very well with the others, while avoiding problems with ill-conditioned modes, very sharp peaks or unobservable modes. The identified models were validated under classical validation techniques for models identified in closed loop operation – see [37].

3.1.3 Identification of Pitch Loop

The identification of the pitch loop usually requires a different algorithm from the torque loop [38], because the pitch loop usually contains non linear time varying controllers. New algorithms had to be developed to deal with this, by extending the CLOE algorithms to deal with a non-linear controller [39]. Once again, although there is a strong dependency between the plant model and the wind speed in the pitch loop, the wind speed is not used in the identification algorithm. The experimental method should also be modified because of the nature of the pitch loop [39].

Six experiments were developed using simulation tools, for wind speeds between 14 and 24 m/s and turbulence intensities between 10% and 15%, as summarized in Table 3.1.

Case	Standard deviation	Turbulence intensity
14 m/s	1.66 m/s	11.58 %
16 m/s	2.57 m/s	15.29 %
17 m/s	1.68 m/s	9.76 %
20 m/s	2.58 m/s	13.07 %
22 m/s	2.69 m/s	11.29 %
24 m/s	3.15 m/s	12.13 %

Table 3.1. Wind characteristics at hub during experiments

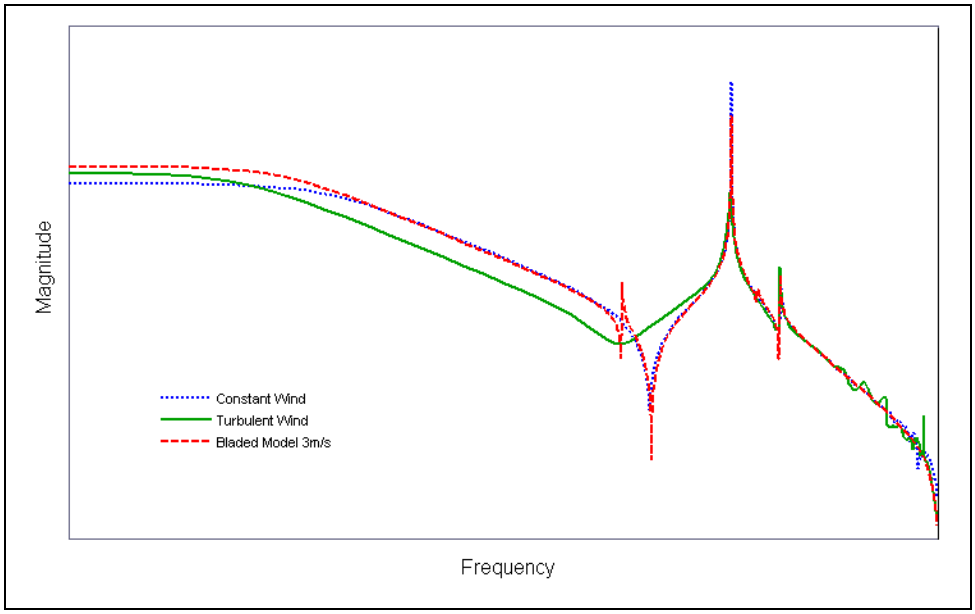

Figure 3.4: Linearized model, Identified model with constant Wind Speed, and Identified model while turbulent wind speed

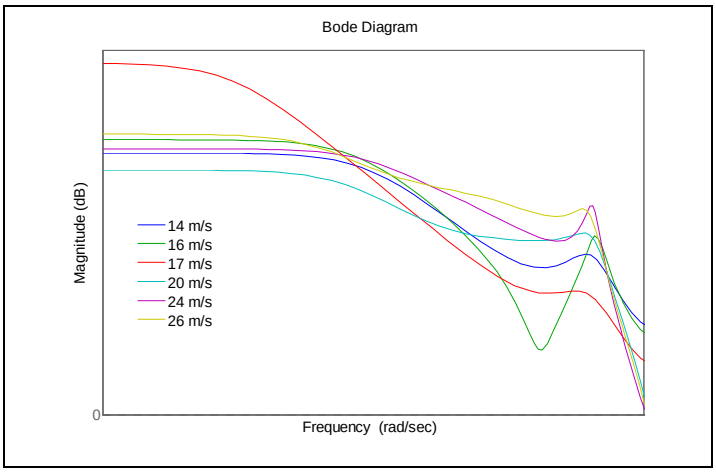

Figure 3.5: Pitch Plant models Identified in closed loop operation

The models obtained in these experiments are represented in the Bode plot of Figure 3.5. This shows important changes in the dynamics of the loop, which correspond with the theory, and which introduce important restrictions in the controller design. These important changes are more evident in Figure 3.6, where the non-minimum phase zeros at the lower wind speeds move to minimum phase in higher winds.

No validation tests were created for this new algorithm, so the validation test selected for this set of models was to design a controller and test it in the simulation tool. According to this, a robust controller was designed, and the non linear effects of the controller were cancelled. Then a linear controller was tested, and the simulation results are presented in Figure 3.7.

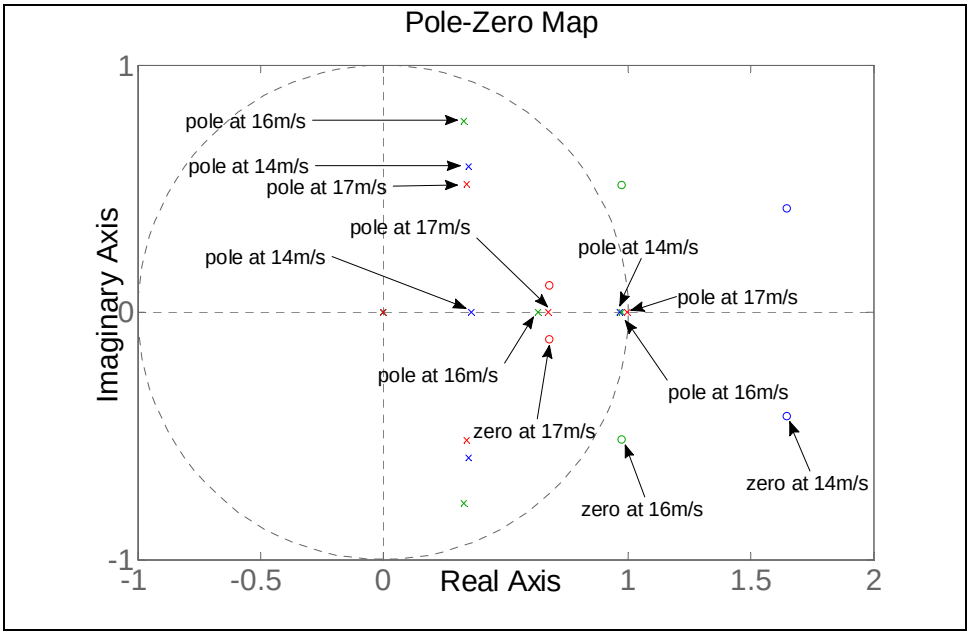

Figure 3.6: Pole Zero map of the Pitch Plant models Identified in closed loop operation

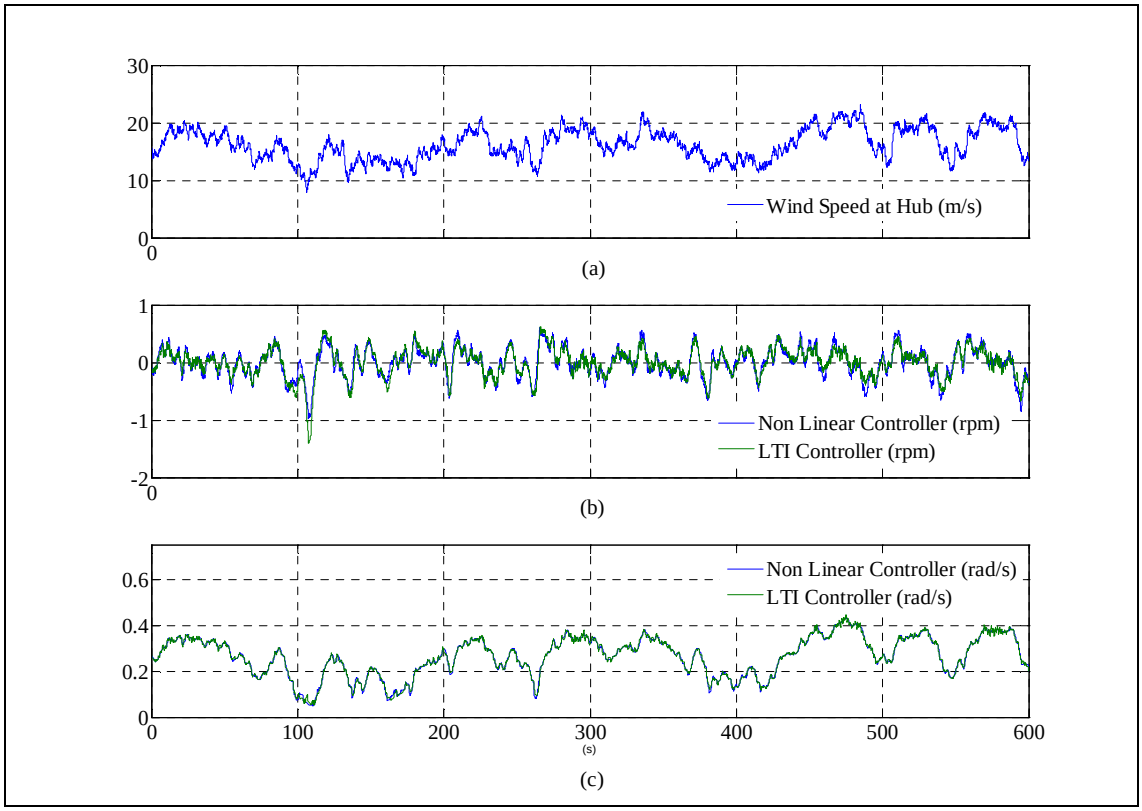

Figure 3.7: Comparison between non linear controller and a robust linear controller for a 600 second simulation with high turbulence wind speed.
(a) Wind speed (b) Rotor Speed (normalized) (c) Pitch Angle.

3.1.4 Real experiments on CART2 and future work.

Experimental protocols for the CART2 turbine at NREL were implemented in cooperation with the NREL control team. Preliminary results from a first set of experiments show the potential of the technique. This work is still under development, and identified models for torque loop will be available soon. This will be followed by similar work on CART2 to identify the pitch loop. In addition, but based on simulation data, it is expected to carry out the identification for obtaining the models needed for IPC, which may reveal new problems, depending on whether the system can be considered SISO or MIMO. Similar work will be developed for the tower damping loop.

This work is reported in detail in Deliverable 5.11 [43].

3.2 Hardware-in-the-loop test rig

This activity focuses on the practical implementation and laboratory testing of control hardware together with the algorithms arising from Task 5.1.1 [8]. The objective is to set up a means of performing hardware-in-the-loop (HITL) simulations in which the performance of the reference 5MW wind turbine in conjunction with actual controller and pitch actuator hardware can be evaluated. The advantage of interfacing the controller with real actuators is to directly measure on the pitch actuator system data such as temperature and motor currents which should be monitored especially when Individual Pitch Control (IPC) is used.

This is a joint task between ECN, IWES and GL-Garrad Hassan and the deliverable will combine the GH Bladed hardware test interface, real-time turbine simulation and the IWES pitch actuator rig. Simulation models from all three participants will be used to guarantee the results.

A suitable scaling based on blade inertia and geometry has been computed and applied to map the 2MW turbine pitch facility dynamics available at IWES, into a realistic 5MW wind turbine pitch actuator model.

3.2.1 Test description

The 5MW reference wind turbine has been modelled and simulated in Bladed, apart from the pitch actuator whose response is directly measured on the test rig and the blade bearing which has been simulated in x-PC Target. The Bladed Hardware Test Module (BHTM) has been used to exchange information between the pitch system, the wind turbine controller and the wind turbine model. Figure 3.8 shows the test set-up where it is possible to identify the pitch actuators and the pc where simulations and controller run.

The turbine model has been suitably reduced in order to be able to run in real time on the machine used in the test. However the accuracy of the model has been maintained and checked against the full more sophisticated model.

A second simulation model and controller was provided by ECN. This 'simulation core' was included in a Simulink diagram which was downloaded in the target-PC that controls the HITL pitch actuators. The wind turbine part of the simulation core is set up by the ECN Turbu environment for real-time controller testing (ETRT). It allows for fast aero-elastic simulation through a set of linear models that covers the whole range of operation. The linear models are derived with the ECN program Turbu and are implemented in discrete time. Switching and interpolation schemes between the models apply. This approach allows for the inclusion of a considerable number of deformation modes for the rotor, drive-train and tower; the accuracy has been checked against a state-of-the-art non-linear aero-elastic model.

Different tests have been performed in order to assess the capability of the test rig to represent the effects of using a Collective Pitch Controller (CPC) and an Individual Pitch Controller (IPC) both on turbine loads and on pitch actuator response.

Tests have been focused on turbulent wind conditions around and above rated (from 10ms to 24ms) where the performance of different pitch control strategies can be estimated.

In order to validate the test configuration the same wind conditions have been simulated in a complete virtual environment where the same controller and an estimated pitch actuator model suitable for a 5MW machine have been employed.

The loads which are mainly affected by the IPC control strategy are blade out of plane bending moment, rotating hub and yaw bearing out of plane loads and for this a fatigue analysis has

been performed. Also pitch actuator fatigue analysis has been performed trying to represent the actuator duty cycle.

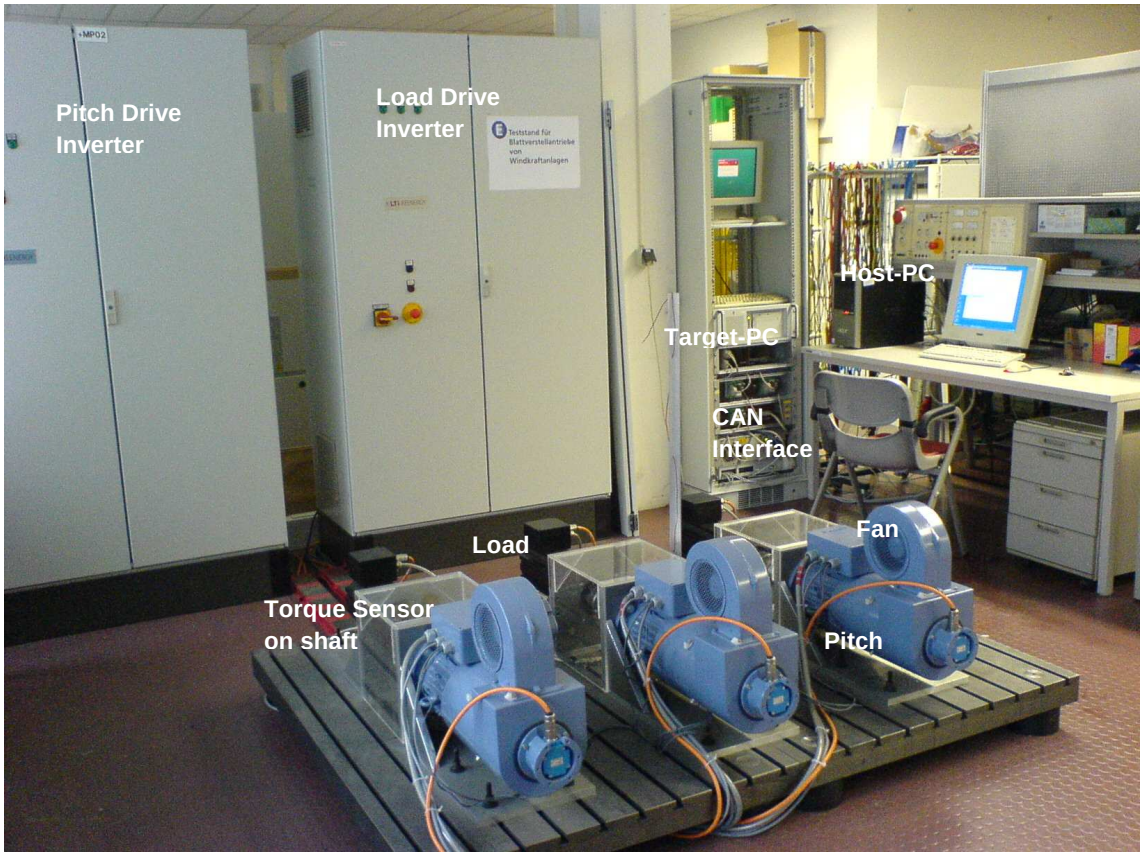

Figure 3.8 HITL Test facility

3.2.2 Results

Table 3.2 summarizes the fatigue load analysis comparison between simulation and HITL tests where the index of performance is defined as

$$\Delta = 1 - \frac{x_{IPC}}{x_{CPC}}$$

The table shows a good agreement in predicting the difference between CPC and IPC control strategies both in terms of load reduction and in terms of increment in pitch actuator activity.

Load component	Simulation			Hardware in the loop test		
	CPC	IPC	Δ	CPC	IPC	Δ
Blade root out of plane [kNm]	13302.2	10494.9	**21.10%**	12631.5	9677.64	**23.38%**
Rotating Hub My [kNm]	18020.1	12562.7	**30.29%**	17176.5	11597.1	**32.48%**
Rotating Hub Mz [kNm]	18141	12644.3	**30.30%**	17184	11506.4	**33.04%**
Yaw bearing My [kNm]	12330	11810	**4.22%**	11420	10860	**4.90%**
Yaw bearing Mz [kNm]	12778.6	12580.8	**1.55%**	11810.5	11533	**2.35%**
Pitch angle [deg]	7.95773	12.426	**-56.15%**	7.92431	12.3915	**-56.37%**
Pitch rate [deg/s]	5.4036	15.7451	**-191.38%**	4.78575	13.7262	**-186.81%**

Table 3.2 Fatigue analysis

Mean wind speed [m/s]	controller	RMS [Nm]			Max [Nm]		
		Shaft1	Shaft2	Shaft3	Shaft1	Shaft2	Shaft3
10	CPC	0.96	0.99	1.46	7.53	7.53	8.60
	IPC	2.12	2.19	2.22	8.52	9.48	9.11
	Diff.[%]	118	121	52	13.1	25.9	5.9
12	CPC	1.44	1.48	1.61	7.01	7.70	8.89
	IPC	2.87	2.95	3.01	8.80	9.55	9.35
	Diff.[%]	98	98	86	25.4	24.0	5.1
14	CPC	1.57	1.63	1.73	7.65	8.53	7.98
	IPC	2.90	3.06	3.07	9.34	9.53	9.48
	Diff.[%]	84	87	76	22.0	11.7	18.7
16	CPC	1.57	1.64	1.72	7.40	7.83	7.67
	IPC	3.06	3.21	3.21	9.55	9.64	9.64
	Diff.[%]	94	95	87	28.9	23.0	25.6
18	CPC	1.57	1.64	1.90	6.98	7.08	8.25
	IPC	3.19	3.33	3.36	9.24	9.80	9.66
	Diff.[%]	102	102	77	32.2	38.3	17.1
20	CPC	1.63	1.70	1.80	7.82	7.32	8.06
	IPC	3.23	3.40	3.41	9.16	9.56	9.58
	Diff.[%]	97	99	89	17.1	30.5	18.8
22	CPC	1.69	1.76	1.87	7.86	8.39	8.17
	IPC	3.42	3.68	3.67	9.86	9.39	9.90
	Diff.[%]	101	108	96	25.3	11.8	21.1
24	CPC	1.69	1.75	1.96	7.26	7.81	8.58
	IPC	3.26	3.44	3.45	9.22	9.78	10.24
	Diff.[%]	92	96	75	27.0	25.1	19.2

Table 3.3 RMS and maximum torque measured on the shaft

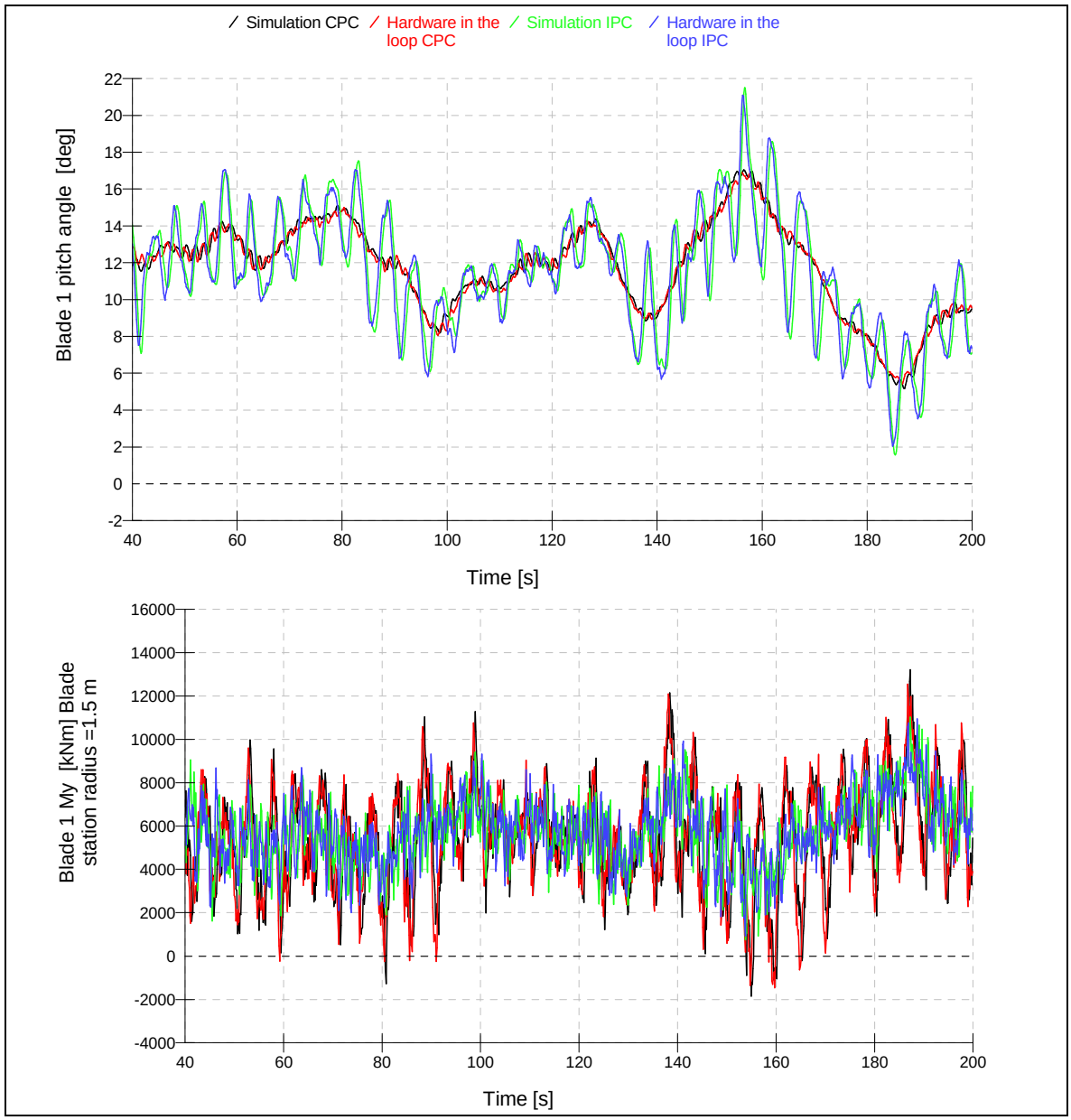

Figure 3.9 Time histories comparison between simulation and HITL tests at 16ms with CPC and IPC

Figure 3.9 shows as an example the comparison in terms of blade root out of plane load prediction and pitch activity between simulation and HITL tests with the tow different control strategies. The diagram shows the good agreement between the two types of tests.

The advantage of performing HITL tests is the possibility of having insight of pitch actuator details and monitor its performance.

A torque sensor on the shaft measures actual torque. The statistical values are written in **Table 3.3**. RMS (root-mean-square) increases up to by 121% and maximum absolute value up to by 38.3%.

Figure 3.10 shows demanded pitch angle out of Bladed is fairly well followed by actual angle of the pitch motor. However IPC causes frequent changes and some aberration is shown between demanded angle in Bladed and actual angle in the motor as reported in Figure 3.11.

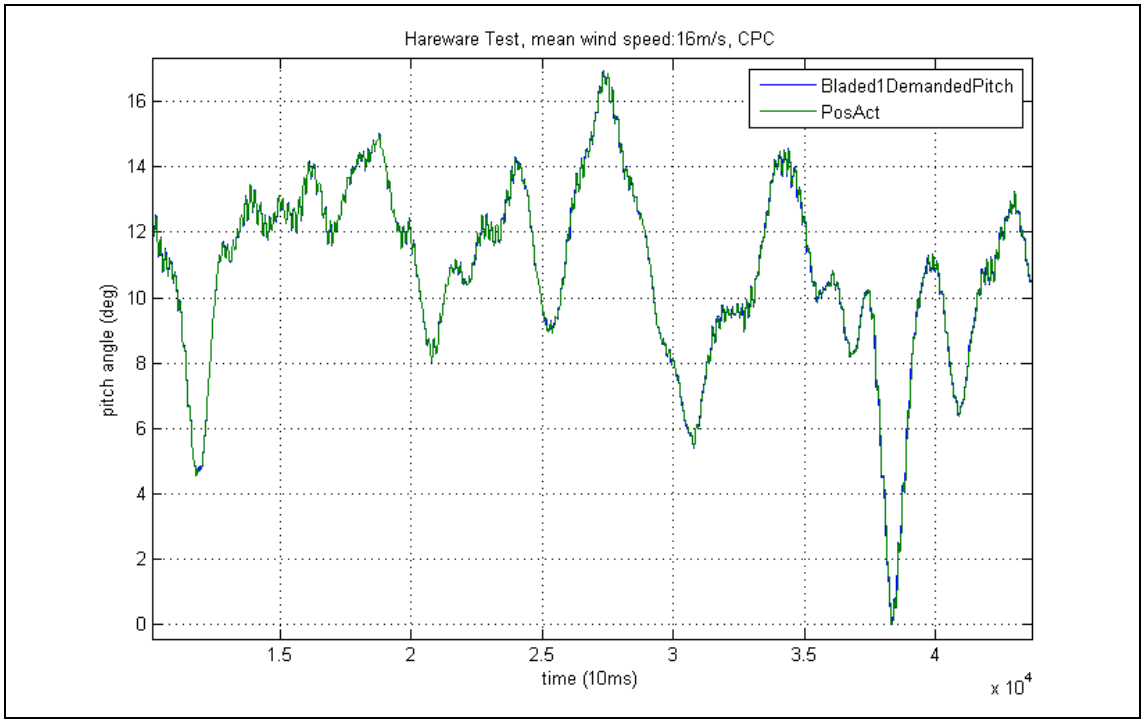

Figure 3.10 Demanded pitch angle in Bladed and measured angle in the pitch motor with CPC at turbulence with 16m/s mean wind speed

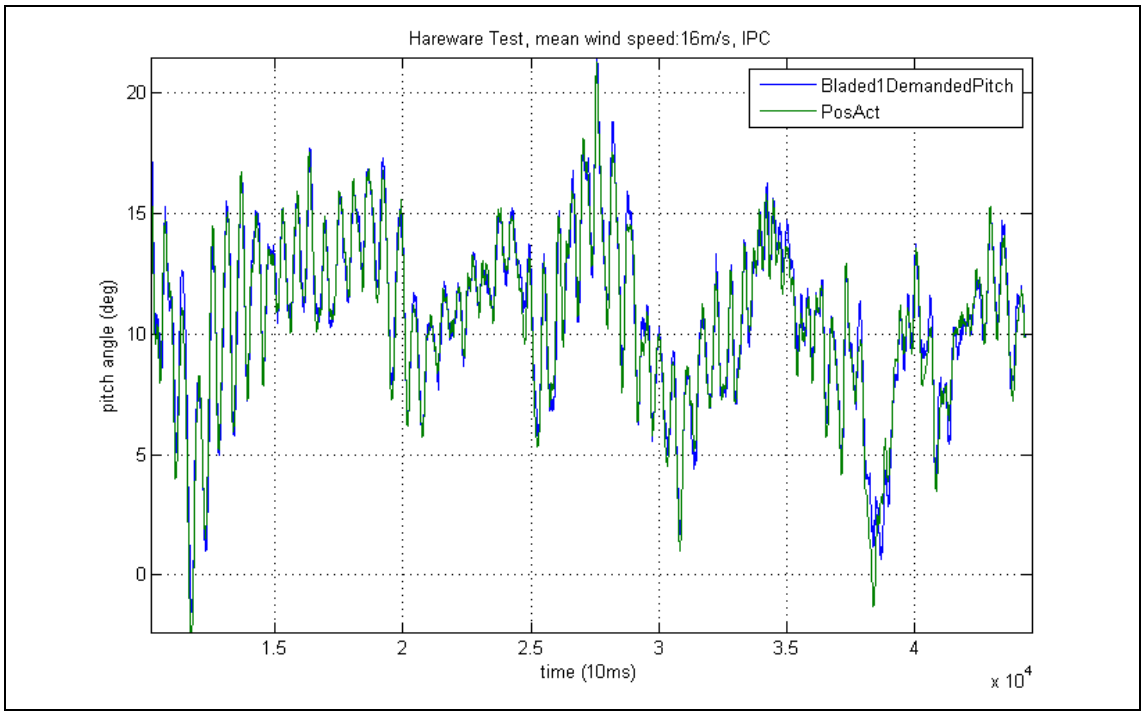

Figure 3.11 Demanded pitch angle in Bladed and measured angle in the pitch motor with IPC at turbulence with 16m/s mean wind speed

The results obtained with the ECN Turbu environment for real-time controller testing (ETRT) are similar to those obtained with the GH Bladed Hardware Test Module (BHTM). Hardware in the loop (HITL) tests and offline simulations were performed with the ETRT In wind speeds of 16, 18, 20, 22 and 24 m/s . The table below lists the damage equivalent fatigue load cycle amplitudes ([MNm]) for the out-of-plane moment, shaft bending moment, and the overturning and torsion moment in the yaw bearing centre (tilt, yaw).

wind [m/s]	16		18		20		22		24		mean		red. by
signal	cpc	ipc	cpc	ipc	cpc	Ipc	cpc	ipc	cpc	ipc	cpc	ipc	ipc [%]
M_{rt} *S*	8.8	6.8	10.3	8.3	10.3	8.1	11.1	8.6	11.8	9.1	10.4	8.2	21.7
M_{rt} *H*	9.0	7.1	10.4	8.7	10.2	8.2	10.0	8.7	11.6	9.3	10.4	8.4	19.6
M_{sh} *S*	8.9	6.2	10.1	6.9	10.7	7.6	11.6	8.2	12.4	8.8	10.7	7.5	29.9
M_{sh} *H*	8.9	6.3	10.1	6.9	10.7	7.6	11.5	8.3	12.3	8.9	10.7	7.6	29.1
M_{lt} *S*	7.1	6.1	7.8	7.2	8.6	7.7	9.2	8.4	9.7	9.0	8.5	7.7	9.0
M_{tl} *H*	7.1	6.3	7.8	7.3	8.5	7.7	9.2	8.5	9.7	9.1	8.4	7.8	7.8
M_{yw} *S*	6.8	6.3	7.8	7.1	8.1	7.8	8.7	8.5	9.3	9.1	8.1	7.8	4.6
M_{yw} *H*	6.8	6.4	7.8	7.3	8.1	7.9	8.7	8.6	9.3	9.2	8.1	7.9	3.4

Fatigue loads for the blade-root moment (M_{rt}), shaft moment (M_{sh}) and tilt and yaw moment (M_{tl}, M_{yw}) [*S* : offline simulation; *H* : HITL test].

It appeared during the experiments that the true delay of the pitch actuators was higher than assumed in the offline simulations. This was accounted for by enhancing the azimuth shift in the cyclo-stochastic IPC additions to the pitch angles around the 1p and 2p frequency. This difference in delays explains that the off-line simulation results are a little better than the HITL results.

Overall, the results are comparable to those obtained with Garrad Hassan's BHTM. There the load reductions from IPC were slightly more favourable for the blade and shaft loading, and slightly less favourable for the tilt and yaw loading.

The extreme pitch rate and acceleration in the HITL tests amounted to 8.5 ^{o}/s and 20.9 ^{o}/s^2 compared to 3.2 ^{o}/s and 10.4 ^{o}/s^2 if IPC was switched off. The corresponding standard deviation pairs were [2.2 ^{o}/s, 4.8 ^{o}/s^2] and [0.5 ^{o}/s, 1.3 ^{o}/s^2]. The offline simulations yielded almost equal values.

The figures below show the power spectrum of the out-of-plane moment at 18 m/s average wind speed from (i) offline simulations with azimuth shift of 21 degrees and *assumed* pitch delay of 0.1s and (ii) HITL tests with a shift of 35 degrees and *true (estimated)* pitch delay of 0.2s

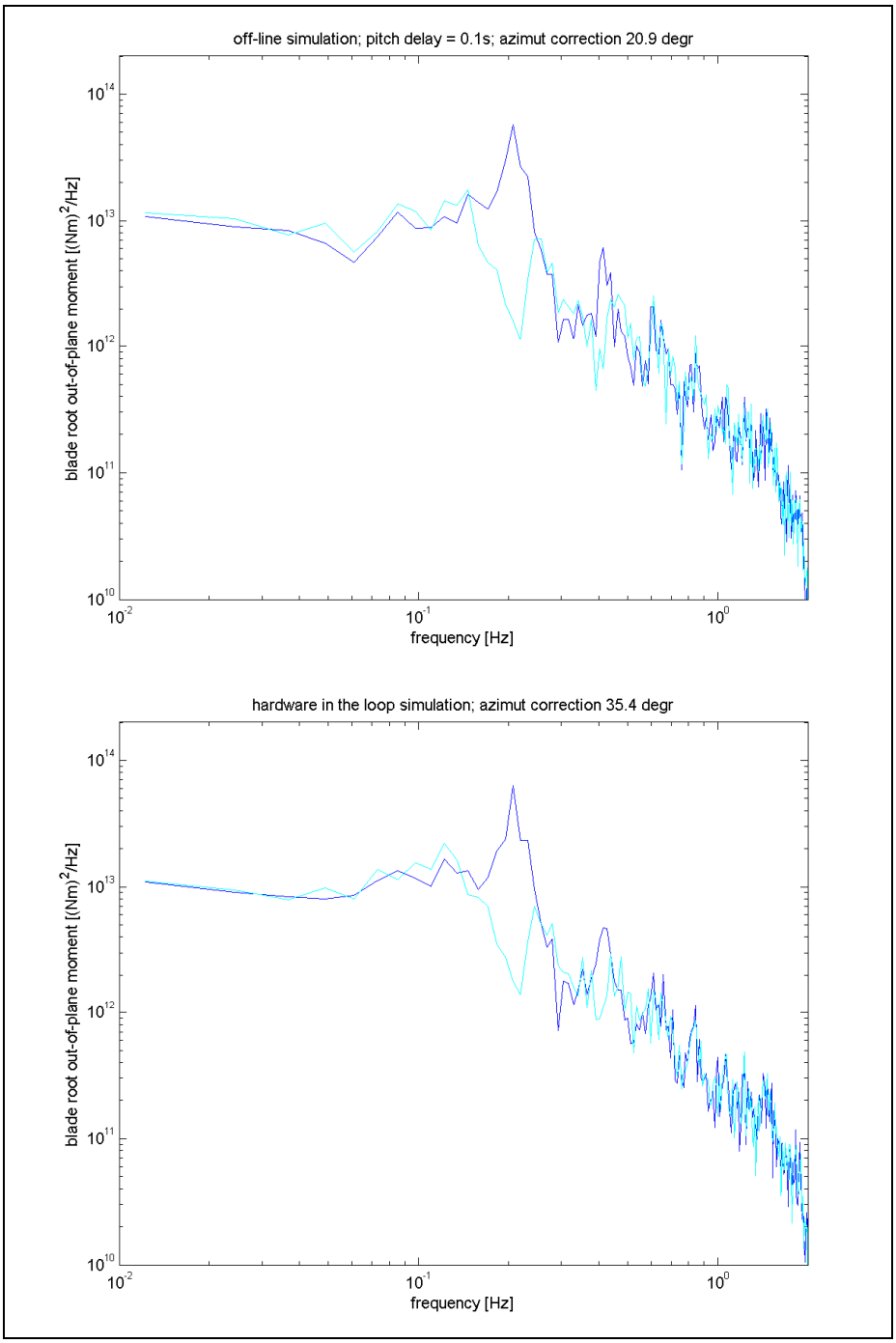

Blade moment power spectrum from simulations (upper) and HITL tests (lower) at 18m/s, with and without IPC

3.2.3 Conclusions

A test facility has been prepared and used to perform HITL tests with IWES pitch actuator facility. Individual and collective pitch control strategies have been used to control a wind turbine model implemented in Bladed where the pitch actuator model has been replaced by the real IWES pitch system. Scaling laws have been applied to map input and output from the 2MW pitch actuator facility to a suitable 5MW wind turbine pitch system response.

The tests showed that the test rig is capable of well representing the different behaviour arising by using the two different control strategies. The results have been compared with the ones obtained by a full simulation environment and good agreement can be found between full simulation and HITL prediction. In particular the relative difference between CPC and IPC is well captured.

Future work might involve the identification of pitch system dynamics in order to upgrade the 5MW reference model.

Further tests might consist in checking the response in terms of extreme events like gusts, failures etc. so that pitch system variables could be monitored in this critical scenarios.
In order to run real time tests the wind turbine model complexity has been reduced yet preserving its capability of suitably representing the full model dynamic response. A faster pc might enable the use of a more detailed model in order to improve simulation accuracy.

This work is reported in detail in Deliverable 5.4 [47].

4. Field testing and evaluation

An important task of the UPWIND project is to use field tests to demonstrate that the very significant load reductions predicted with advanced load-reducing controllers such as individual pitch control (IPC) can really be achieved in practice. Previously the only published results came from simulation models [1], so field test results are vital for increasing confidence of turbine designers to use IPC in their new designs, to improve cost-effectiveness. Initially a field test programme using a REpower turbine was intended, but for commercial reasons the testing of IPC in particular could not be carried out by REpower. Therefore a new three-pronged test programme was conceived, making use of the two 'Controls Advanced Research Turbines' (CART) situated at the National Renewable Energy Lab in Colorado, USA, and a separate experiment on a REpower turbine.

The three field tests were designed to test different aspects of load reducing control. The NREL turbines consisted of the two-bladed, teetered CART2 turbine and the three-bladed CART3. Although at 42m diameter these turbines are smaller than current commercial models, this in no way detracts from the validity of the tests. The opportunity to test a two-bladed machine is also useful, as this concept is still under consideration for large offshore machines where the principal disadvantages of noise and visual appearance do not really apply. In both cases, the advanced control features to be tested included both individual pitch control (IPC) and fore-aft tower damping (FATD). Although some validation of FATD has previously been published [5], it was easy to extend the NREL tests to include this technique and so provide more extensive validation on very different machines. The CART3 additionally provided the opportunity to test second-harmonic or 2P IPC, which brings further load reductions in the case of three blades. The REpower experiment was used to test some new tower damping algorithms, including side-side damping which is of particular relevance for large offshore turbines operating in conditions of wind-wave misalignment.

4.1 Load reducing controller testing on CART2

The detailed results of the CART2 field tests are presented in Deliverable 5.6.1 [10]. Some key results are summarised here.

4.1.1 The CART2 turbine

The CART2 turbine is 42m in diameter, with a rated output of 660 kW. It is two-bladed with a teetered hub. The aim of the IPC is to avoid the need for a teetered hub, but the turbine has a teeter brake which was applied during the tests to lock the teeter hinge.

The CART-2 is fitted with conventional strain gauges, but these are very stable, robust and well calibrated. This is partly because of the mounting position, made possible by the spindle bearings used for pitching, which also results in very low pitch bearing friction and very fast actuator response, which is very suitable for IPC. This is excellent for proving the control principles, even if it does not allow experience to be built up with the use of fibre-optic load sensors (which are more likely to be chosen for commercial applications) or the effect on more conventional pitch bearings or actuation systems.

4.1.2 CART2 controller design

A *Bladed* model of the CART-2 turbine was built from information supplied by NREL [6] and used to design a power production control algorithm incorporating IPC and FATD. This was based on up-to-date principles regularly used by GH for commercial controller design work [1],[7], and also applied to the UPWIND 5MW reference turbine as reported in Deliverable 5.1.1 [9].

The controller includes the following features:

- Optimal power production, maintaining peak Cp over the whole nominal operating speed range
- Speed regulation by interacting PI-based torque and collective pitch control loops
- Drive train damping filter in torque controller
- Damping of fore-aft tower vibration by collective pitch control (FATD)
- PI-based 1P individual pitch control to reduce rotating and non-rotating loads (IPC)

The tuning of the control loops has been carried out using classical design techniques. The FATD and IPC loops are largely independent of the rest of the controller, which was written in such a way as to allow these advanced features to be switched on and off easily during operation. By switching these features on and off every 10 minutes during the field test data collection periods, it was possible to evaluate the effects of the IPC and FATD by comparing 'on' and 'off' datasets in similar wind conditions.

4.1.3 CART2 field tests

Following simulation testing using *Bladed* [2], the new CART2 controller was installed in the turbine in early 2009, but testing could not start until February 2010 because of a gearbox failure followed by a poor winter wind season. The controller included conventional torque control for optimal power production below rated and speed regulation by torque and collective pitch control, as well as the IPC and FATD which were the focus of the field testing. The conventional power and speed control worked well from the start and required no further attention, and the very first results already demonstrated good performance of the advanced load reduction features of the controller, as shown below. Only one adjustment was required: the nacelle acceleration signal used as input to the FATD was found to have a large mean offset, causing the fine pitch angle to drift. This problem was very easily fixed by passing the acceleration signal through a 0.1 Hz high pass filter, which removed the offset without significant effect on the phase.

For the field testing, the IPC and FATD action could be switched on and off during operation without affecting speed regulation, so by comparing test data with and without the advanced features, the load reduction could be quantified across a variety of wind conditions. First some typical results from individual 10-minute samples are compared, and then the results from all the tests are binned to show the overall effect.

4.1.4 CART2 results

Comparing results from individual 10-minute samples with and without the IPC and FATD is not straightforward because inevitably the incident wind will be different. Two comparisons are shown here, between datasets with similar mean wind speeds and turbulence intensities, as shown in Table 4.1. The estimated shear is a rough fit to the mean wind speeds measured at heights of 3, 15, 36.6 and 58.2m on the nearby met mast.

Comparison	Dataset	IPC & FATD	Mean wind speed (m/s)	Turbulence intensity (%)	Estimated shear exponent
A	02050253	OFF	16.3807	15.95	.09
	02050317	ON	15.481	18.47	.14
B	02050340	OFF	12.4217	21.55	.13
	02020007	ON	12.0926	20.70	.08

Table 4.1: Individual datasets for comparison

Looking first at the tower damping, Figure 4.1 shows the spectrum of tower base fore-aft bending moment for these four cases, with the thicker lines representing the two cases with IPC and FATD switched 'ON'. A clear reduction is seen on both 'ON' cases at the first tower frequency around 0.9 Hz, confirming that the damping algorithm is working as intended. The low frequency levels are more variable, lower in one 'ON' case and higher in the other; this is simply because the underlying slow wind speed variations were different in each sample, and is not caused by the controller dynamics.

Turning to the IPC performance, Figure 4.2 compares the spectra of blade root out of plane bending moment. The low frequency changes are not important for exactly the same reason as in Figure 4.1. The complete removal of the 1P peak at 0.7 Hz confirms that the IPC is working perfectly as intended. Figure 4.3 shows the main shaft bending moment, calculated as the difference between the out of plane moments at the two blade roots. This means that the low frequency effects due to gross thrust variations cancel out, and again the dominant 1P load peak is removed exactly as expected.

Transforming these loads into the non-rotating frame we get the nodding and yawing moments. The yaw moment is shown in Figure 4.4. Here we expect the low frequency and 2P peaks to be reduced, and again this is clearly achieved, although once again the low frequencies are very dependent on slow wind field variations. Not predicted by simulations is the peak at 1P. This is unaffected by the IPC and is caused by imbalance effects – perhaps including occasional slipping of the teeter brake which is clearly observed in the measured teeter angles [3]. The nodding moment shows very similar behaviour.

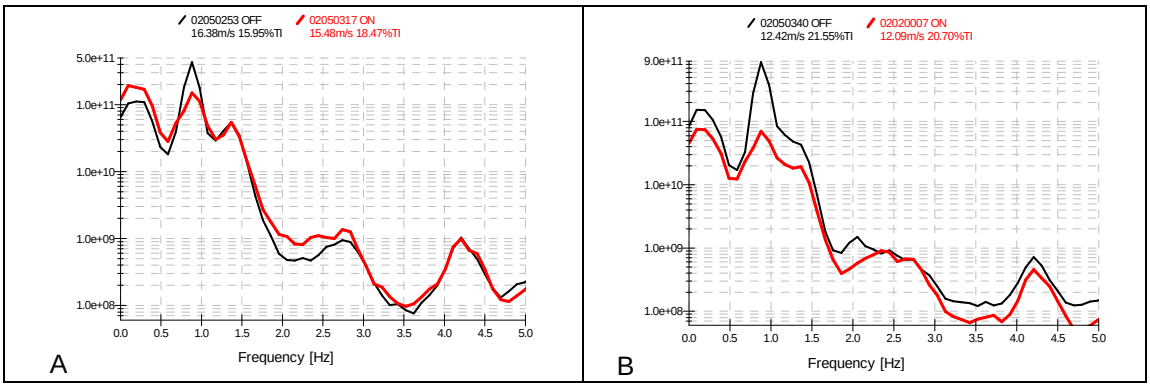

Figure 4.1: Spectra of tower base fore-aft bending moment

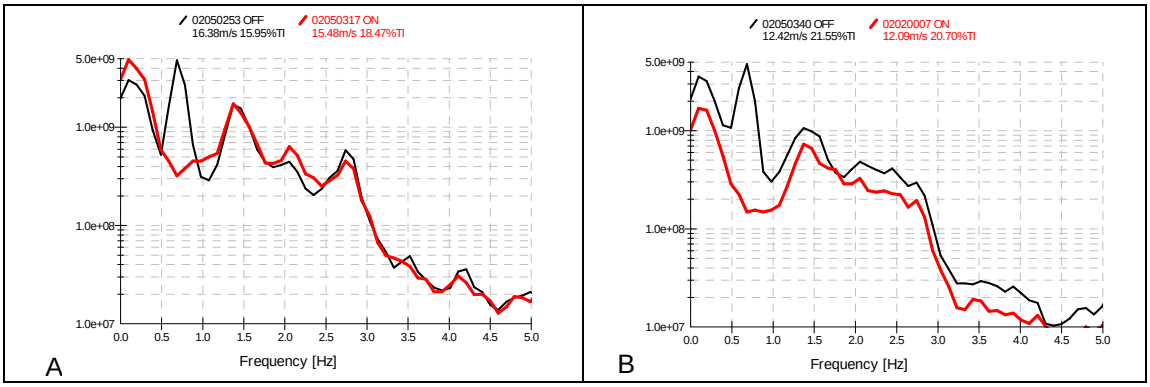

Figure 4.2: Spectra of blade root out of plane bending moment

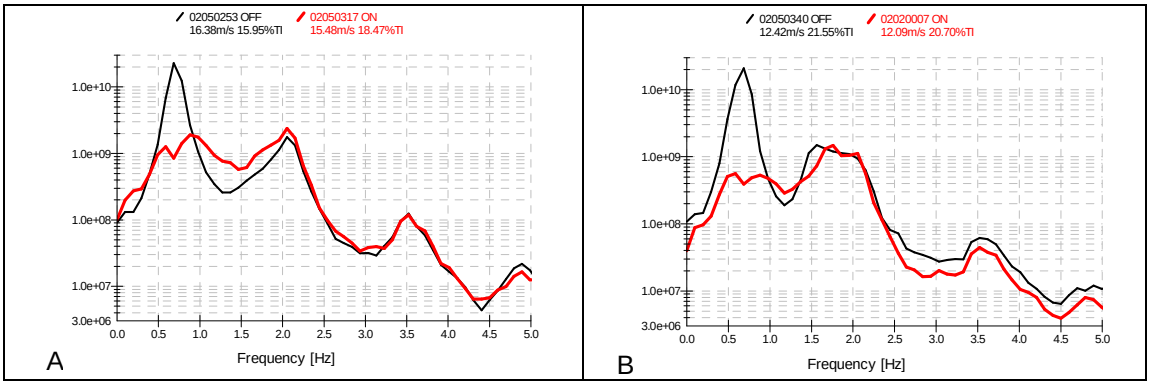

Figure 4.3: Spectra of shaft bending moment

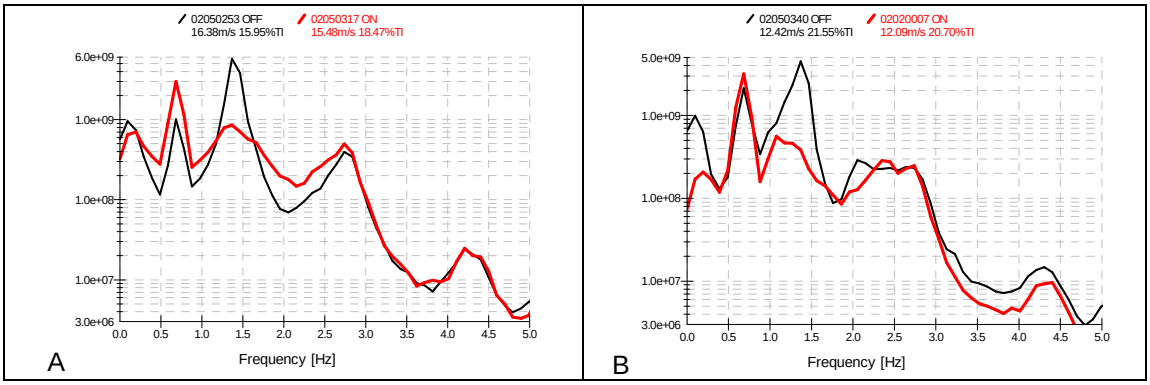

Figure 4.4: Spectra hub yawing moment

These results already demonstrate fairly conclusively that the predicted load reductions from IPC and FATD are achieved in practice. For a more complete assessment, a whole series of 10-minute datasets were processed to estimate the reduction in key damage equivalent loads and also to confirm that the loss of power production is negligible. Over 130 10-minute datasets were collected between 1st February and 13th April 2010. A number were not useful as the wind speed was falling away, and in some the turbine was only operating for part of the time, although some extracts of less than 10 minutes were still usable from these. In all 127 full or partial datasets were used in the analysis presented here.

For each dataset the mean wind speed and turbulence intensity at the hub height met mast was calculated. Only datasets with turbulence intensities within the range 10% - 25% and more than 300s in length were retained. This resulted in 48 datasets with the advanced features OFF and 56 with them ON. The distribution of points is shown in Figure 4.5.

These datasets were then processed in Bladed to calculate the 1Hz damage equivalent loads (DELs) as a measure of fatigue damage, using Wöhler exponent 4 (appropriate for steel) or 10 (for GRP composites). Plotting the DELs against wind speed already showed the reductions due to the advanced control, but inevitably there was scatter due to varying wind speed and turbulence. By binning the data into 1 m/s wind speed bins as in Figure 4.6 to Figure 4.11, the load reduction trends are clearly visible. The mean percentage damage equivalent load reductions for bins above 12 m/s are shown in Table 4.2.

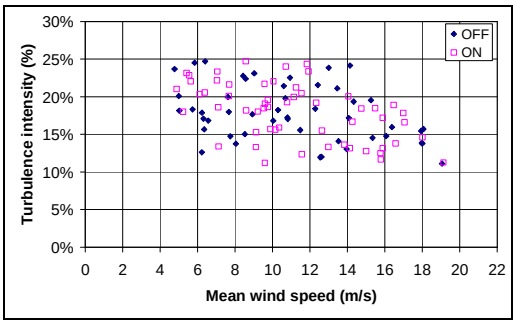

Figure 4.5: Spread of datasets

Blade root My, steel	9.4%
Blade root My, GRP	7.3%
Shaft My, steel	26.0%
Nod My, steel	10.0%
Yaw My, steel	14.4%
Tower My, steel	12.6%

Table 4.2: Load reductions above 12 m/s

Finally Figure 4.12 shows that there is no loss of output above rated as a result of IPC and FATD – in fact the power seems to be slightly increased in the 12 – 14 m/s region. In lower winds there is evidence of a slight decrease in power; but in the normal situation the IPC would be phased out in low winds anyway, as the loads are lower and the additional pitch action would not be justified.

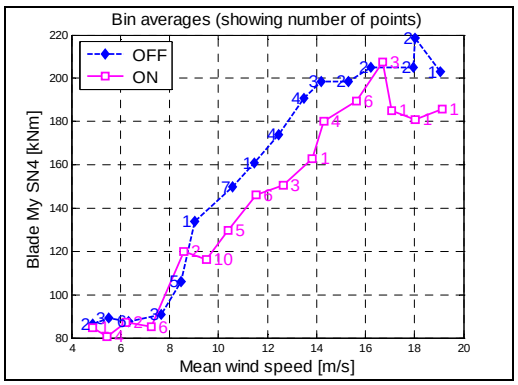

Figure 4.6: Blade root My DEL (steel)

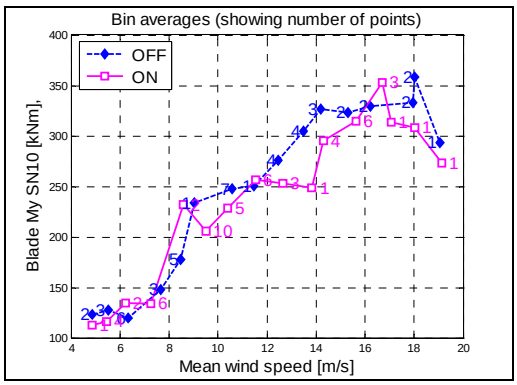

Figure 4.7: Blade root My DEL (GRP)

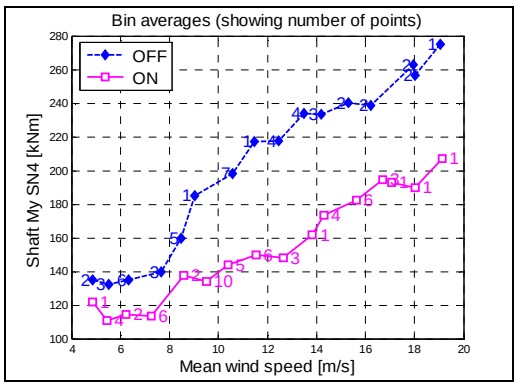

Figure 4.8: Shaft My DEL (steel)

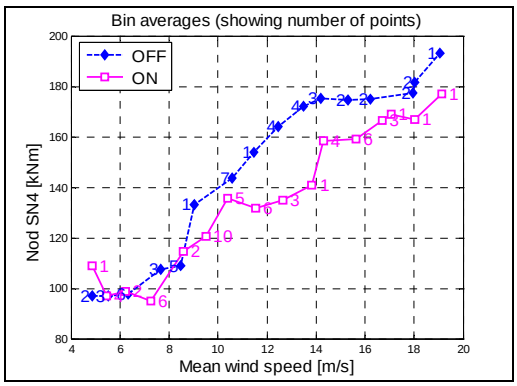

Figure 4.10: My Nod moment DEL (steel)

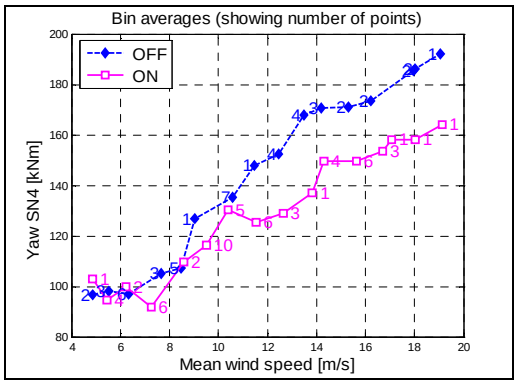

Figure 4.9: Mz Yaw moment DEL (steel)

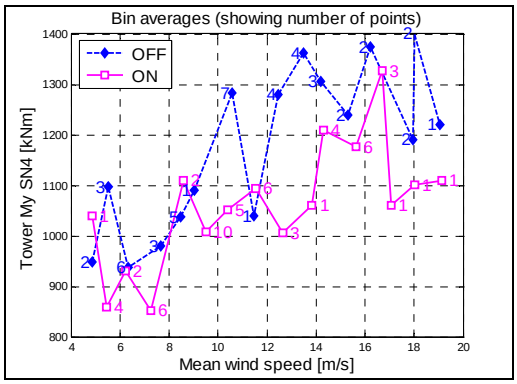

Figure 4.11: Tower My DEL (steel)

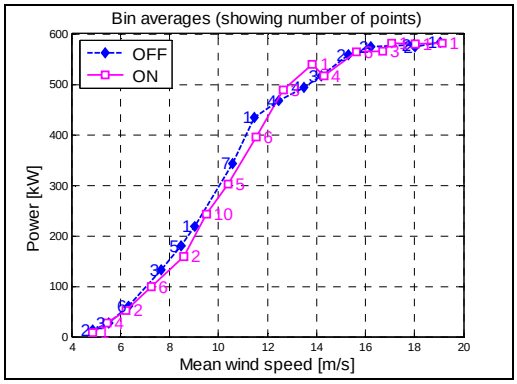

Figure 4.12: Power output

4.1.5 Conclusions from the field tests

The data collected from the CART2 field tests clearly shows that both the individual pitch control and the fore-aft tower damping algorithms work as expected, and that the load reductions predicted by simulations can be realised in practice, without significant loss of energy output. The fact that no adjustments of any significance needed to be made to the algorithms or parameter values confirms that these controller features are robust, and should provide the confidence required by turbine designers to be able to use these techniques as an integral part of turbine design in future.

4.2 Load reducing controller testing on CART3

Following the CART2 field tests, a similar exercise was undertaken using the 3-bladed CART3 turbine. The principal objectives were to demonstrate that the principles of IPC can also be applied successfully on 3-bladed turbines, and also to demonstrate that I this case, second-harmonic or 2P IPC can be added to achieve more significant fatigue load reduction on the non-rotating components. As with CART2, the tests also included tower damping (FATD).

The detailed results of the CART3 field tests are presented in Deliverable 5.6.2 [44].

4.2.1 The CART3 turbine

The CART3 turbine is a modified CART2, fitted with a new hub and three blades of a different design. The generator and power converter are also different. The turbine was intended to run at the same rated power and rotational speed as the CART2 (about 600 kW at 42 rpm). The turbine was first run in this configuration in early 2010, but significant dynamic problems were encountered. Significant efforts were made by NREL to understand these problems [46], and eventually the most likely cause was thought to be in the power electronics. Pending a final solution, the problems could be avoided by running at reduced speed and power (about 550 kW at 37 rpm), and these settings were therefore used for the field tests reported here.

A *Bladed* model of the CART3 turbine was built from information supplied by NREL, and used for an initial controller design incorporating IPC and FATD. The model was subsequently changed as a result of new parameter estimations resulting from data collected during the commissioning of the machine, and used to re-rune the controller before the tests started.

4.2.2 The CART3 controller

As in the case of the CART2, a power production control algorithm was designed for the CART3 based on up-to-date principles regularly used by GH for commercial controller design work [1],[7], and also applied to the UPWIND 5MW reference turbine as reported in Deliverable 5.1.1 [9]. The application of these techniques to the CART3 is similar and therefore not elaborated here in detail.

The controller includes the following features:

- Optimal power production, maintaining peak Cp over the whole nominal operating speed range
- Speed regulation by interacting PI-based torque and collective pitch control loops
- Drive train damping filter in torque controller
- Damping of fore-aft tower vibration by collective pitch control
- PI-based 1P and 2P individual pitch control loops to reduce rotating and non-rotating loads

For the field testing, the IPC and FATD action can be switched on and off during operation without affecting speed regulation, so by comparing test data with and without the advanced features, the load reduction can be quantified across a variety of wind conditions.

4.2.3 Simulation testing

To verify the controller design, a series of turbulent wind simulations were carried out using Bladed 4.0, with and without IPC and FATD, at 6, 9, 12, 15, 18, 21 and 24 m/s mean wind speeds, with turbulence intensities of 20% (longitudinal), 15% (lateral) and 10% (vertical). A small number of example plots from these runs are presented here, to illustrate the key features of the advanced control action. More results are presented in Deliverable 5.6.2 [44].

The effect of the 1P and 2P IPC is well illustrated in Figure 4.13, showing the effect on rotating loads, and Figure 4.14 for the non-rotating loads. The shaft bending moment spectra in Figure 4.13,show that dominant 1P peak is effectively removed by the 1P IPC action, but that there is also a significant peak at 2P, which the 2P IPC action removes. The tower top yaw moment spectra in Figure 4.14 demonstrate the reduction in low frequency (0P) loading by the 1P IPC action, because of the transformation to the non-rotating frame, and it also shows how the fatigue-dominating 3P load peak is removed by the 2P IPC action.

Figure 4.15 demonstrates the reduction in tower base loading at the first fore-aft tower frequency caused by the FATD action in the collective pitch control.

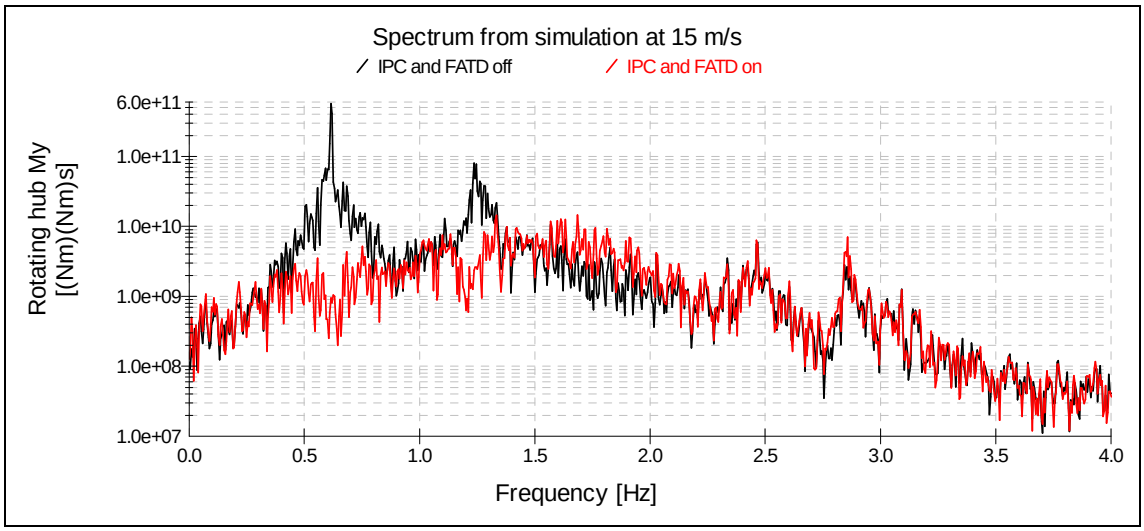

Figure 4.13: Shaft moment spectra at 15 m/s

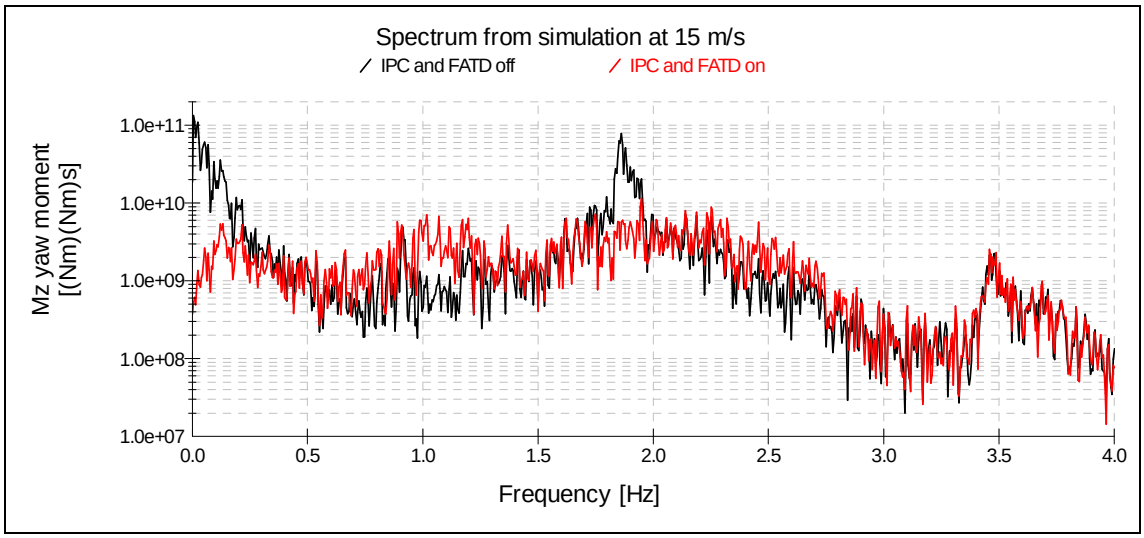

Figure 4.14: Yaw moment spectra at 15 m/s

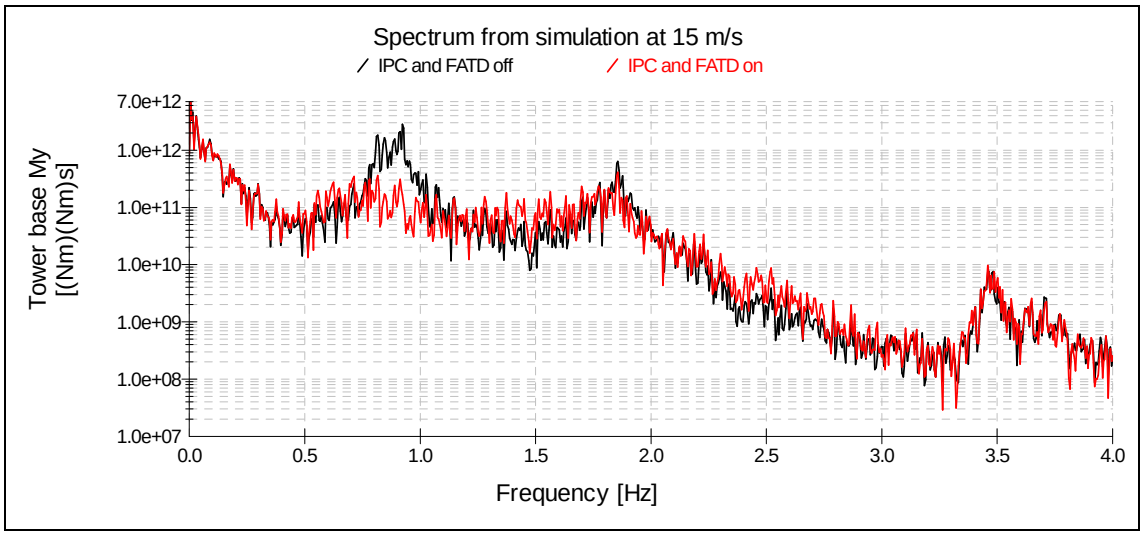

Figure 4.15: Tower base fore-aft bending moment spectra at 15 m/s

4.2.4 Field testing

After the above-mentioned dynamic problems on the CART3 were resolved, the turbine was finally commissioned and ready for testing in November 2010. Some initial running revealed various minor problems which had to be rectified before allowing extended operation with the new controller. This included a memory overrun caused by the DLL, a timestep overrun on the first DLL call, incorrect initialisation of the tower acceleration feedback integrator, and the need for two additional filters: a low-pass filter to prevent pitch actuator problems arising from high-frequency noise on the pitch demands, and a notch at the drive train frequency to prevent excitation by the collective pitch control. From mid-January 2011 a lack of wind prevented significant further data collection, so only some very preliminary indications are available at the time of writing. For example, Figure 4.16 shows two brief samples of IPC operation for a little over 100 seconds each, indicating a distinct reduction in shaft bending moment when IPC is switched on (red line at 100%). This is however at a low wind speed (8 m/s) when IPC would not normally be active.

GH and NREL have agreed to continue the programme of work so that a sufficient amount of data for detailed analysis can be obtained covering a range of wind speeds above rated.

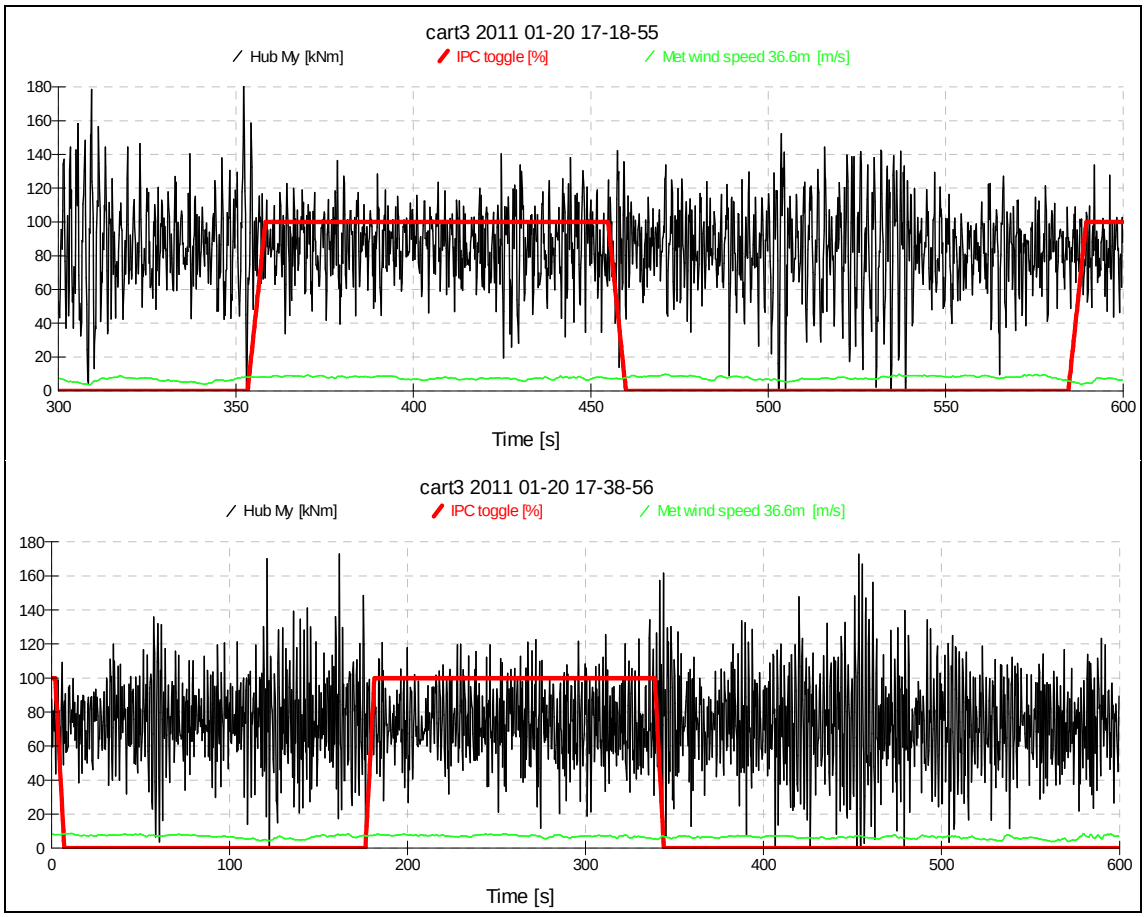

Figure 4.16: Brief data samples showing effect of IPC operation on shaft moment

4.3 Tower damping controller testing on a REpower turbine

The detailed results of the REpower field tests are presented in Deliverable 5.6.3 [45]. Some key results are summarised here.

REpower performed a half year field test to validate a new side-side tower damper that acts via individual blade regulation and a well known fore-aft damper, together referred as “tower damper”. Two neighbouring MM92 production turbines with 100 m hub height have been chosen as prototype, since turbines with high towers respond very well to active tower damping. Measurement results were compared quantitatively and qualitatively to former simulation output.

4.3.1 Active tower damping algorithms

The considered active tower damper consists of two controller components that operate independently from each other: a collective pitch controller to reduce fore-aft movements of the tower (tfa damper) and a cyclic pitch controller to reduce side-side movements of the tower (tss damper). Both components are add-ons to the standard speed controller and can be switched on and off during operation. Figure 4.17 shows the control structure design.

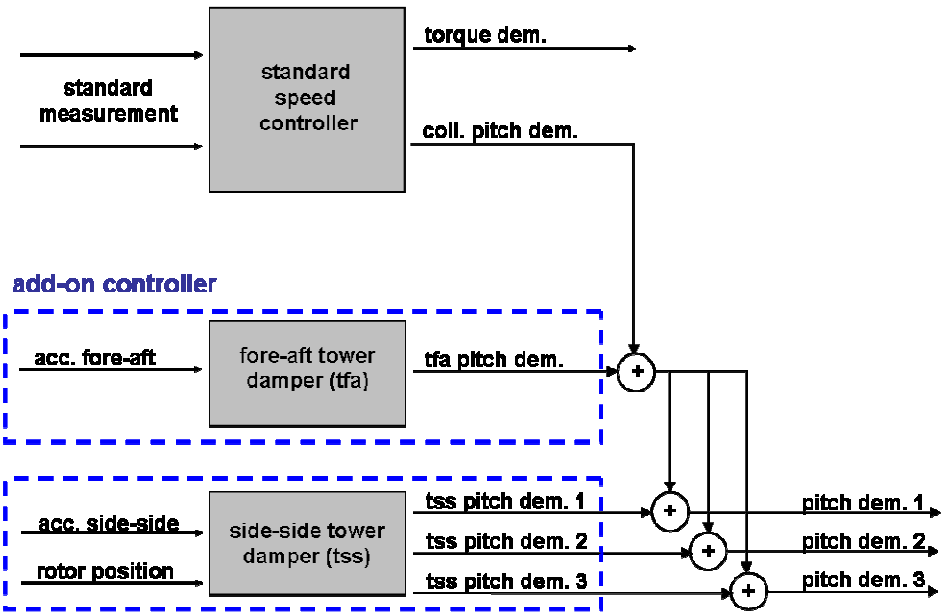

Figure 4.17: Control structure with standard speed controller, fore-aft tower damper and side-side tower damper

To implement a fore-aft tower damper an accelerometer is installed in the nacelle aligned to the fore-aft direction of the turbine. From the measured acceleration the algorithm calculates an additional collective pitch angle demand to regulate the thrust of the rotor. As a basic concept the blades are pitched in counter-phase with the tower displacement and thereby increase the aerodynamic damping of the tower. The tfa damper is configured to be active only close to and above rated wind. Thus, additional loads for the pitch device are moderate and it avoids negative effects on the energy production. This restriction has only small impact on the tower damage load reduction, as most damage occur above rated wind when the aerodynamic damping of the fore-aft vibration is lowered by pitch interaction of the speed controller.

The side-side tower damper requires the side-side acceleration and rotor position signals to calculate additional cyclic, individual pitch demands for each blade. The asymmetrical blade position results in a sidewise force at rotor hub that counteracts the side-side movements of the tower. There is only a light natural damping of side-side tower movements and even small rotor asymmetry of few tenths of a degree cause significant damping. The side-side damping is switched off below rated wind, so additional pitch drive loads are minimised and there is no negative influence on the energy yield.

The two tfa and tss dampers do not influence each other within certain bounds. Both algorithms are always switched on and off together in the following analysis.

4.3.2 Simulation results

Figure 4.18 illustrates the results of the full fatigue load simulation using Flex5 with IEC 2A conditions as an example. Depending on the component material the resulting damage equivalent loads are calculated for Wöhler exponent m = 4 (steel) or Wöhler exponent m = 10 (composite). Further the weighted standard deviation of the pitch rate is calculated to demonstrate the pitch activity. The graphic shows the relative change of damage equivalent loads by using active tower damping.

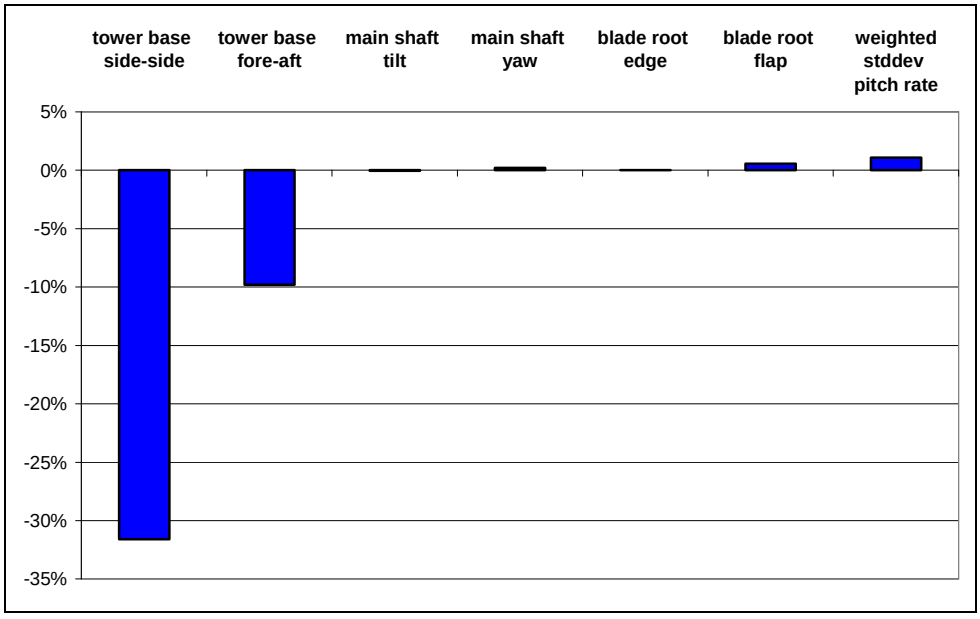

Figure 4.18: Relative change of damage equivalent loads by active tower damping in simulation, IEC 2A, m = 4 for tower base and main shaft and m = 10 for blade roots

Obviously both damping algorithms operate as expected and reduce the relevant loads without considerable negative side-effects:

- Reduction of tower base side-side loads by more than 30%
- Reduction of tower base fore-aft loads by more than 10%

There is almost no influence on main shaft and blade root loads visible. Even the pitch activity does not increase significantly (approx. 1%) and the power curve is untouched. Additional extreme load simulations verify that there is no considerable negative influence on any values.

4.3.3 Measurements

Two neighbouring turbines with quite similar inflow in the main wind direction are chosen as prototypes. One of the test turbines operates with active tower damping and simultaneously, the other turbine operates without active tower damping. To eliminate the influence of turbine and site particularities e. g. rotor imbalances, the turbines are switched in a 6-hours cycle.

The load measurement is carried out according IEC 61400-13 with a reduced set of considered load cases and sensors. Only power production is taken into account while the tower base bending moments are measured with strain gauges.

The loads are measured over 10-minute periods, and damage equivalent loads are generated through rain-flow counting procedures. As a basis a mean wind speed of 8.5 m/s according to IEC 61400-1 ed.3 class II has been taken into account. Since measurements do not cover the whole operating wind range, the Weibull distribution is modified: The time portions for high wind speeds with no data available are summed up and dispensed evenly to the more frequented wind bins above rated wind speed.

Figure 4.19 shows the measured and simulated relative mitigation of damage equivalent loads by using active tower damping for the modified Weibull distribution. The relative mitigation of fore-aft tower loads in the simulation is a little bit bigger than the measured one while the simulated side-side tower load mitigation is somewhat smaller than in the measurement. Considering general uncertainties in load comparisons the load mitigations match astonishingly well. The power curve is not influenced by the tower damper, neither was increased pitch activity noticed.

Frequency analysis of measured fore-aft and side-side acceleration confirm the proper performance of the active tower damping as well.

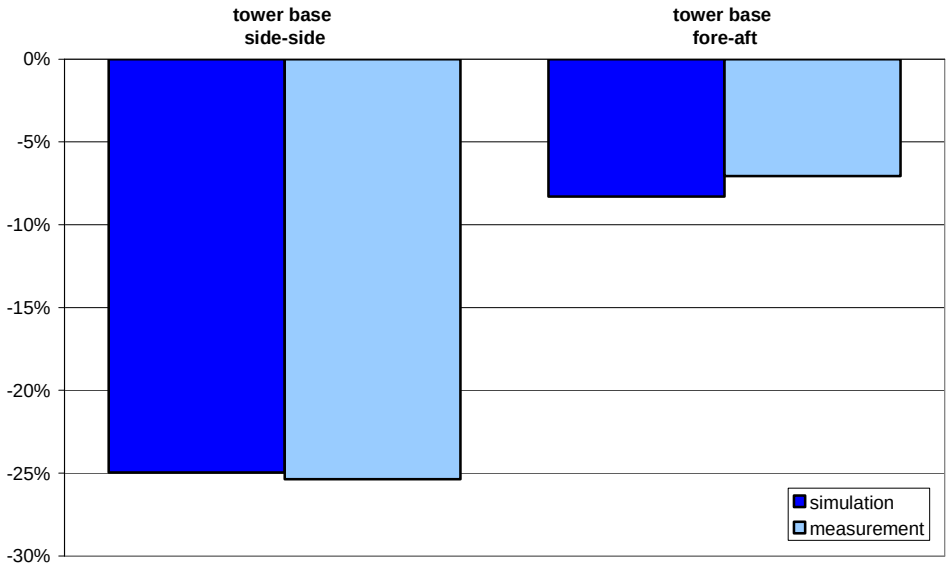

Figure 4.19: Relative mitigation of damage equivalent loads by active tower damping in simulation and measurement for modified Weibull distribution, m=4

4.3.4 Conclusion

Simulations show that the tower damping algorithms allow a reduction of tower fatigue loads without significant negative side-effects to other loads. Especially the reduction of side-side loads by using the new side-side tower damper is high. Load measurement results demonstrate that the load reductions predicted by simulation can be obtained in reality. Now the algorithms may be applied to series turbines, e. g. to upgrade an established turbine type to match higher wind class conditions, which is done presently. The active tower damping should be considered too, when designing offshore towers and foundations, even though another validation might be advisable as especially side-side excitations by waves are much stronger than by wind.

5. Electrical interaction with the network

As turbines become larger and as penetration of wind energy increases, it becomes increasingly important to control the interactions between the turbines themselves and the electrical network, both from the point of view of the loading seen by the turbine during network transients and from the point of view of network security and power quality.

5.1 Review of electrical drive train topologies

One of the first tasks in the work package was to examine the various options available for generators and power converters, and to assess their suitability for different turbine designs and for complying with network requirements.

Various turbine options were considered, including:

- Fixed Speed Induction Generator (FSIG)
- Variable Ratio Transmission (VRT)
- Variable Slip Induction Generator (VSIG)
- Double Fed Induction Generator (DFIG)
- Full Converter connected generator (FC)

The variable speed options (DFIG, FC) are now most commonly used, the latter sometimes in combination with direct drive transmissions requiring a large multipole generator. The FC option usually uses a synchronous generator, using either permanent magnets or a wound rotor.

Each option was examined from the point of view of the principal network compatibility criteria:

- Frequency and voltage tolerance
- Fault Ride through
- Reactive power and voltage control capability
- Operating margin and frequency regulation
- Power ramping

The detailed results are presented in Deliverable 5.8 [40], but Table 5.1 presents a brief summary table, indicating that the full converter option is most likely to satisfy all requirements effectively.

	Wind Turbine Type			
Grid Code Req.	**FSIG**	**DFIG**	**FC**	**VRT**
Voltage & Frequency Range	✓	✓✓	✓✓✓	✓
Fault Ride Through	✓	✓✓	✓✓✓	✓✓
Reactive Power	✓	✓✓	✓✓✓	✓✓
Operating Margin & Frequency Regulation	✓	✓✓	✓✓✓	✓✓✓
Power control	✓✓	✓✓	✓✓✓	✓✓✓

Table 5.1: Scoring of WTG types against Grid Code requirements

5.2 Riding through grid faults

DFIG wind turbines have experienced a massive employment during the last years because of their capabilities to deal with grid faults, their well-know generator and power converter technologies, and relatively low cost. This fact motivates the implementation of an accurate model of the DFIG to study its behaviour under grid disturbances so that the fulfilment of the different Grid Codes can be analysed and the wind turbine control can be improved to reduced loads. These later studies have been done compiling this DFIG model implemented in Simulink© into a dynamic link library (DLL) and linking it with an aeroelastic wind turbine model developed in GH Bladed©.

This section describes both electrical and control parts of the DFIG and their modelling, explaining its behaviour under grid fault conditions (FRT) and showing the model validation methodology with a comparison between simulations and tests.

The full results are presented in Deliverable 5.9.2 [42].

5.2.1 DFIG model: electrical and control description

The electrical system of the wind turbine consists of a generator, which is a Doubly Fed Induction Generator (DFIG), whose rotor is supplied by a bidirectional converter (Machine Side Converter (MSC) and Line Side Converter (LSC)) based on IGBT technology having three phase legs of IGBTs connected to the generator rotor windings, a DC bus and a second set of three phase legs connected to the grid by means of a power transformer. This can be seen in Figure 5.1.

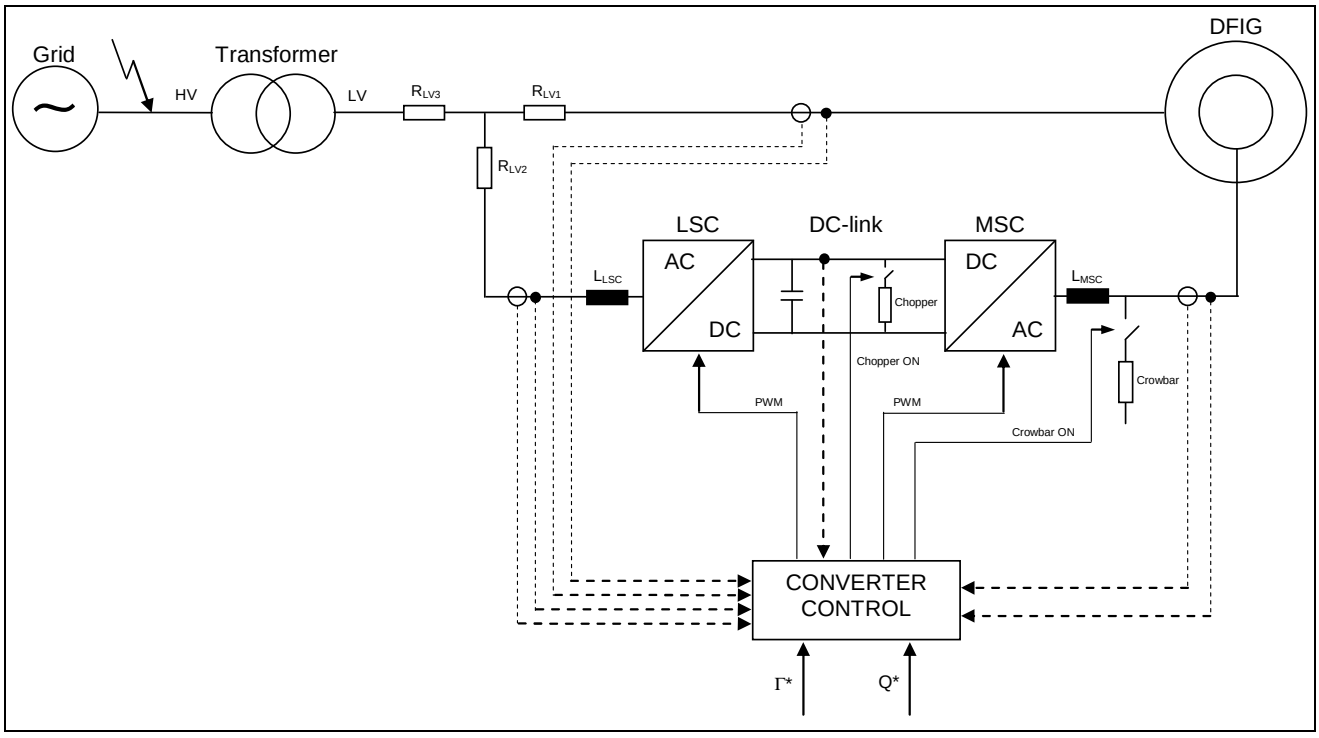

Figure 5.1: Single line diagram of the wind turbine: electrical and control systems modelled

This system has been modelled in Simulink© without considering the effects of high switching frequency components, like power converters. This means that these components are replaced

with their low-frequency average counterparts, without having the computational burden of high-frequency details.

A detailed converter control diagram implemented in the model can be seen in Figure 5.2. The converter control receives torque (active power is also possible) and reactive power references (PF is also possible) to apply from the wind turbine control in base on an internal speed control loop (torque reference) and the current grid requirements (reactive power). These references are converted into d-q desired currents on the MSC and LSC, and by means of an internal current loop results both d-q MSC and LSC voltages to apply by the converters.

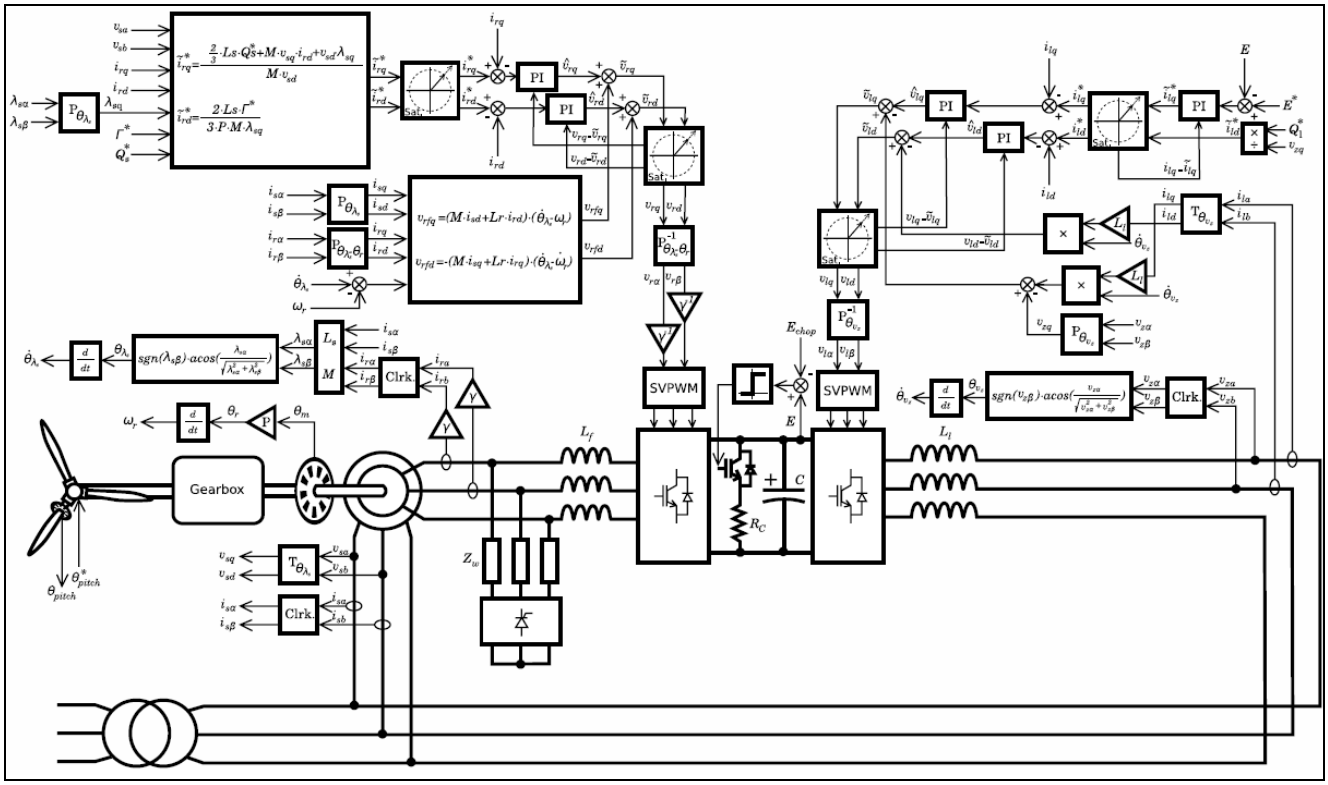

Figure 5.2: Detailed converter control diagram implemented

5.2.2 Fault Ride Through operation mode – basic description

In order to withstand line faults the electrical system is equipped as shown in Figure 5.1. Two key elements protect the machine against overvoltages/overcurrents and permit to remain connected to the grid when a fault is provoked: a Chopper and a Crowbar.

The Chopper consists of an active switching means (IGBTs) and series-connected resistor. This element balances power fluctuations in the intermediate link of the converter caused by grid faults. Measuring the DC-voltage the Chopper is switched on when a critical DC-link voltage threshold is exceeded. Beneath a lower uncritical DC-link voltage threshold, the measuring device switches the Chopper off. The excessive power is dissipated in the Chopper resistor.

As back-up protection means for the converter in case of Chopper failure, a Crowbar is installed parallel to the MSC. It consists of three thyristors (SCR) and a three-phase series-connected damping-resistor. If the DC-link voltage exceeds a defined threshold above the Chopper threshold, a malfunction of the Chopper is detected and the Crowbar is switched on. In this case the system separates from the grid.

Once a fault is detected by the converter, an especial strategy is applied to fulfil the Grid Code of the country where the machine is installed. That means to provide active current (active power) if it is necessary and to deliver/consume reactive current (reactive power) during the fault according to the specifications. To comply with active current requirements, the wind turbine control is in charge of demanding to the converter a proper torque/power reference. On the other hand, reactive current commands are directly managed by the convert control, having parameterised a proper *voltage-reactive current* characteristic to set these reactive current commands depending on the voltage level.

5.2.3 Comparison between simulations and tests

A voltage dip test campaign (SAT) was carried out in the ECO100 prototype wind turbine during the second term of 2009. This has provided useful information and measurements to validate and adjust the model of this machine, taking into account the methodology followed in Figure 5.3.

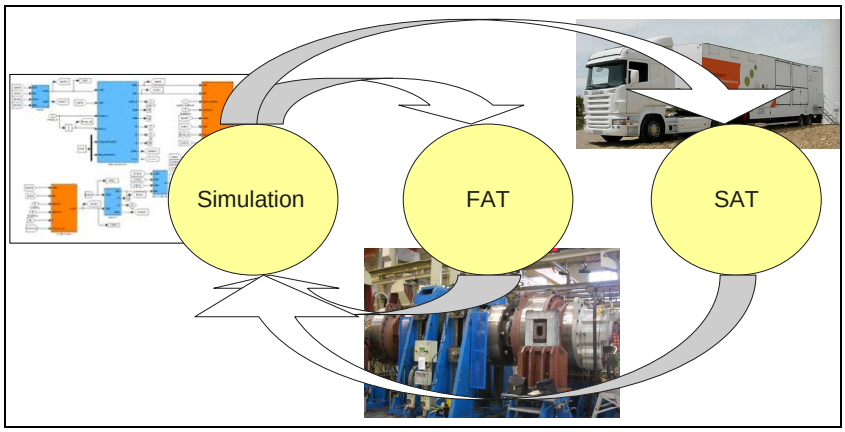

Figure 5.3: Simulation and tests methodologies for the validation of models (FAT: Factory Acceptance Test, SAT: Site Acceptance Test)

Figure 5.4 to Figure 5.6 show the comparison between simulation and test of the above mentioned wind turbine in case of a 3 phase 50% 710 ms voltage dip (included in the UK Grid Code), proving a very good agreement between them.

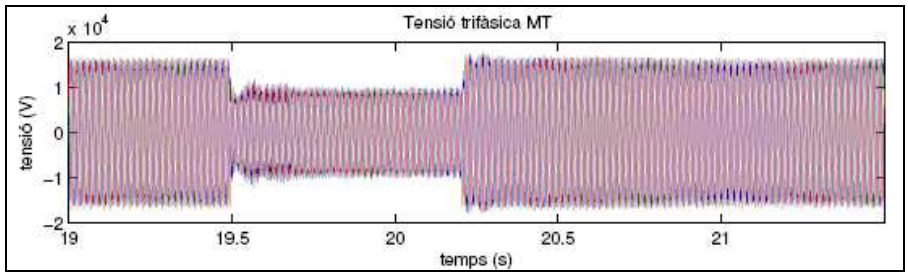

Figure 5.4: A 3ph 50% 710 ms voltage dip on HV point shown in Figure 5.1 (both simulation and test)

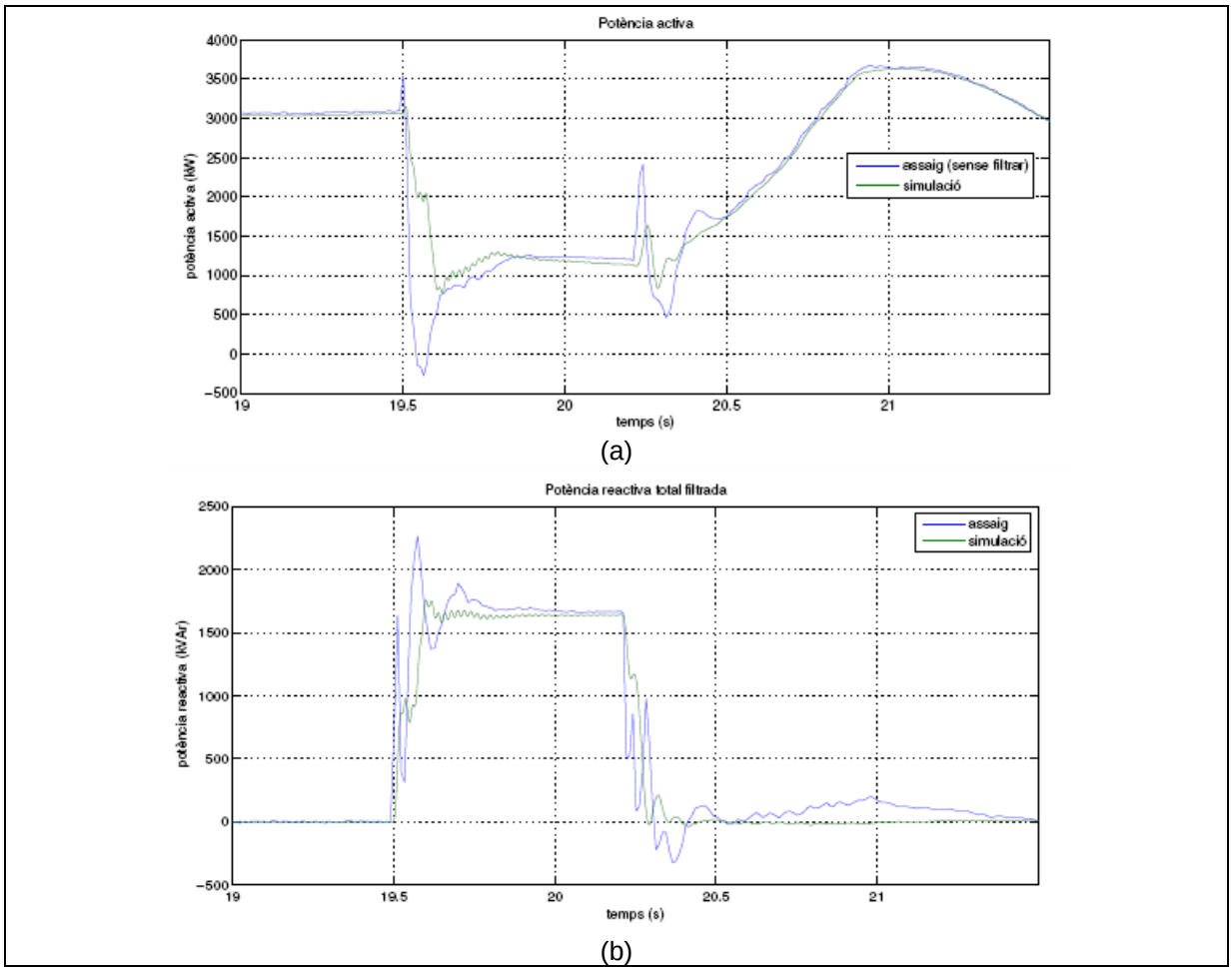

Figure 5.5: (a) Active power (blue line: test, green line: simulation), (b) Reactive power (blue line: test, green line: simulation)

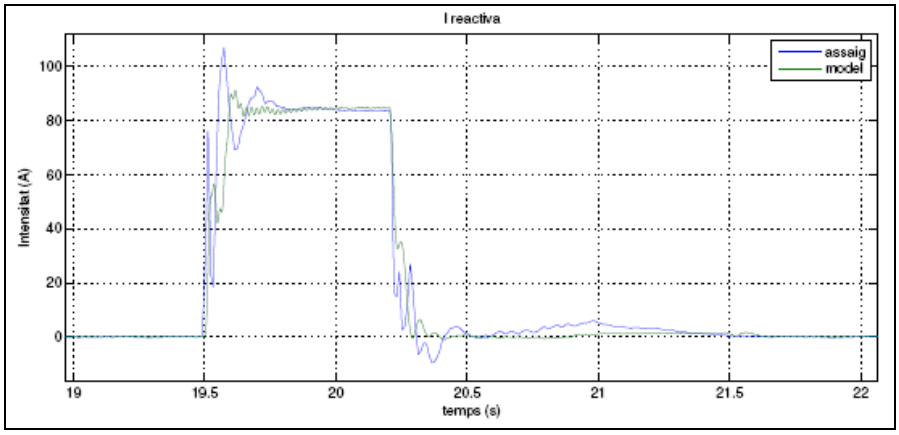

Figure 5.6: Reactive current (blue line: test, green line: simulation)

5.2.4 Conclusion

This work has demonstrated how the coupled dynamics of the turbine structure, control system and electrical system can be modelled accurately and in sufficient detail to allow grid code requirements to be fully taken into account during the design of the whole system.

5.3 Impact of drive train on wind farm VAr control

Utilities generally require wind farms to maintain the voltage at the point of interconnection (POI) to the grid. This can be performed by actively regulating the reactive power from wind turbine generators, a scheme that is often termed wind farm VAR control.

The work reported here is based on a case study for a future large-scale offshore wind farm and the evaluation of the impact of the choice of drive train on wind farm-grid performance in terms of voltage control. The detailed results are presented in Deliverable 5.9.1 [41]. The study investigated:

- The effect of long cables and how well the voltage is controlled
- Setting up a criterion for evaluating the performance of the wind farm VAR control
- Voltage compensation under system disturbances
- Voltage regulation with and without high bandwidth power electronics within the system
- The effect of grid strength level and the number of connected wind turbines on tuning the wind farm VAR control

A large-scale offshore wind farm was the focus of this study where the turbine rating and size of the farm are in line with the future needs of the industry, and the farm layout was based on case studies developed in the Upwind work package WP9.4.2 [48].

5.3.1 Modelling

The performance of the systems was modelled and investigated using the GE PSLF load flow and dynamic simulation software [49]. Various aspects that were modelled included:

- Drivetrain topologies involving power electronic grid interfaces, such as for Doubly Fed Induction Generators (DFIG) and Full converter Connected generators (FC). For such devices (Figure 5.7) the electrical dynamic performance is dominated by the converter
- Variable Ratio Transmission (VRT) with synchronous machine interfaces, which along with their associated excitation system govern the system dynamics. Both static and brushless excitations systems were investigated
- Collector and transmission system including HV cables (Figure 5.8).
- Wind farm VAR control system which includes the individual WTG terminal voltage and reactive power loops, along with the farm level supervisory VAR control which regulates the voltage at the POI by allocating reactive power commands to the WTGs. Different control structures were examined including the impact of explicitly limiting the reactive power command to take into account WTG capability.

An aggregate approach to modelling the generators was used. The system shown (Figure 5.8) included a single WTG model rated at 360MVA (324MW) representing the aggregation of 54 WTGs each of 6MW, along with an aggregate WTG transformer and a 34.5kV feeder medium voltage collector system. A 360 MVA substation transformer was included to step-up the MV distribution system level to the high voltage (HV) system level, which eass assumed to be at 150kV (Bus 2). An equivalent impedance was used to represent the HV subsea transmission cables for power transmission to shore. A transmission distance of 30 km was used in the case study.

Different grid short circuit ratios (SCRs) at the POI were considered, representing relatively weak to strong grid systems and the impact of changing the number of WTGs online was also examined. Methods for tuning the control systems, and the impact on performance under various scenarios were examined.

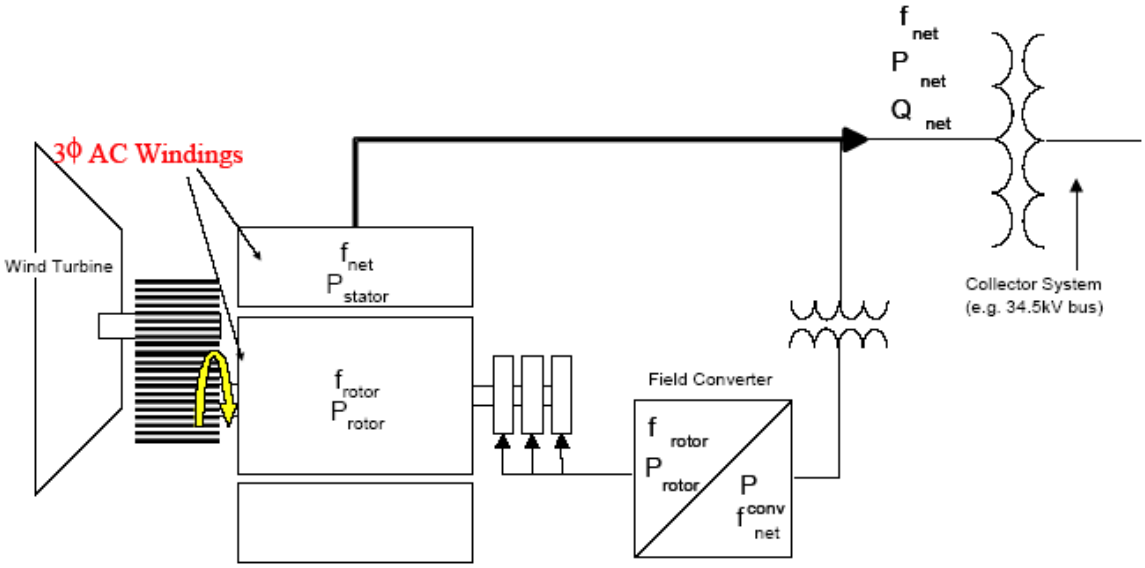

Figure 5.7: DFIG system major components.

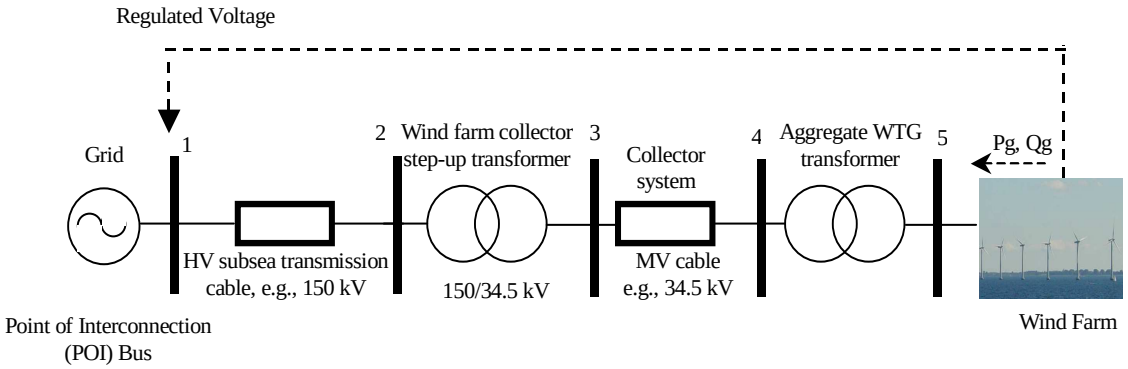

Figure 5.8: Test System.

5.3.2 Impedance Allocation of Test System Components

Figure 5.9 shows the impedance in percent of the different system components with different SCRs. It shows that the equivalent WTG transformer and collector transformer as well as the grid impedances constitute the major parts of the total system impedance and should be carefully considered. The distance of the wind farm from the shore and therefore the length of the HV transmission cables has relatively little impact on the system impedance.

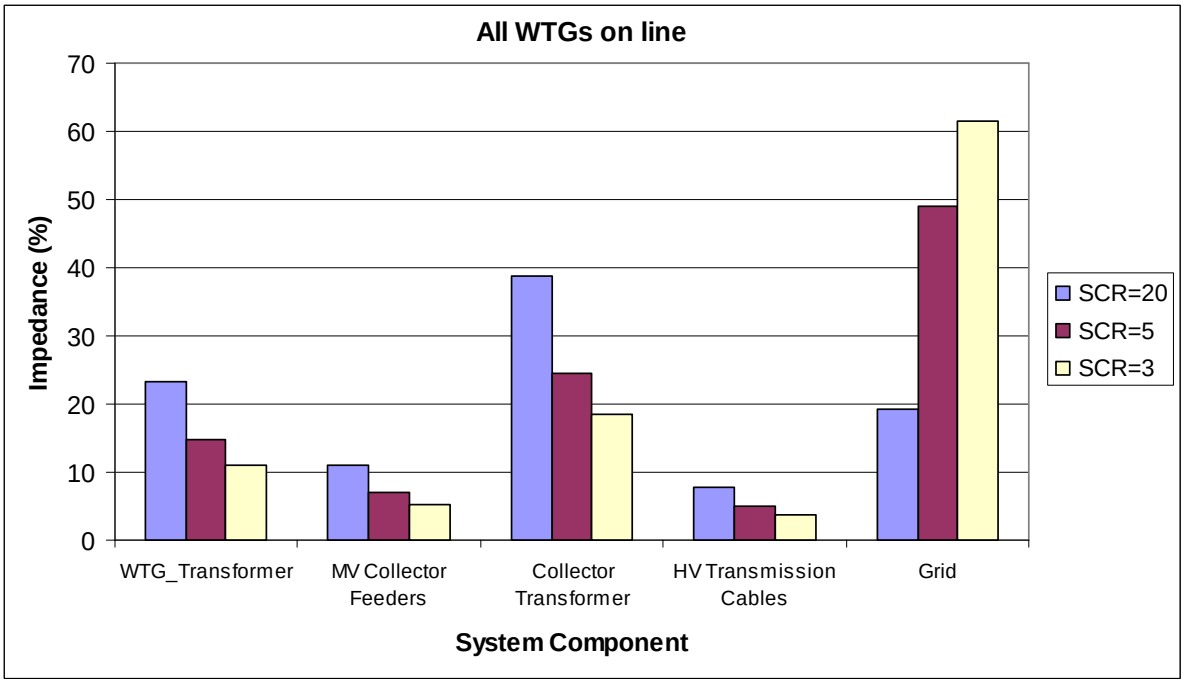

Figure 5.9: Impedance allocation of system components with all WTGs online.

5.3.3 VAR Control

The main factors affecting the wind farm VAR control were investigated in detail with the following findings:

- The grid short circuit ratio (SCR) level has a major impact on the control design and response.
- Monitoring the number of connected WTGs is important for updating the control parameters. With over 50% of connected WTGs online, the impact is relatively insignificant. However with lower fraction of WTGs online, adapting the control scheme parameters is recommended for more robust control and for achieving roughly the same VAR control time response with different numbers of connected WTGs.
- In general a trade-off is observed between the performance of the systems and robust stability properties in the presence of grid impedance variations
- With well-tuned control parameters, the VAR control performance with the conventional synchronous machines could have similar time responses to that obtained with the DFIG or FC machine types with power electronics grid interface.

For synchronous machine WTG types, two VAR control strategies were investigated.

- The first strategy had only a WTG voltage control loop. This did not take into account the machine reactive power capability, which can be exceeded particularly with higher SCR systems. In this case voltage collapse caused by system disturbances was found to be a possibility if control parameters were chosen so that the VAR control response was faster than that of the WTG excitation system. This is important particularly with the brushless excitation system, which has a slower time response.
- The second VAR control strategy included an additional reactive power control loop, with slightly slower overall response, but maintaining stability and respect the machine reactive power capability.

6. Conclusions

This report summarises some key findings arising from the Control Systems work package of UPWIND which have the potential to improve the cost-effectiveness of future wind turbine designs. Most of these results are presented in more detail in published reports covering each specific area.

The principle of load reduction through control action is well known, but there has been a need for field test data to provide confidence in these methods. The three sets of field tests undertaken by this work package have made a significant contribution here. The tests on the NREL CART2 turbine have clearly demonstrated successful and robust operation of individual pitch control (IPC) on a real machine, while the REpower tests have convincingly demonstrated a side-side tower damping technique using cyclic pitch control, which could be valuable especially offshore. Tests on the NREL CART3 turbine are not yet completed but early indications are positive; this should provide confidence in higher-order IPC for additional load reduction. All three tests included fore-aft tower damping through collective pitch action, which is now well validated. These results should provide the confidence which turbine designers need to incorporate these techniques in future designs.

There as also been a concern that the fatigue load reduction effect achieved by individual pitch control may be tempered by increased extreme loads. This has been resolved by developing a relatively simple modification allowing IPC to be phased out in advance of possible shutdowns. Using the 5MW reference turbine, a complete set of load calculations according to the IEC standard has demonstrated that using IPC, the extreme loads are no greater than with collective pitch control but the fatigue loads are still reduced as expected.

The possibility of dual pitching blades has been investigated and shown to provide large potential benefits in reduced blade loads. This must be traded against the cost and reliability implications of the additional mechanism.

Advanced control action requires additional sensors, which also have some cost and reliability implications. Work on load estimation has demonstrated how appropriate algorithms can be used to estimate certain loads, reducing the need for additional sensors. Again, field tests have demonstrated the operation of these algorithms.

A Lidar system to measure approaching winds is also a sophisticated additional sensor. Although still somewhat expensive, early results demonstrate their effectiveness in reducing loads, which may well lead to an overall improvement in cost-effectiveness of large turbines.

The characteristics of a real wind turbine will always differ to some extent from those assumed at the design stage, which may mean that controller re-tuning may be necessary during commissioning. System identification techniques are used to characterise the as-built turbine. Closed loop identification algorithms have been developed which allow the characteristics to be identified safely while the turbine is in closed loop operation.

Simulations are vital during the design process, but hardware-in-the-loop simulations are increasingly being used to validate the systems as far as possible prior to actual commissioning in the field. Turbine controllers are tested by linking to detailed dynamic simulations of the rest of the turbine so that they can be tested under realistic conditions. A pitch actuator test rig has now also been linked into a hardware-in-the-loop simulation, so that real pitch actuator motors replace the simulated actuators, allowing the real performance of the pitch actuators during IPC operation to be measured, and confirming that the effectiveness of the IPC action is not compromised by any limitations of the real actuators.

As the penetration of wind energy on the electricity network increases, a number of system integration issues are becoming increasingly important. Three specific aspects of this have been covered by this work package: low voltage ride-through (LVRT) capability, VAR control, and soft cut-out strategies for high wind.

LVRT is becoming mandatory, and to study this properly, a complete and integrated simulation model is required which includes not only the turbine aeroelastic, structural and controller dynamics but also the electrical dynamics. Such a model was constructed by linking the *Bladed* wind turbine simulation package to a detailed electrical model of a DFIG generator and converter system, and the complete model validated against field test data collected during voltage dip tests. The model can now be used to optimise the turbine control action to ensure that the constraints of turbine loading and grid code compatibility can be satisfied simultaneously.

VAR control is increasingly required, meaning that utilities require wind farms to maintain the voltage at the point of interconnection (POI) to the grid. This can be performed by actively regulating the reactive power from wind turbine generators. A case study for a future large-scale offshore wind farm has examined the options for VAR control in different situations and evaluated the impact of the choice of drive train on voltage control performance.

Finally, the conventional high-wind cut-out strategy, usually when the mean wind speed exceeds 25 m/s, means that as a storm passes, the wind power output from a region may suddenly fall dramatically as turbines shut down. Also the predictability of the output is very poor because the predicted output can change by 100% as a result of a very small error in wind speed prediction. This problem can be mitigated by more gradual shut-down strategies, but it is important to consider the effect of this strategy on wind turbine loading, both fatigue and extreme, and on energy capture. The work package has examined the effect of such soft cut-out strategies, and concluded that if sufficient care is taken over tower vibration (both fore-aft and side-side), and as long as the full effect of idling loads in the conventional case is considered, a suitable speed and torque ramping strategy can be designed which has the desired effect without significant increases in any of the critical loads, and without compromising energy production.

7. References

[1] E Bossanyi, Developments in Individual Blade Pitch Control, “The Science of making Torque from Wind”, Delft University of Technology, The Netherlands, April 19-21 2004.

[2] E. Bossanyi, A. Wright, Field testing of individual pitch control on the NREL CART-2 wind turbine, proc. European Wind Energy Conference 2009.

[3] E. Bossanyi, A. Wright and P. Fleming, Further progress with field testing of individual pitch control, proc. European Wind Energy Conference 2010.

[4] E. Bossanyi, A. Wright and P. Fleming, Progress with field testing of individual pitch control, proc. Conference on the science of making torque from wind, The European Academy of Wind Energy, June 2010.

[5] M. Rossetti, E. Bossanyi, Damping of tower motions via pitch control – theory and practice, proc. European Wind Energy Conference 2004.

[6] K A Stol, Geometry and Structural Properties for the Controls Advanced Research Turbine (CART) from Model Tuning, August 25, 2003–November 30, 2003, NREL/SR-500-32087, http://www.nrel.gov/docs/fy04osti/32087.pdf

[7] E Bossanyi, Wind Turbine Control for Load Reduction, Wind Energy 2003 vol 6 pp 229-244.

[8] E. Bossanyi and D Witcher, A state-of-the-art controller for the 5MW UPWIND reference wind turbine, Proceedings of European Wind Energy Conference 2009.

[9] E Bossanyi and D Witcher, Controller for 5MW reference turbine, Upwind Work Package 5 deliverable report 11593/BR/04, 10th July 2009, http://www.upwind.eu/Shared%20Documents/WP5%20-%20Publications/D%205.1.1.%20Controller%20for%205MW%20reference%20turbine.pdf

[10] E. Bossanyi, A. Wright and P. Fleming, Controller field tests on the NREL CART2 turbine, Upwind Work Package 5 deliverable report 11593/BR/08, 22/06/2010, http://www.upwind.eu/Shared%20Documents/WP5%20-%20Publications/D%205.6.1.pdf

[11] E.A. Bossanyi, “Further load reductions with individual pitch control”, Wind Energy, 8, 2005.

[12] B. Savini, E.A. Bossanyi, “Supervisory Control Logic Design for Individual Pitch Control”, Poster presented at EWEC 2010, Warsaw Poland, April 20-23 2010.

[13] B. Savini, R Lupton, “Supervisory controller and load calculation for 5MW reference turbine”, Upwind Work Package 5 deliverable report 11593/BR/06/B, January 2011, http://www.upwind.eu/Paginas/Publications/5%20Control%20systems.aspx.

[14] E. A. Bossanyi. (2000). Developments in Closed Loop Controller Design for Wind Turbines. *ASME Wind Energy Symp.*, Reno, NV, US, pp. 64–74.

[15] M. Hau. (2008). Promising load estimation methodologies for wind turbine components. Upwind Deliverable 5.2, 29/05/2008, www.upwind.eu/Shared%20Documents/WP5%20-%20Publications/D5.2_PromisingLoadEstimationMethodologies.pdf.

[16] B. Jasniewicz. (2010) Online estimation of mechanical load for wind turbines. Upwind Deliverable 5.3, 9th February 2011, http://www.upwind.eu/Paginas/Publications/5%20Control%20systems.aspx.

[17] E. A. Bossanyi. (2003). Individual blade pitch control for load reduction. *Wind Energy,* 6, pp. 119–128.

[18] C. L. Botasso, A. Croce. (2009). Cascading Kalman Observers of Structural Flexible and Wind States for Wind Turbine Control, Dipartimento di Ingegneria Aerospaziale, Politecnico di Milano, DIA-SR 09-02

[19] K. Selvam, S. Kanev, J. W. van Wingerden, T. van Engelen and M. Verhaegen. (2009). Feedback-feedforward individual pitch control for wind turbine load.

[20] P. Caselitz, W. Kleinkauf, T. Krüger, J. Petschenka, M. Reichardt, K. Störzel. (1997). Reduction of Fatigue Loads on Wind Energy Converters by Advanced Control Methods. *Proceedings of the European Wind Energy Conference EWEC*, Dublin Castle, Ireland.

[21] A. D. Wright, L. J. Fingersh, K. A. Stol. (2007). Designing and testing controls to mitigate tower dynamic loads in the controls advanced research turbine. 45th AIAA Aerospace Sciences Meeting and Exhibit, Wind Energy Symposium. Reno, NV, US.

[22] G. Bir. (2008). Multiblade Coordinate Transformation and Its Application to Wind Turbine Analysis. *ASME Wind Energy Symp*., Reno, NV, US.

[23] H. Kwakernaak, R. Sivan. (1972). *Linear optimal control systems*. Wiley, New York.

[24] S. Skogestad, I. Postlethwaite. (2005). *Multivariable Feedback Control*. Wiley.

[25] Multibrid GmbH. (2010, June 8). M5000 Technical Data. Retrieved from http://www.multibrid.com/fileadmin/infomaterial/MB_Datenblatt_UK.pdf.

[26] Schlipf, D. and Kühn, M.: *Prospects of a Collective Pitch Control by Means of Predictive Disturbance Compensation Assisted by Wind Speed Measurements*, Proc. DEWEK 2008, Bremen, Germany, 2008.

[27] Rettenmeier, A., Bischoff, O., Hofsäß, M., Schlipf, D., Trujillo, J. J., and Kühn, M.: "*Wind field analyses using a nacelle-based LIDAR system*, Proc. EWEC, Warsaw, Poland, 2010.

[28] Lindelöw, P.: *Fiber Based Coherent Lidars for Remote Wind Sensing*, Ph.D. thesis, Danish Technical University, Copenhagen, Denmark, 2008.

[29] Schlipf, D., Trabucchi, D., Bischoff, O., Hofsäß, M., Mann, J., Mikkelsen, T., Rettenmeier, A., Trujillo, J. J., and Kühn, M.: *Testing of Frozen Turbulence Hypothesis for Wind Turbine Applications with a Scanning LIDAR System*, Proc. ISARS, Paris, France, 2010.

[30] T.G. van Engelen, Control design based on aero-hydro-servo-elastic linear models from TURBU (ECN), in Sc. Proc. European Community Wind Energy Conf., 2007, Milan, Italy.

[31] J.B. Dragt, Atmospheric turbulence characteristics in the rotating frame of reference of a WECS rotor, in Proc. European Community Wind Energy Conf., 1990, Madrid, Spain.

[32] T.G. van Engelen, P. Schaak, Huge Oblique Inflow Model for Assessing Wind Turbine Controllers, internal ECN note and delayed submitted to Conf. of Making Torque from Wind, 2007, Copenhagen, Denmark.

[33] E Bossanyi, Probabilities of sudden drop in power from a wind turbine cluster, Proc. 4th international symposium on wind energy systems, September 21-24 1982.

[34] H Markou and T Larsen, Control Strategies for operation of pitch regulated turbines above cut-out wind speeds, Proc. European Community Wind Energy Conference 2009, Marseille.

[35] Iribas M. Closed loop Identification for Wind Turbines. CENER Ref IN-08.00289. 2006.

[36] Burton T. Sharpe D. Jenkins N. Bossanyi E.. Wind Energy Handbook. Wiley 2001.

[37] Iribas M., Landau I.D. Identification of wind turbines in closed loop operation in the presence of three dimensional turbulence wind speed. Wind Energy Journal 2009; 12:660-675.

[38] Iribas M., Landau I.D. Closed Loop Identification of Wind Turbines Models for Pitch Control. Mediterranean Control Conference 2009.

[39] Iribas M., Landau I.D. A New Algorithm for the Identification of Wind Turbines Models for Pitch Control in closed loop operation. Wind Energy Journal. Under Revision.

[40] L Greedy, Review of electrical drive-train topologies, Upwind Deliverable 5.8, report 11593/BR/01, http://www.upwind.eu/Shared%20Documents/WP5%20-%20Publications/Review%20of%20electrical%20drive-train%20topologies.pdf

[41] Vyas P and Ahmed E., Impact of Drivetrain on Wind Farm VAR Control, Deliverable 5.9.1, http://www.upwind.eu/Shared%20Documents/WP5%20-%20Publications/UpWind_D591_Final.pdf.

[42] Carlo E Carcangiu, DFIG modelling & LVRT Deliverable 5.9.2, 10th February 2011, http://www.upwind.eu/Paginas/Publications/5%20Control%20systems.aspx.

[43] Mikel Iribas, Wind Turbine Identification in Closed loop operation, Deliverable 5.11, 9/02/2011, http://www.upwind.eu/Paginas/Publications/5%20Control%20systems.aspx.

[44] E Bossanyi, A. Wright and P. Fleming, Controller field tests on the NREL CART3 turbine, Deliverable 5.6.2, 10/02/2011, http://www.upwind.eu/Paginas/Publications/5%20Control%20systems.aspx.

[45] Svenja Wortmann, Matthias Heinicke, Martin von Mutius, REpower Field Test of Active Tower Damping, Deliverable 5.6.3, 26/01/2011, http://www.upwind.eu/Paginas/Publications/5%20Control%20systems.aspx.

[46] P A Fleming, A D Wright, L J Fingersh and J-W van Wingerden, Resonant vibrations resulting from the re-engineering of a constant-speed 2-bladed turbine to a variable-speed 3-bladed turbine, 49th AIAA Aerospace Sciences Meeting, 2011.

[47] Martin Geyler, Jung Chul Choi, Barbara Savini, Dennis Wouters and Tim van Engelen “Hardware-in-the-loop testing of pitch controller algorithms and actuators”, Upwind deliverable 5.4, 10/02/2011, http://www.upwind.eu/Paginas/Publications/5%20Control%20systems.aspx.

[48] Upwind Project WP9.4.2 – Electrical Grid, “Design of Large Scale Offshore Wind Farms”, GE-GRC Munich

[49] General Electric, Positive Sequence Load Flow (PSLF) Manual